AD-A086 217 PHYSICS INTERNATIONAL CO SAN LEANDRO CA F/G 18/3
ASYMMETRIC COLLAPSE OF LOS PIPE.(U)
JUL 79 E T MOORE, R FUNSTON DNA001-77-C-0155
UNCLASSIFIED PIFR-1034 DNA-5023F NL

1 OF 2
AD
A086217

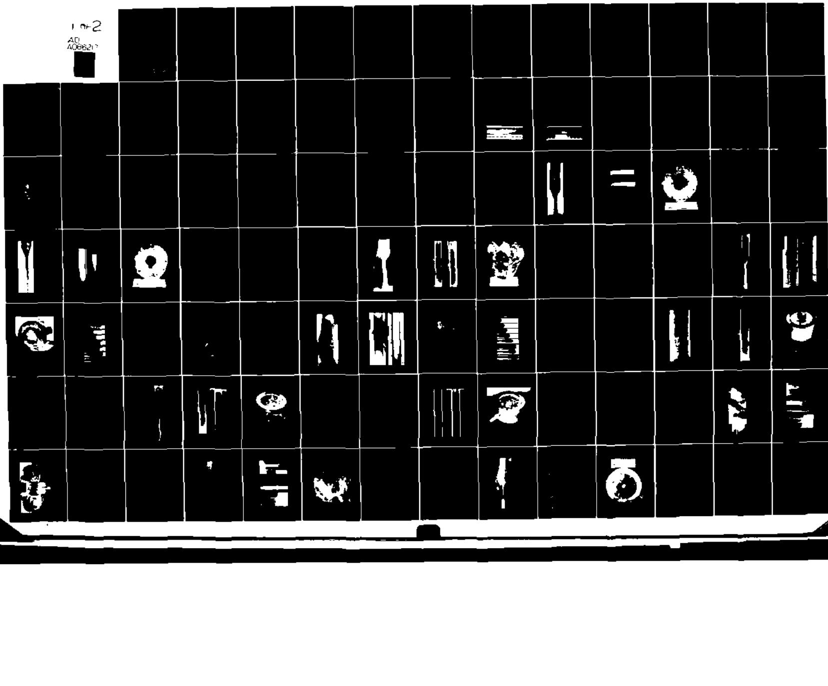

(12) LEVEL II

AD-E300820

DNA 5023F

ADA086217

ASYMMETRIC COLLAPSE OF LOS PIPE

E. T. Moore, Jr.
R. Funston
Physics International Company
2700 Merced Street
San Leandro, California 94577

17 July 1979

Final Report for Period 28 February 1977—31 May 1977

CONTRACT No. DNA 001-77-C-0155

APPROVED FOR PUBLIC RELEASE;
DISTRIBUTION UNLIMITED.

DDC FILE COPY

THIS WORK SPONSORED BY THE DEFENSE NUCLEAR AGENCY
UNDER RDT&E RMSS CODE B345079462 J24AAXYX98363 H2590D.

Prepared for
Director
DEFENSE NUCLEAR AGENCY
Washington, D. C. 20305

Destroy this report when it is no longer needed. Do not return to sender.

PLEASE NOTIFY THE DEFENSE NUCLEAR AGENCY, ATTN: TISI, WASHINGTON, D.C. 20305, IF YOUR ADDRESS IS INCORRECT, IF YOU WISH TO BE DELETED FROM THE DISTRIBUTION LIST, OR IF THE ADDRESSEE IS NO LONGER EMPLOYED BY YOUR ORGANIZATION.

UNCLASSIFIED

SECURITY CLASSIFICATION OF THIS PAGE (When Data Entered)

REPORT DOCUMENTATION PAGE

READ INSTRUCTIONS BEFORE COMPLETING FORM

1. REPORT NUMBER: DNA 5023F	2. GOVT ACCESSION NO.: AD-A086 217
3. RECIPIENT'S CATALOG NUMBER:	
4. TITLE (and Subtitle): ASYMMETRIC COLLAPSE OF LOS PIPE	5. TYPE OF REPORT & PERIOD COVERED: Final Report for Period 28 Feb [redacted]—31 May 77
	6. PERFORMING ORG. REPORT NUMBER: PIFR—1034
7. AUTHOR(s): E. T. Moore, Jr. R. Funston	8. CONTRACT OR GRANT NUMBER(s): DNA 001-77-C-0155
9. PERFORMING ORGANIZATION NAME AND ADDRESS: Physics International Company 2700 Merced Street San Leandro, California 94577	10. PROGRAM ELEMENT, PROJECT, TASK AREA & WORK UNIT NUMBERS: Subtask J24AAXY983-63
11. CONTROLLING OFFICE NAME AND ADDRESS: Director Defense Nuclear Agency Washington, D.C. 20305	12. REPORT DATE: 17 Jul[redacted]979
	13. NUMBER OF PAGES: 156
14. MONITORING AGENCY NAME & ADDRESS (if different from Controlling Office)	15. SECURITY CLASS (of this report): UNCLASSIFIED
	15a. DECLASSIFICATION DOWNGRADING SCHEDULE

16. DISTRIBUTION STATEMENT (of this Report)

Approved for public release; distribution unlimited.

17. DISTRIBUTION STATEMENT (of the abstract entered in Block 20, if different from Report)

18. SUPPLEMENTARY NOTES

This work sponsored by the Defense Nuclear Agency under RDT&E RMSS Code B345079462 J24AAXYX98363 H2590D.

19. KEY WORDS (Continue on reverse side if necessary and identify by block number)

Nuclear	Stemming
Underground	Line-of-Sight
Explosives	Jetting
Containment	

20. ABSTRACT (Continue on reverse side if necessary and identify by block number)

Laboratory experiments are described that were performed to investigate the potential of using asymmetries to inhibit the formation and progression of high energy jets from the collapse of thin-walled metal tubes. The experiments were designed to simulate the collapse of a line-of-sight (LOS) pipe in an underground nuclear test. Results indicate that helical asymmetries on the internal surface of the tubes may eliminate or suppress jetting.

PREFACE

This work was sponsored by the Defense Nuclear Agency (DNA) under Contract No. DNA001-77-C-0155 in support of the DNA stemming and containment program for underground nuclear tests. The authors are particularly indebted to DNA's Contracting Officers' Representative, Carl Keller. They appreciate the background experience, ideas, insights and suggestions which he provided to the work reported here.

The authors are also indebted to Dan Patch of Pacifica Technology and James Barthel of Systems, Science and Software for their calculational support, to J. L. Ploss of Lockheed Missiles and Space Company for line-of-sight pipe information, to Tom McKown of Los Alamos Scientific Laboratory and Dennis Whann of EG&G, Las Vegas, for the time domain reflectometry instrumentation, and to Russell Duff of Systems, Science and Software for his comments and suggestions.

CONVERSION FACTORS FOR U.S. CUSTOMARY TO METRIC (SI) UNITS OF MEASUREMENT

To Convert From	To	Multiply By
angstrom	meters (m)	1.000 000 X E -10
atmosphere (normal)	kilo pascal (kPa)	1.013 25 X E +2
bar	kilo pascal (kPa)	1.000 000 X E +2
British thermal unit (thermochemical)	joule (J)	1.054 350 X E +3
cal (thermochemical)/cm² §	mega joule/m² (MJ/m²)	4.184 000 X E-2
calorie (thermochemical) §	joule (J)	4.184 000
calorie (thermochemical)/g§	joule per kilogram (J/kg)*	4.184 000 X E +3
curie§	giga becquerel (GBq)+	3.700 000 X E +1
degree (Celsius)‡	degree kelvin (K)	$T_K = T_{°C} + 273.15$
degree (angle)	radian (rad)	1.745 329 X E -2
degree Fahrenheit	degree kelvin (K)	$T_K = (T°F + 459.67)/1.8$
electron volt§	joule (J)	1.602 19 X E -19
erg§	joule (J)	1.000 000 X E -7
erg/second	watt (W)	1.000 000 X E -7
foot	meter (m)	3.048 000 X E-1
foot-pound-force	joule (J)	1.355 818
gallon (U.S. liquid)	meter³ (m³)	3.785 412 X E -3
inch	meter (m)	2.540 000 X E -2
jerk	joule (J)	1.000 000 X E +9
joule/kilogram (J/kg) (radiation dose absorbed)§	gray (Gy)*	1.000 000
kilotons§	terajoules	4.183
kip (1000 lbf)	newton (N)	4.448 222 X E +3
kip/inch² (ksi)	kilo pascal (kPa)	6.894 757 X E +3
ktap	newton-second/m² (N-s/m²)	1.000 000 X E +2
micron	meter (m)	1.000 000 X E -6
mil	meter (m)	2.540 000 X E -5
mile (international)	meter (m)	1.609 344 X E +3
ounce	kilogram (kg)	2.834 952 X E -2
pound-force (lbf avoirdupois)	newton (N)	4.448 222
pound-force inch	newton-meter (N-m)	1.129 848 X E -1
pound-force/inch	newton/meter (N/m)	1.751 268 X E +2
pound-force/foot²	kilo pascal (kPa)	4.788 026 X E -2
pound-force/inch² (psi)	kilo pascal (kPa)	6.894 757
pound-mass (lbm avoirdupois)	kilogram (kg)	4.535 924 X E -1
pound-mass-foot² (moment of inertia)	kilogram-meter² (kg·m²)	4.214 011 X E -2
pound-mass/foot³	kilogram-meter³)	1.601 846 X E +1
rad (radiation dose absorbed)§	gray (Gy)*	1.000 000 X E -2
roentgen§	coulomb/kilogram (C/kg)	2.579 760 X E -4
shake	second (s)	1.000 000 X E -8
slug	kilogram (kg)	1.459 390 X E +1
torr (mm Hg, 0° C)	kilo pascal (kPa)	1.333 22 X E -1

*The gray (Gy) is the accepted SI unit equivalent to the energy imparted by ionizing radiation to a mass of energy corresponding to one joule/kilogram.
+The becquerel (Bq) is the SI unit of radioactivity; 1 Bq = 1 event/s.
‡Temperature may be reported in degree Celsius as well as degree kelvin.
§These units should not be converted in DNA technical reports; however, a parenthetical conversion is permitted at the author's discretion.

CONTENTS

ILLUSTRATIONS

SECTION 1

INTRODUCTION AND SUMMARY

1.1 BACKGROUND

Line-of-sight (LOS) pipes are frequently used in underground nuclear tests to collimate and transmit the radiation from a nuclear source to an experimental test station. The radiation is followed by a spherically divergent ground shock that causes the LOS pipe to collapse and form a very high-energy plasma jet. This jet represents a serious threat not only to the experiments located at the test station but also to the successful stemming and containment of the radioactive gases generated by the nuclear explosion. As a result, various techniques have been developed and used to delay, attenuate, or eliminate the high-energy flow in LOS pipes. Baffles, energy absorbers, debris barriers, high explosive valves, and fast-acting doors are examples of protection techniques that have been used together and separately with mixed results. Although stemming and containment have been successful in recent nuclear tests, the efficacy and reliability of these elaborate (and expensive) techniques are still uncertain.

1.2 OBJECTIVE

The objective of the work reported here was to conduct an experimental program to investigate the use of asymmetries that could potentially be used to inhibit the formation and progression of the high-energy axial jet that occurs in the collapse of an LOS pipe. Specific emphasis was directed toward the evaluation of practical and cost-effective methods which would cause an off-axis collapse of the pipe and thereby either eliminate the jet or minimize the energy contained in the jet.

1.3 SUMMARY OF RESULTS

Two different types of experiments were used to simulate the ground shock collapse of an LOS pipe, explosive drivers and high explosive spheres. Both methods produced high-energy jets from the collapse of evacuated, small-diameter, thin-walled stainless steel tubes (LOS models). In the explosive driver experiments, the LOS models were collapsed by the progressive detonation of a cylinder of high explosive surrounding the model. In the spherical high explosive experiments, the models were embedded in saturated sand and collapsed by the shock wave diverging from a sphere of high explosive. The major results of these experiments are presented below. Special emphasis is given to the effect of asymmetries. More detailed results will be found in the relevant sections of this report.

1.3.1 Spherical High Explosive Experiments (LS-1 and LS-2).

- Helical asymmetries on the internal surface of an LOS model appear to eliminate or suppress jet formation.
- Helical asymmetries on the external surface of an LOS model do not reduce the energy of the jet.
- Thin liners on the inside surface of an LOS model form a jet. The jet energy seems to be highly dependent on the material properties of the liner.

* Increasing the wall thickness (by adding mass uniformly to the external surface) of an LOS model produces a higher energy jet than models with no external liners.

* The target damage from one standard LOS model (i.e., no asymmetries) was approximately 80 percent greater than a second standard model evaluated in the same experiment.

* The jet formation conditions resulting from the collapse of an LOS model by a spherically diverging shock wave are considerably different from those resulting from the explosive collapse of a model. Asymmetries that are effective for one type of collapse may not be effective for the other.

1.3.2 Explosive Driver Experiments (APC Series).

* Helical asymmetries on the external surface of an LOS model appear to eliminate or suppress jet formation. Lead and foam helixes produced comparable results.

* An LOS model with a square cross-section showed less jetting than models with a circular cross-section.

* One atmosphere of air in an LOS model suppressed jet formation.

* The jet from a standard LOS model (no asymmetries) was characterized. The jet was reproducible. It had a velocity of approximately twice the detonation velocity of the explosive used. The jet was not discernable on radiographs capable of resolving 0.0025 mm of steel. Models with steel and stainless steel tubes produced comparable jets.

* Explosively collapsed tubes cannot be used to simulate the collapse of a tube by a spherically diverging shock wave.

1.4 COMMENTS AND RECOMMENDATIONS

The experimental results reported here indicate that internal asymmetries *may* be a promising method of reducing or eliminating the jetting phenomena in small, evacuated steel tubes that are collapsed by spherically diverging shock waves. However, the number of experiments and the scale of the experiments were too small to postulate the efficacy of using similar asymmetries on a full-scale LOS pipe in an underground nuclear test environment. Such use should only be considered after a more comprehensive investigation provides a better understanding of jetting and the effects of asymmetries.

Increasing the data base should be the first priority of further investigations of asymmetries. Initial efforts should be directed at experiments designed specifically to determine the reproducibility of the jetting/nonjetting phenomena. Experiments should also be performed to understand the source of jetting and to establish whether internal asymmetries eliminate the cause or suppress the results of jetting. These experiments should be well instrumented to characterize the dynamic and thermodynamic properties of the jet.

A parametric study should also be conducted after the reproducibility and source of jetting have been established. The results of these experiments would establish the sensitivity of specific asymmetry parameters on the collapse and jetting process. They would also provide an experimental data base for modeling the process.

Candidate LOS pipe designs should be developed during the final phase of the parametric study. Still, separate experiments should be performed to evaluate specific designs. As much as possible, the experiments should be designed to simulate the conditions that would be expected in an underground nuclear test. Particular emphasis should be placed on: (1) the scale of the experiment; (2) the LOS pipe material and geometry; (3) the effect of a particular testing site; (4) the presence of grout; (5) blow-off gases in the pipe, and (6) the yield of the nuclear device.

Finally, a small-scale, proof-of-concept experiment could be added to the underground nuclear test program. Successful results from such an experiment would not only validate the concept of using asymmetries, it would validate the methods used to select and design the asymmetries and maximize the probability of success on a full-scale LOS pipe.

SECTION 2

EXPLOSIVE DRIVER EXPERIMENTS

2.1 BACKGROUND

Explosive drivers were selected as a vehicle for producing jets in the laboratory that were similar to those generated by the ground-shock collapse of an LOS pipe. This selection was based on the results of extensive theoretical and experimental investigations of jetting and nonjetting explosive drivers performed by Physics International Company during the past 15 years. A comprehensive summary of these results, including a description of the operating characteristics of explosive drivers, is given in References 1 through 8.

Jetting in an explosive driver can be enhanced or suppressed by the choice of certain experimental parameters or combinations of parameters. For example, the experiments illustrated in Figure 1 show the effect of the initial pressure of the gas contained in an explosive driver (Reference 1). Diluted nitromethane with a detonation velocity of approximately 0.55 cm/μs was used for these experiments to progressively collapse a 0.794-cm- (3/16-inch-) diameter steel tube having a wall thickness of 0.074 cm (0.029 inch). It is seen that the shock velocity increases as the initial pressure is decreased. Furthermore, when the tube is evacuated the shock velocity is approximately twice the detonation velocity. Since this doubling

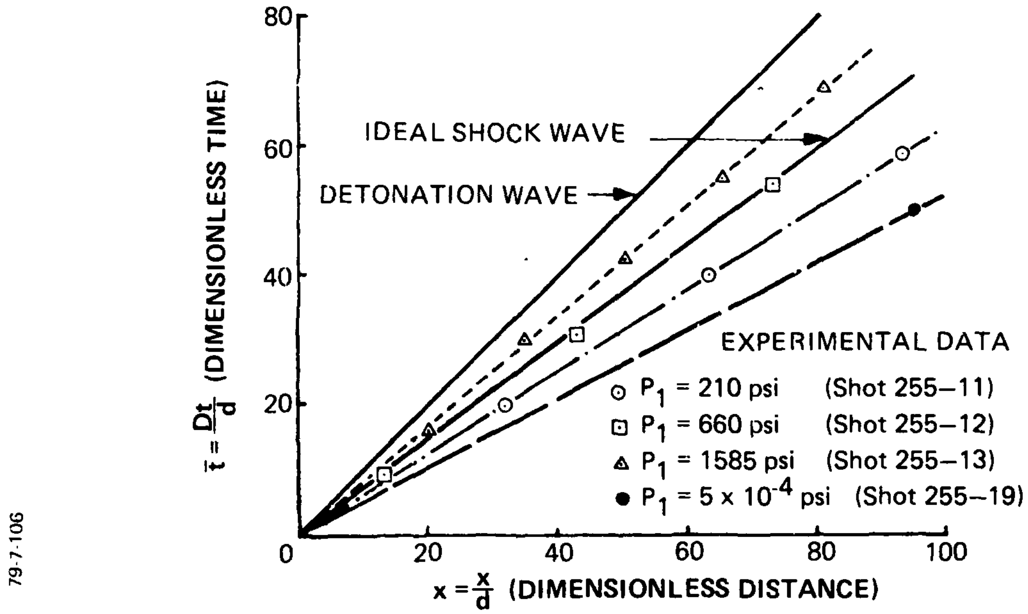

Figure 1 Explosive driver trajectories showing the effect of initial gas pressure.

represents the theoretical limit of jet formation, it can be inferred that the high velocity is a result of jetting tube material.

Figure 2 shows the results of an experiment performed specifically to examine the character of a jet from an explosive driver. A 50 cm length of polymethyl methacrylate (PMMA) tubing was used to extend the driver and contain any jetting material so that high-resolution radiographic diagnostics could be used. The radiograph taken at 60 μs shows the existence of a high-density metal jet (Figure 2b). Furthermore, the observed shock trajectory indicates severe mixing of the jet with the shocked gas, causing the jet tip to be quite close to the shock front. As a comparison, Figure 3 shows the trajectory and radiograph of a driver with a higher initial pressure in which jetting did not occur.

The results of these experiments provide the background and basis for selecting the explosive driver techniques to investigate the jetting in LOS pipes. The specific designs and design methods used in this program are given in the following section.

2.2 DESIGN OF JETTING EXPLOSIVE DRIVER

Explosive drivers were used in this program primarily for testing and evaluating various methods of using asymmetries to eliminate or reduce jetting in a collapsing pipe. It was well recognized that the collapse generated by the drivers is a steady-state process and cannot be used to rigorously simulate the nonsteady collapse of the entire length of an LOS pipe by a

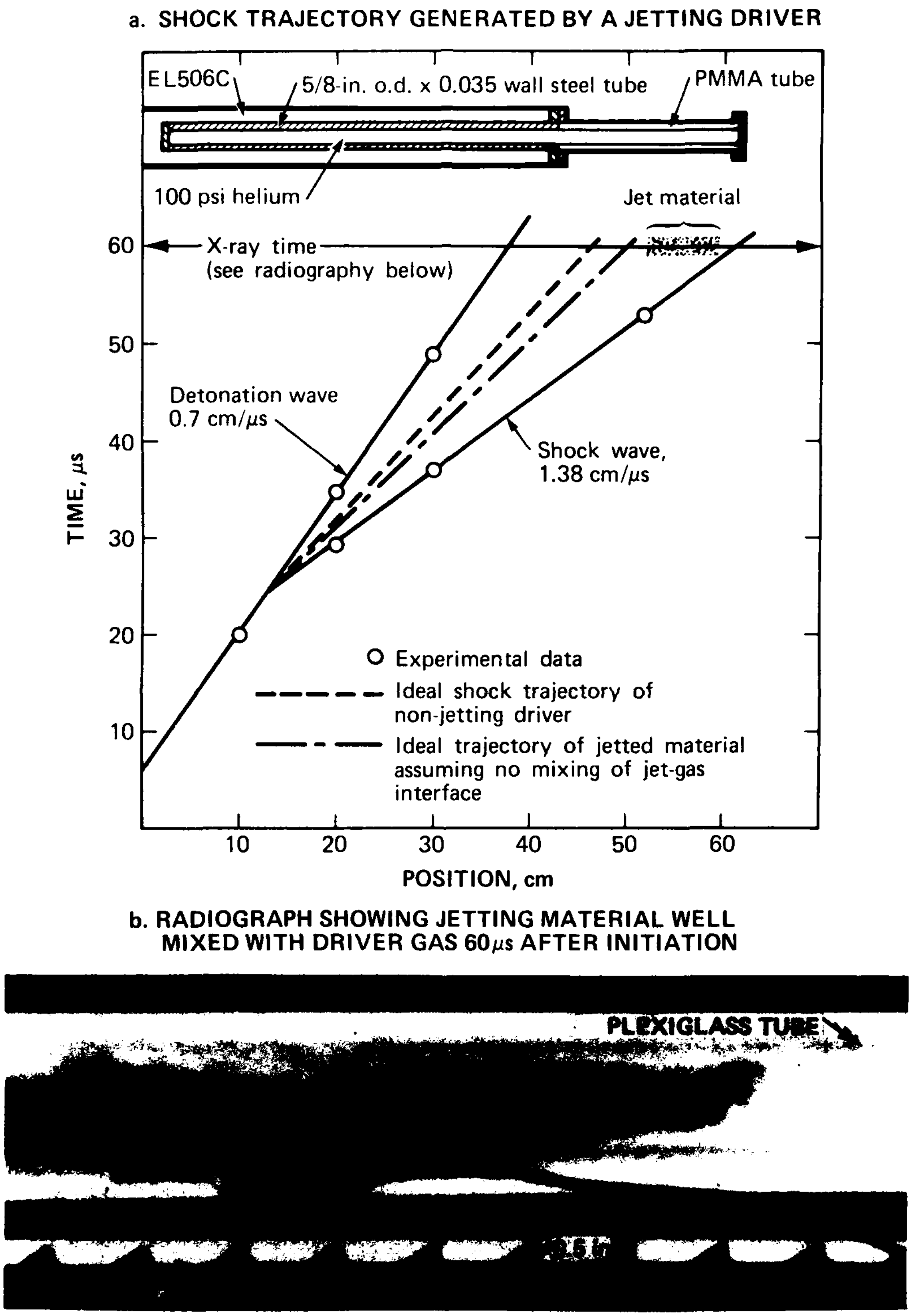

Figure 2 Performance characteristics of a jetting driver (shot 255-26 from Reference 1).

a. SHOCK TRAJECTORY GENERATED BY FIRST-STAGE DRIVER

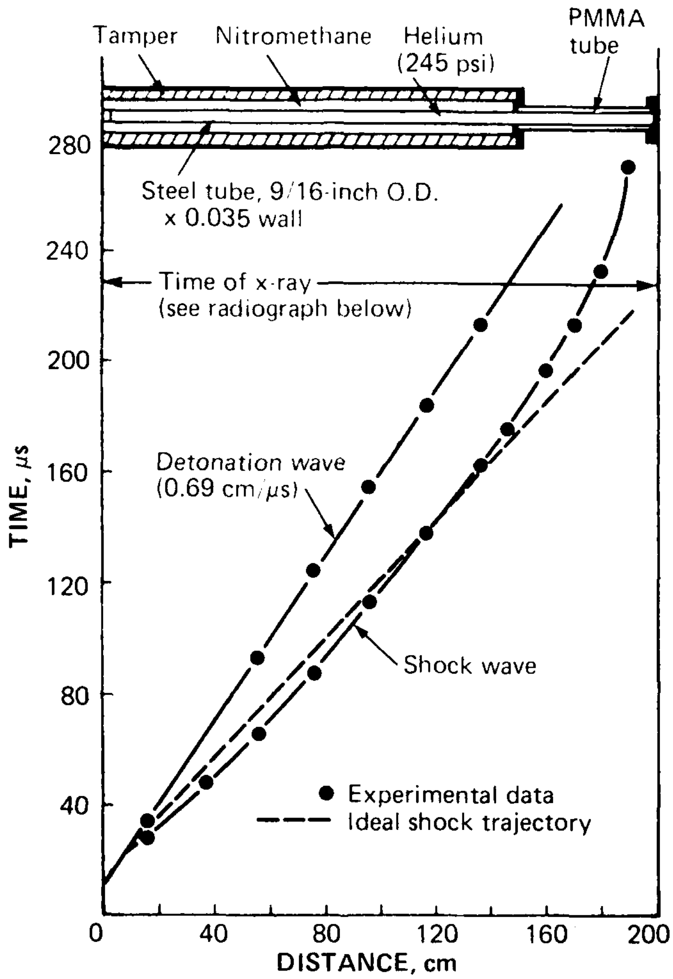

b. RADIOGRAPH OF SHOCKED DRIVER GAS 222μs AFTER INITIATION

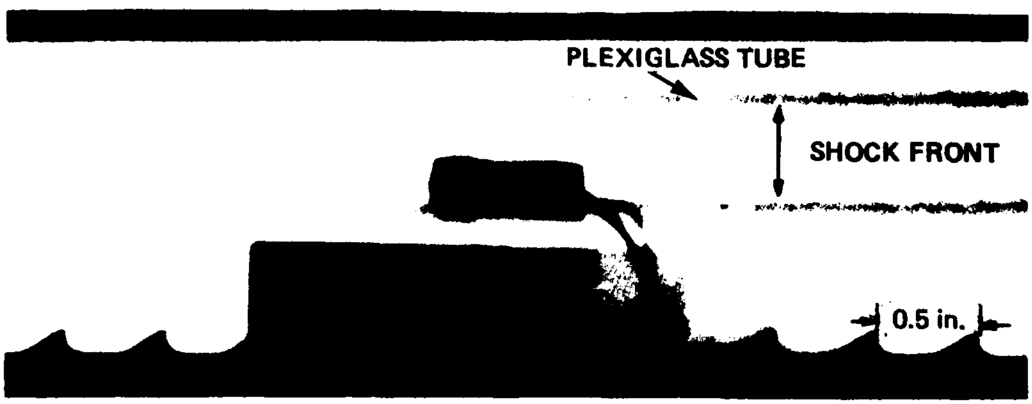

Figure 3 Results of an experiment to investigate the possibility of jetting in an explosive driver (shot 255-28). (See Reference 1.)

spherically divergent ground shock. Therefore, the design approach was based on the reproduction of those critical parameters that were expected to contribute most significantly to the collapse and jetting of an LOS pipe. Mighty Epic and Diablo Hawk were used as representative underground nuclear tests. Where appropriate, these events were analyzed to establish the baseline environment, collapse conditions, and LOS pipe configurations.

The first step in the design process was to define the collapse conditions at a distance from the nuclear source where the peak stresses in the free-field were comparable to the stresses that can be generated by chemical high explosives. Figure 4 shows the peak radial stress calculated as a function of distance from the Mighty Epic source. This figure also shows the detonation pressure of typical high explosives, comparable to the free-field stress at ranges between 10 meters (HMX) and 14 meters (nitromethane).

The LOS pipe collapse conditions were calculated from "close-in" data from the Mighty Epic event. The curves given in Figure 5 from Reference 9 summarize some of these conditions. These curves show the trajectories of the ground shock and collapse point for a range between 11 meters, where the LOS pipe begins, and 25 meters. While the pipe collapse angle was judged to be 15.6 degrees ± 1.3 degrees over this range, the axial and radial collapse velocities given in this figure are based on a constant collapse angle of 15.6 degrees. With this assumption, Figure 5 shows an axial collapse velocity between 0.73 cm/μs and 0.39 cm/μs for the range interval of 11 to 14 meters.

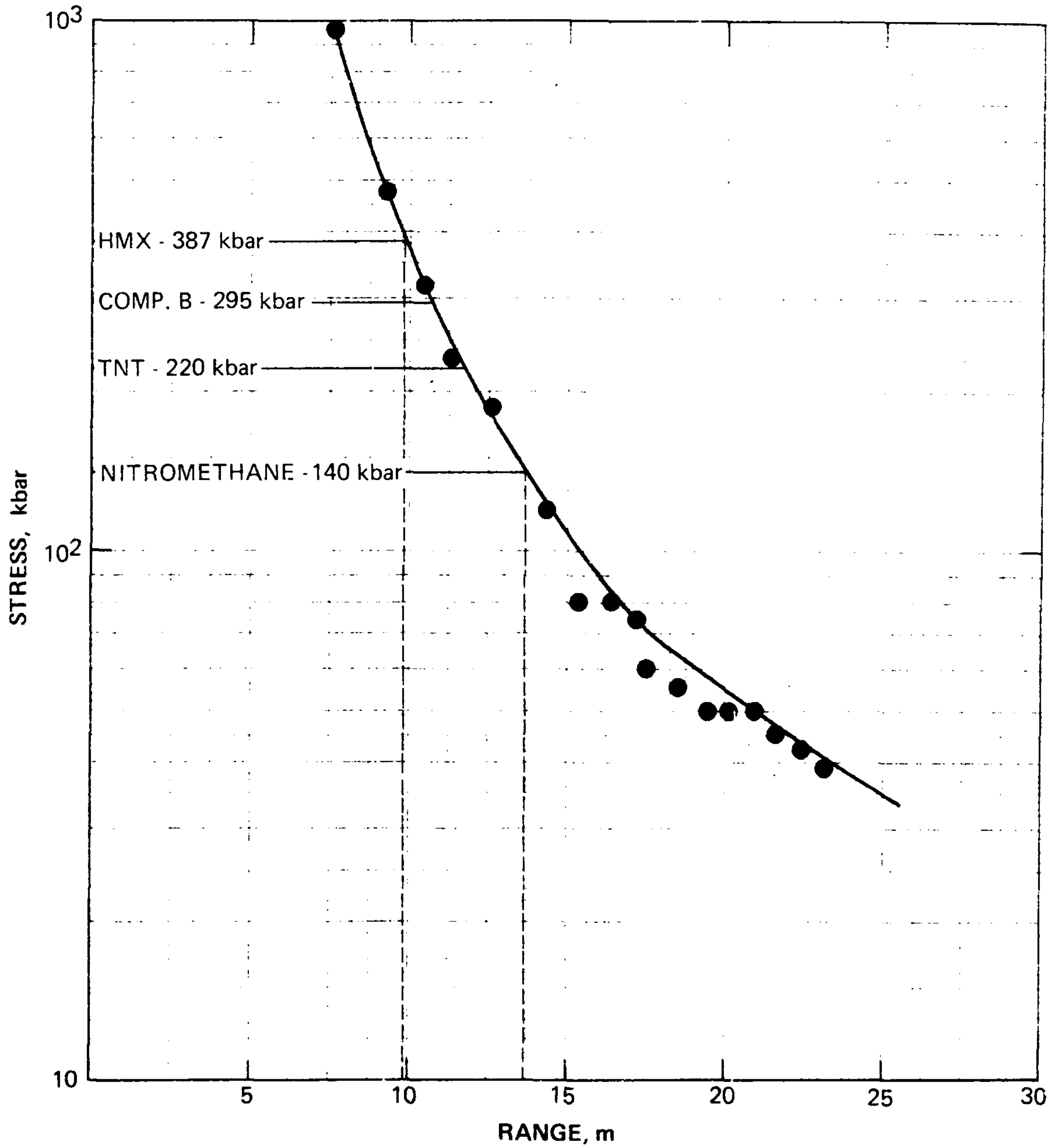

Figure 4 Calculated peak radial stress versus range for Mighty Epic and the detonation pressure of various high explosives.

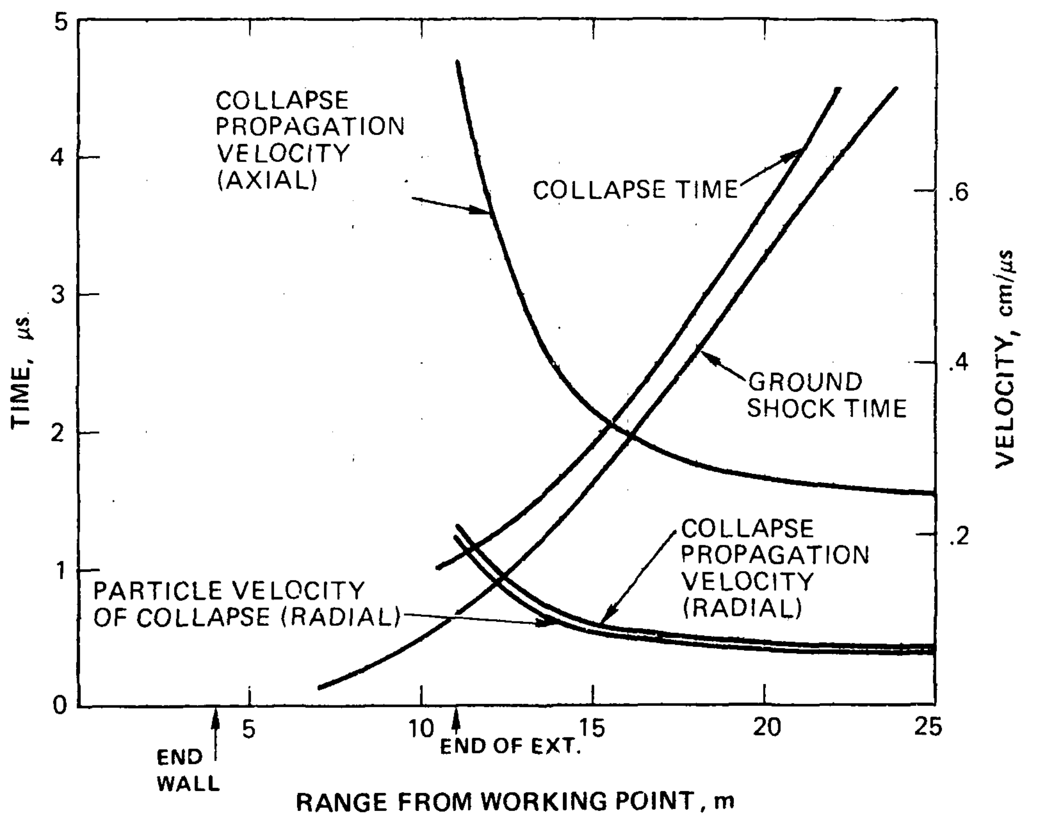

Figure 5 LOS collapse characteristics for Mighty Epic (Reference 9).

Nitromethane was selected as the driver explosive. The detonation pressure 14 mPa (140 kbar) and detonation velocity of approximately 0.62 cm/μs for this explosive are comparable, respectively, to the values for the free-field peak stress and the axial pipe collapse velocity in the range of 11 meters to 14 meters. In addition, the procurement, manufacturing, and assembly procedures for using this liquid explosive are considerably less difficult than those associated with most other explosive candidates.

The most critical parameter affecting jetting phenomena in explosively collapsed tubes is the collapse angle (illustrated in Figure 6). Here, a metal tube is deflected through a collapse angle, β, by the detonation pressure of a cylindrical charge of explosive surrounding the tube. As the tube converges and impacts on the axis, a jet is formed. Classical jetting theory (Reference 10) shows that the collapse velocity, V_o, the detonation velocity, U_d, and collapse angle, β, are related by

$$\sin \frac{\beta}{2} = \frac{V_o}{2U_d}$$

The ratio of the mass in the jet, m_j, to the mass in the tube, m_o, is given by

$$\frac{m_j}{m_o} = \sin^2 \left(\frac{\beta}{2}\right) .$$

Furthermore, the jet velocity, V_j, would be

$$V_j = \frac{V_o}{\tan \frac{\beta}{2}} = 2\ U_d .$$

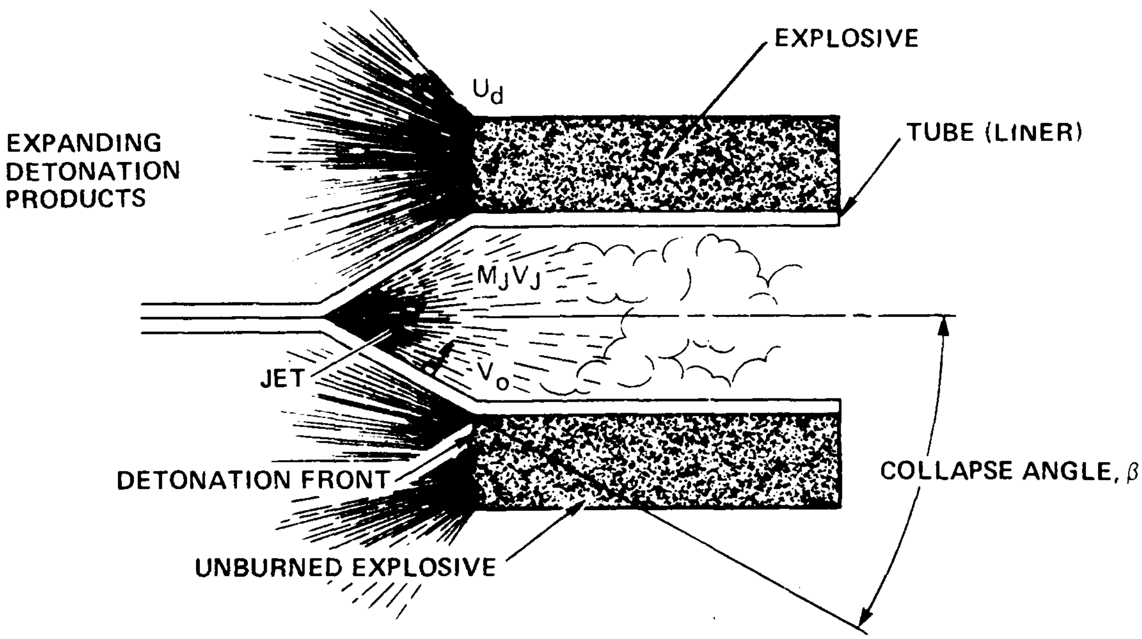

Figure 6 Illustration of a jetting explosive driver.

These equations show that the collapse velocity of a tube surrounded by nitromethane (U_d = 0.62 cm/μs) would vary between 0.15 cm/μs and 0.18 cm/μs for the range of collapse angles, 15.6 ± 1.3 degrees, calculated for the Mighty Epic event. Since the mass contained in the jet is larger for larger collapse angles, the upper end of this range (~ 17 degrees) was selected for the driver design in order to generate the highest energy flow possible in the collapsed tube.

Having selected the explosive and the collapse angle, the remaining task was to establish the tube dimensions. The engineering drawings for the LOS pipe used for the Mighty Epic and Diablo Hawk events showed a tapered steel pipe design with a wall thickness of 0.476 cm (3/16 inch) and an inside diameter of 37.008 cm (14.57 inches) at a range of 14 meters (Reference 11). These dimensions could not be scaled down precisely to the dimensions of standard tubing and still obtain the desired collapse angle. However, a close approximation could be achieved by using a standard 7.937 cm (3-1/8 inch o.d. PMMA tubing with a wall thickness of 0.317 cm (1/8 inch) to contain nitromethane around a steel tube with an outer diameter of 5.042 cm (1.985 inch) and a wall thickness of 0.071 cm (0.028 inch). This latter specification can be met merely by grinding 0.018 cm (0.007 inch) from the outside surface of commercially available steel tubes (5.08 cm o.d. [2 inches] with a wall thickness of 0.089 cm [0.035 inch]). One-dimensional, time-dependent finite difference calculations of the collapse of this configuration indicated a collapse velocity of 0.18 cm/μs and a collapse angle of 17 degrees.

Figure 7 shows an engineering sketch of the explosive drivers used in this program. A PMMA tube having approximately the same inner diameter as the steel driver tube was used to extend the steel tube to mock up the sections of an LOS pipe that do not collapse, to facilitate radiographic measurements of the jet, and to minimize the blast and debris effects on the aluminum targets. The results from experiments using this driver design are given in the following section. Any deviations from this design are appropriately noted.

2.3 EXPLOSIVE DRIVER EXPERIMENTS

A complete list of the APC series of explosive driver tests is given in Table 1. The objectives of the tests designated APC-1 through APC-4 were to investigate the jetting characteristics of the drivers. Asymmetries were then included in tests APC-5 (lead wrapped), APC-7 (foam wrapped), and APC-8 (square cross-section). The air pressure inside the steel tubes was reduced to a few millimeters of mercury except for APC-6, which was a test to examine the effects of 1 atm. of pressure. Stainless steel tubes were intoduced in tests APC-9 through APC-11 in preparation for the large spherical high-explosive experiment described in Section 3. The variety of wall thicknesses commercially available in small-diameter stainless steel tubing reduced the magnitude and expense of this experiment.

2.3.1 Instrumentation and Data Presentation. The typical instrumentation used for the explosive driver tests includes: (1) ionization pins for measuring the time of arrival of the

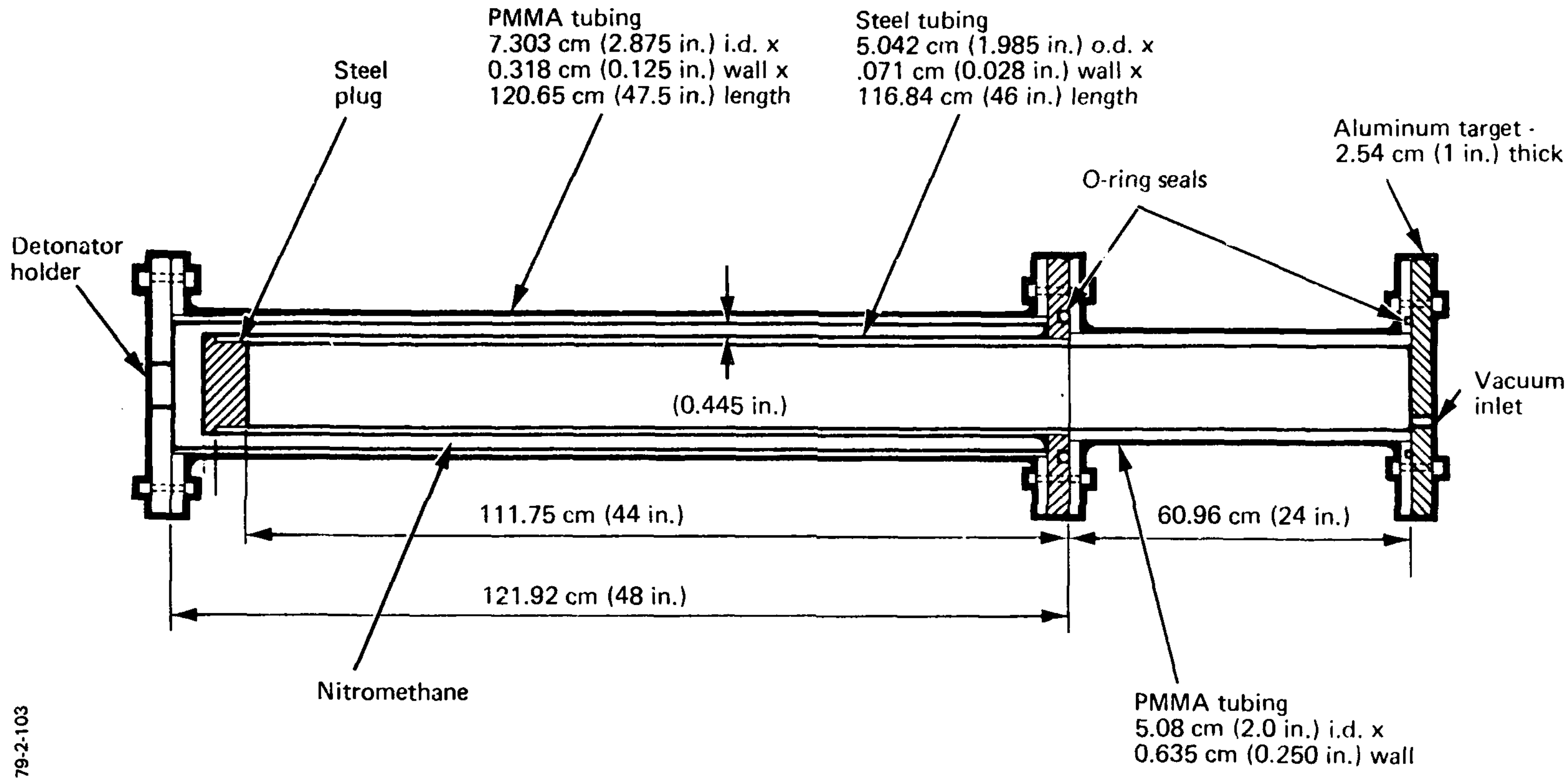

Figure 7 Explosive driver for evaluating asymmetric collapse of LOS pipe.

TABLE 1

EXPLOSIVE DRIVER EXPERIMENTS

Experiment Number	Purpose of Experiment	DRIVER TUBE Material	DRIVER TUBE Outside Dimensions cm (inches)	DRIVER TUBE Wall Thickness cm (inches)	DRIVER TUBE Length cm (inches)	PMMA EXTENSION TUBE Outside Dimensions cm (inches)	PMMA EXTENSION TUBE Wall Thickness cm (inches)	PMMA EXTENSION TUBE Length cm (inches)	TEST DATA Initial Air Pressure (mm Hg)	TEST DATA Detonation Velocity (cm/μs)	TEST DATA Jet Velocity (cm/μs)	TEST DATA Collapse Angle (degrees)	Observations	Figure Numbers
APC-1	To determine jet characteristics	Steel	5.08 (2.0)	0.07 (0.028)	117.48 (46.25)	6.35 (2.50)	0.64 (0.250)	60.96 (24)	1.0	0.61	--	16.5	Total penetration of 2.54-cm-thick target with a 5.08-cm-diameter hole.	9-12
APC-2	Same as APC-1	Steel	5.08 (2.0)	0.07 (0.028)	117.48 (46.25)	6.35 (2.50)	0.64 (0.250)	60.96 (24)	1.2	0.61	--	16.0	Same as APC-1.	13-16
APC-3	Same as APC-1 and 2, but increased length of the extension tube to extend X-ray coverage of jet characteristics	Steel	5.08 (2.0)	0.07 (0.028)	117.48 (46.25)	5.72 (2.25)	0.32 (0.125)	121.92 (48)	0.9	0.61	1.21	17.0	Total penetration and fracture of 10-cm-thick target. Jet not visible in high resolution X-rays.	17-20
APC-4	To establish a standard design and baseline test data optics and flow wires were added to investigate jet characteristics	Steel	5.08 (2.0)	0.07 (0.028)	117.48 (46.25)	5.72 (2.25)	0.32 (0.125)	121.92 (48)	1.4	0.60	1.25	17.0	Deformation and ablation of of flow wires visible in radiographs. Same evidence of annular flow.	21-25
APC-5	A spiral wrap of lead was added to the driver tube to establish effects of asymmetries.	Steel	5.08 (2.0)	0.07 (0.028)	117.48 (46.25)	5.72 (2.25)	0.32 (0.125)	121.92 (48)	1.9	0.60	1.15	~ 17.0	No target damage.	26-31
APC-6	Establish effects of 1 atmosphere of air inside tube	Steel	5.08 (2.0)	0.07 (0.028)	117.48 (46.25)	5.72 (2.25)	0.32 (0.125)	121.92 (48)	760	0.60	0.85	~ 17.0	No target damage.	32-35
APC-7	A spiral wrap of low density foam was added to driver tube as asymmetry	Steel	5.08 (2.0)	0.07 (0.028)	117.48 (46.25)	5.72 (2.25)	0.32 (0.125)	121.92 (48)	2	0.61	1.23	~ 17.0	Slight target damage.	36-39
APC-8	A square pressure tube and extension tube was used as asymmetry.	Steel	5.08 x 5.08 2.0 x 2.0	0.12	117.48	6.35	0.64	121.92	2	0.62	1.24	--	Modest target damage.	40-42
APC-9	Driver tube was changed to stainless steel	Stainless Steel	5.08 (2.0)	0.07 (0.028)	117.48 (46.25)	5.72 (2.25)	0.32 (0.125)	121.92 (48)	1.7	0.61	1.22	17.0	Same result as steel tubes.	43-46
APC-10	Driver tube O.D. was changed to 1.91 cm to determine scalability. Only vertical dimensions were scaled. Horizontal dimensions were same as APC-4 (standard)	Stainless Steel	1.91 (0.75)	0.03 (0.011)	117.48 (46.25)	3.81 (1.50)	4.76 (1.875)	121.92 (48)	1.1	0.61	1.21	18.5	No damage. Suspect jet expanded in large diameter extension tube. Large collapse angle.	47-50
APC-11	Exact scaled version of APC-4. This is standard used for spherical experiment.	Stainless Steel	1.91 (0.75)	0.03 (0.011)	47.94 (18.875)	2.22 (0.875)	0.16 (0.0625)	46.05 (18-1/8)	1.6	0.60	1.17	18	1 [illegible] hole to a depth of 8.4 cm. Crater [illegible] of [illegible] cm³.	51-54

detonation wave in the explosive at six axial locations; (2) ionization pins for measuring the time of arrival of the jet at five locations in the PMMA tube that extended beyond the explosive driver; (3) a radiograph of the collapsing tube using a 1-MeV Pulserad Model 107A X-ray generator with a pulse length of 30 ns; (4) flash radiographs of the jetting phenomena in the Lucite tube extension of the driver using 80 kV, 5 kA pulsed X-ray generators (COBRA's) with a pulse duration of 40 ns, (5) an aluminum target to permanently record the damage caused by each jet; and (6) a single ionization pin located on the front surface of the aluminum target to determine the time of arrival of the leading edge of the jet at the target. In addition, high-speed photography and break-wires were used to investigate the characteristic of the jet in tests APC-4 and APC-5, respectively.

2.3.2 Format for Data Presentation. The top of Figure 8 shows a sketch of a typical experiment using standard instrumentation. This figure also shows the format used for presenting the experimental data in this section. An x-t plot is used to present the arrival time of the detonation wave and jet as a function of the distance from the detonator used to initiate the explosive. The locus of these points will define the trajectories of the detonation wave and the jet, and the slope will be used to define their velocity. It should be noted that the abscissa in Figure 8 is the distance axis (x) and provides a one-to-one correspondence with the axial dimensions of the explosive driver experiment sketched at the top of this plot. It also includes the axial extent of instrumentation. For example, radiography coverage is given as a horizontal bar positioned at the time the X-ray was taken and extending for a length that is

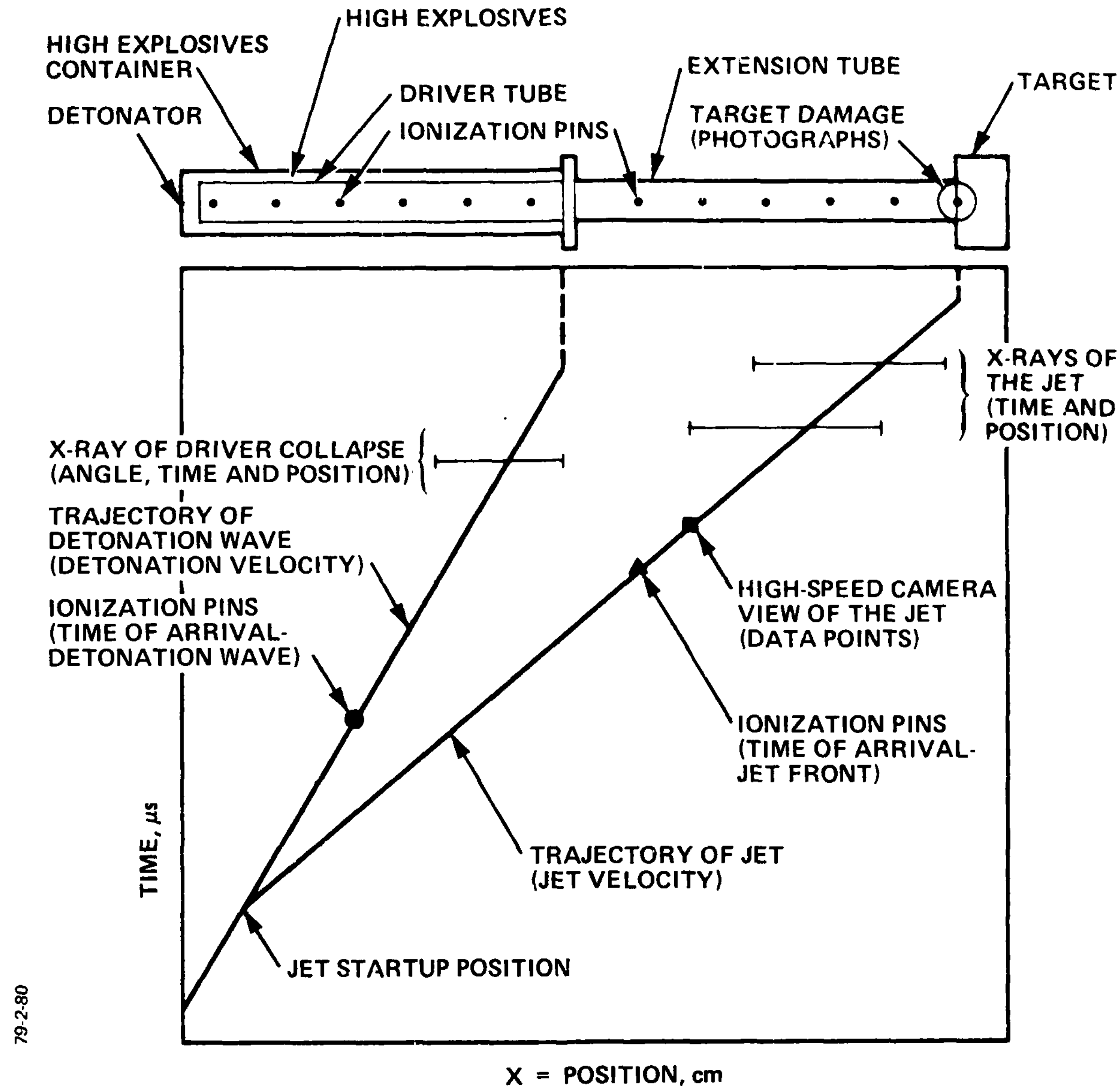

Figure 8 Format used for presenting experimental results.

equal to the axial field of view of the X-ray film used. Actual radiographs for each experiment are presented after each x-t plot. These radiographs will be followed by photographs which show the jet damage to the aluminum targets.

2.3.3 Experimental Results.

Tests APC 1 and 2 (symmetrical). The fist two explosive driver tests, APC-1 and APC-2, were identical except for the radiographic coverage of the jet. Each driver was separate from a 2.54-cm- (1-inch-) thick aluminum target by a 60.96 cm (24 inch) length of PMMA tube with an inside diameter of 5.08 cm (2 inches) and a wall thickness of 0.635 cm (1/4 inch). The driver tubes were evacuated to a pressure in the range of 1 to 1.5 mm Hg. In test APC-1, the location and timing of the radiographic diagnostics were based on obtaining a jet with an assumed velocity approximately twice the detonation velocity of nitromethane, or 1.22 cm/µs. Therefore, two radiographs were used to determine the location, condition, and velocity of the jet after emerging from the explosive driver section and before impacting the aluminum target. The time of arrival obtained from a single ionization pin located on the front surface of the target would confirm the velocity of the jet.

The results of APC-1 are presented in Figures 9 through 12. The x-t plot given in Figure 9 shows that the nitromethane had a detonation velocity of 0.61 cm/µs. The time of arrival for the ionization pin located on the front surface of the aluminum target (183 cm) was 181.9 µs. This value is in very good agreement with a predicted arrival time of 176 µs based on

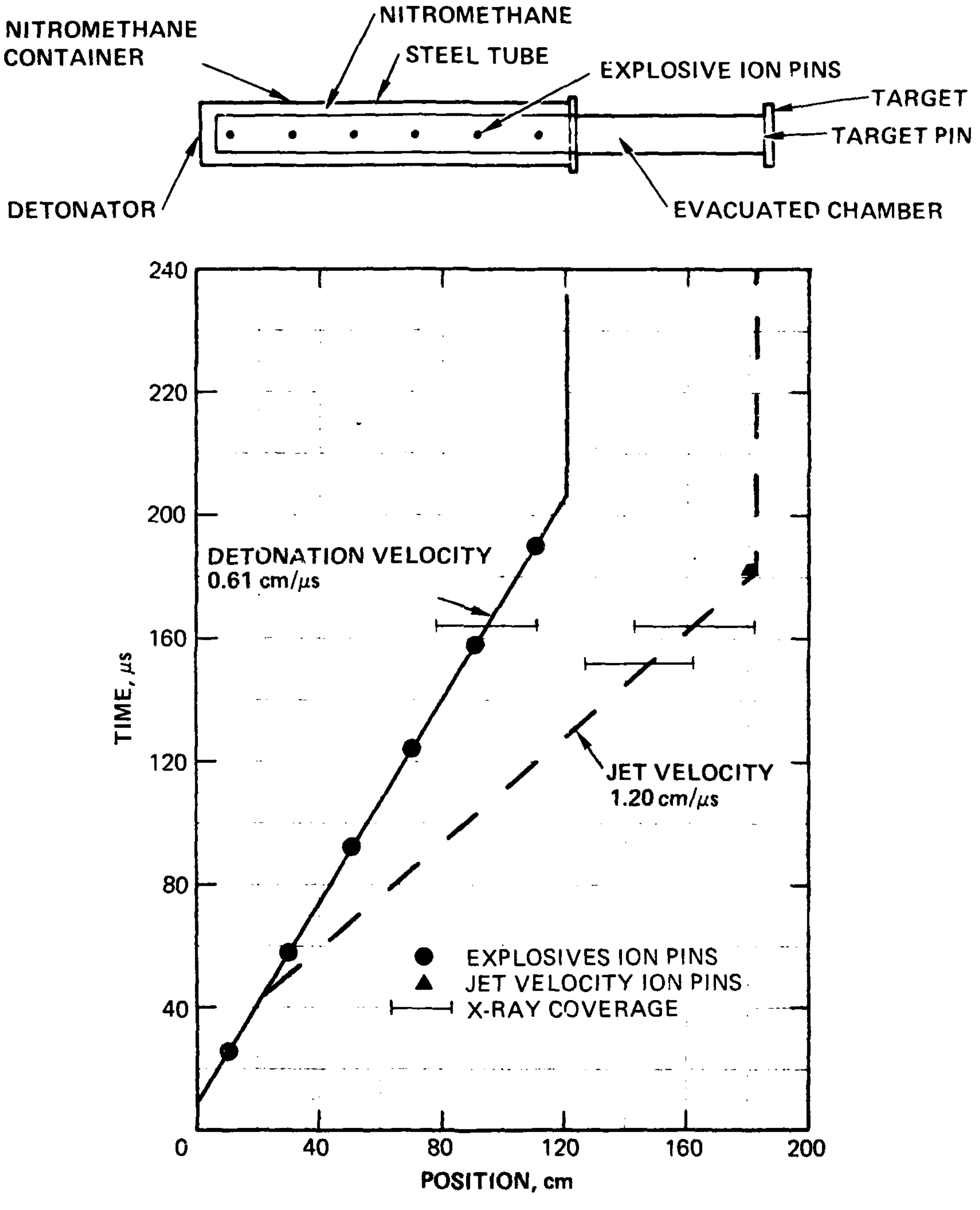

Figure 9 Results from explosive driver test APC-1.

A4098

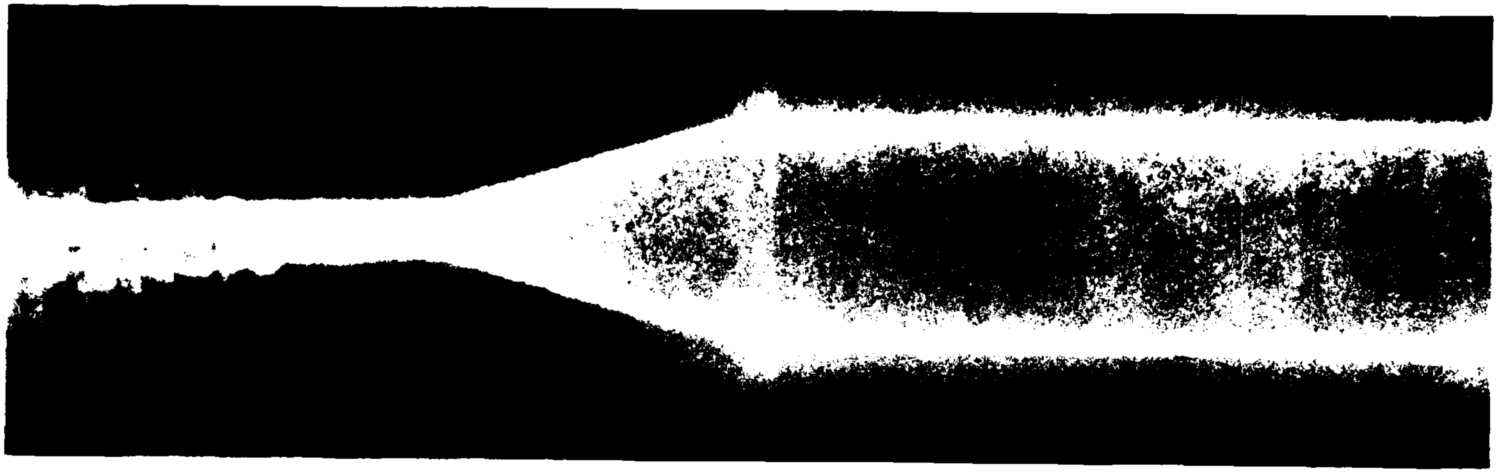

Figure 10   Radiograph of collapsing steel tube in test APC-1.

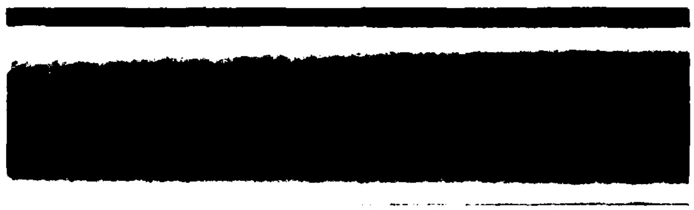

(a) t = 153 μs   163 cm $\geqslant$ x $\geqslant$ 127 cm

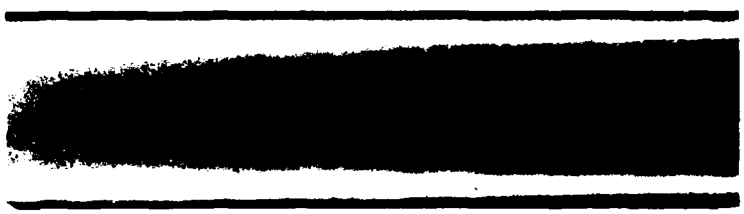

(b) t = 165 μs   180 cm $\geqslant$ x $\geqslant$ 143 cm

Figure 11   Radiographs of PMMA extension tube downstream of jetting explosive driver in test APC-1.

A4103

Figure 12 Aluminum target from test APC-1.

A4108

the assumption that a continuous jet is formed instantaneously on the axis of the driver tube 13 μs after the passage of the detonation wave, which is the time required for the inner surface of the tube to reach the axis. The prediction also assumes that the jet has a velocity twice that of the detonation velocity of the explosive (dashed line in Figure 9). Figure 10 is a radiograph of the explosively collapsing tube. The collapse angle of 16.5 degrees was in very good agreement with the desired value of 17 degrees. Based on the jet predictions and the time of arrival at the target surface, the leading edge of a jet was expected in the center of the radiographs taken at 152 μs and 164 μs. These radiographs, given in Figure 11, showed no visible evidence of jetting. However, there was extensive damage to the 2.54 cm (1 inch) aluminum target as shown by the photographs in Figure 12. The target had been completely penetrated and had a hole diameter approximately equal to the internal diameter of the PMMA tube. On the basis of such conflicting evidence of jetting, it was postulated that either the jet was diffuse (gaseous or liquid droplets) and beyond radiographic resolution, or the target damage was a late-time phenomenon caused by low velocity debris, jets, or slugs from the termination of the driver explosive. The latter possibility was investigated in the second experiment, APC-2.

The radiography coverage for APC-2 was relocated to examine the collapse process near the end of the explosive and to record any slow moving fragments or jets that might account for the target damage in the previous experiment. X-ray location and timing were selected to record velocities as low as 0.4 cm/μs. Figures 13 through 16 indicate that the experimental results of

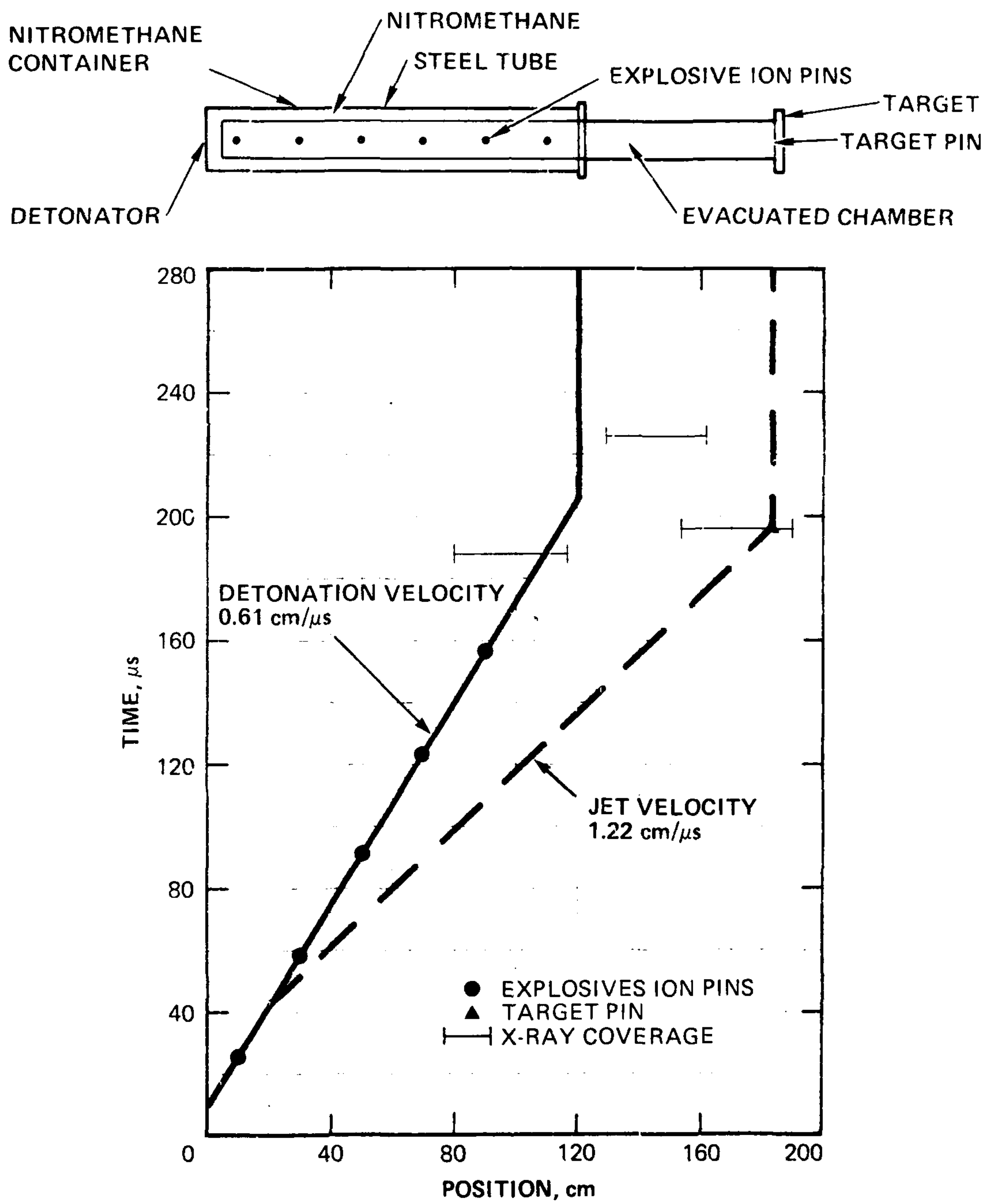

Figure 13 Results from explosive driver test APC-2.

Figure 14   Radiograph of collapsing steel tube in test APC-2.

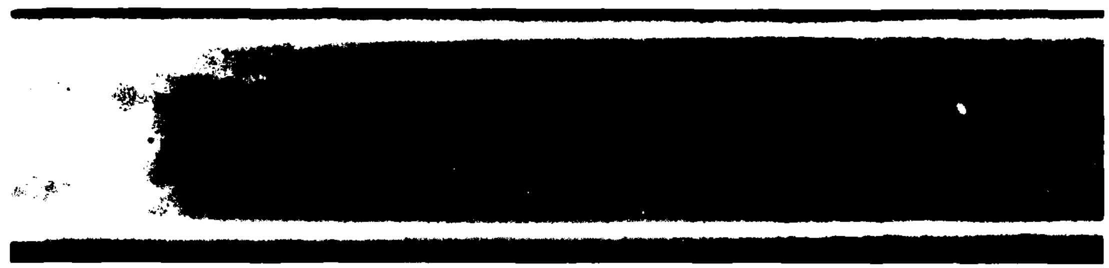

(a) $t = 197\ \mu s$ $162\ cm \geq x \geq 128\ cm$

(b) $t = 235\ \mu s$ $183\ cm \geq x \geq 153\ cm$

Figure 15 Radiographs of PMMA extension tube downstream of jetting explosive driver in test APC-2.

Figure 16 Aluminum target from test APC-2.

A4110

APC-2 were quite comparable to those of APC-1. The x-t plot, given in Figure 13, shows a detonation velocity of 0.61 cm/μs. A radiograph made near the end of the explosive, Figure 14, appeared normal and showed a collapse angle of 16 degrees. Still, there was no evidence of jetting, early or late, in the radiographs taken at 197 μs and 224 μs, and presented in Figure 15. However, once again the target was completely penetrated (Figure 16).

<u>Test APC-3 (Symmetrical--Additional Instrumentation)</u>. Even though jets were not resolvable in the radiographs of the two initial driver tests, the target damage and target arrival times were consistent with a very high velocity, but diffuse, plasma jet. Additional diagnostic techniques were added to this experiment to obtain a better understanding of the jet characteristics. Several dimensional changes were made in the experimental configuration to accommodate these techniques and to assist in the interpretation of results.

The length of the PMMA tubing between the explosive driver and the aluminum target was increased from 60.96 cm (24 inches) to 121.92 cm (48 inches) in order to record the entire jet (tip-to-tail) on two adjacent X-ray cassettes. In addition, the wall thickness of this tubing was decreased from 0.635 cm (1/4 inch) to 0.317 cm (1/8 inch) to reduce the X-ray attenuation and thereby increase the resolution of the jetting material on the X-ray film. A steel step wedge, with 0.0025 cm (0.001 inch) steps, was mounted on the outside of the tube to provide a density resolution standard on the X-ray film. Five ionization pins were added to the PMMA tubing to measure the velocity of the leading edge of the plasma jet. Finally, the thickness of the aluminum target was increased from 2.54 cm (1 inch) to 10.15 cm (4 inches) so that the depth, diameter, and volume of jet penetration in aluminum could be determined.

The results from this experiment are presented in Figures 17 to 20. The trajectories presented in Figure 17 show a detonation velocity of 0.61 cm/μs and an average jet velocity of 1.21 cm/μs. However, it should be noted that the actual differences in the time of arrival for adjacent ionization pins indicate jet velocities ranging between 1.06 and 1.33 cm/μs. This difference could either indicate that the diffuse jet is nonplanar (i.e., tilted or oscillating during transit) or that the ionization environment causes a nonreproducible response from the pins used. A collapse angle of 17 degrees was obtained from examination of the collapse radiograph given in Figure 18. Jets were not evident in the radiographs taken at 174 μs and 211 μs. While the energy density of the jet was sufficient to deform and ablate the ionization pins as shown in Figure 19, the jet could not be resolved with high contrast printing, image enhancement, or densitometry. Still, the target damage was extensive. Figure 20 shows that the plasma jet had not only penetrated the full 10.16 cm (4 inch) aluminum target but also caused the target to fracture longitudinally into six different segments.

On the basis of the radiographic data, it would appear that the jet is either a gas, or it is composed of individual droplets or particles that are smaller than the 0.0025 cm (0.001 inch) steps in the steel step wedge. However, one would expect to see a well defined gradient near the leading edge of the jet if it

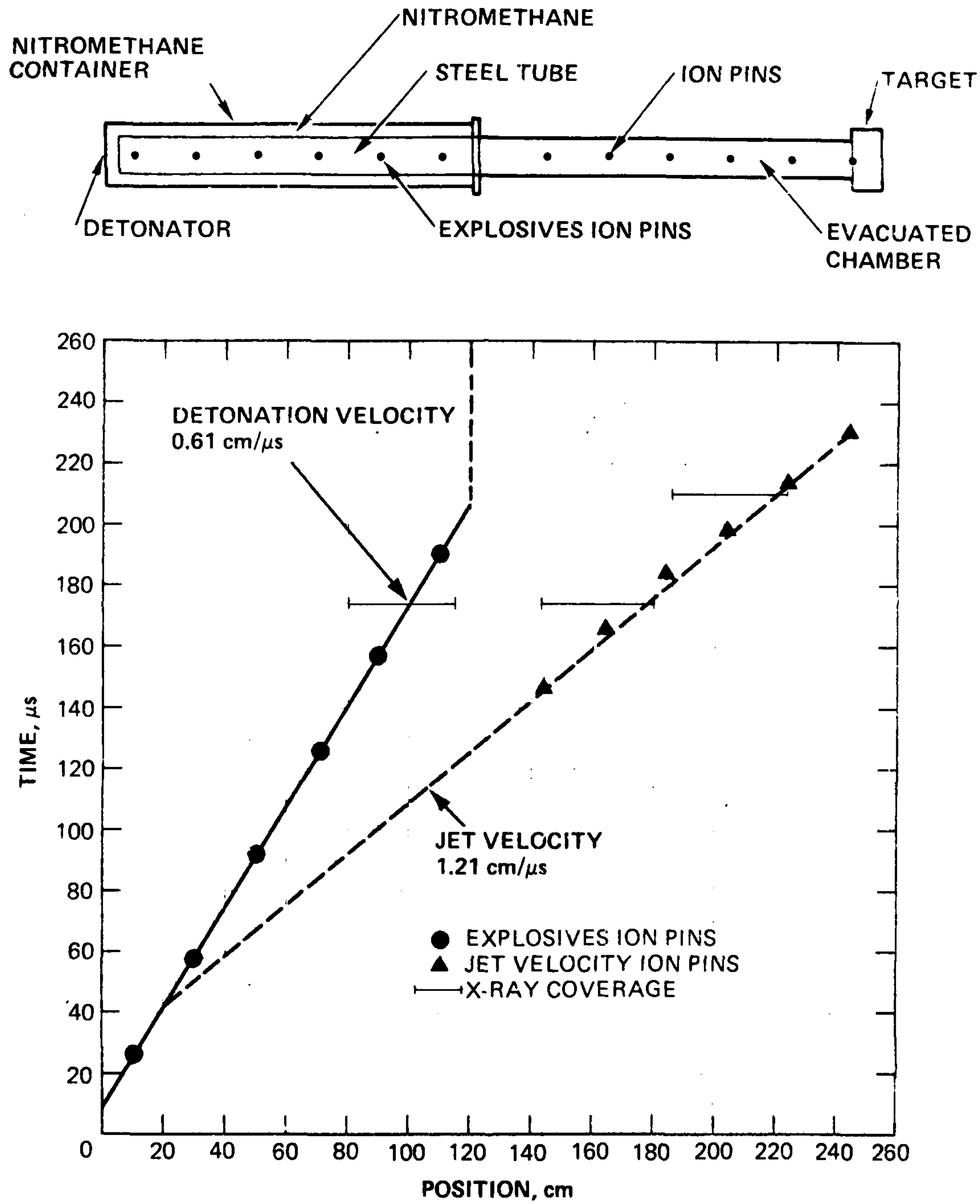

Figure 17 Results from explosive driver test APC-3 (helical lead ribbon).

Figure 18 Radiograph of collapsing steel tube in test APC-3.

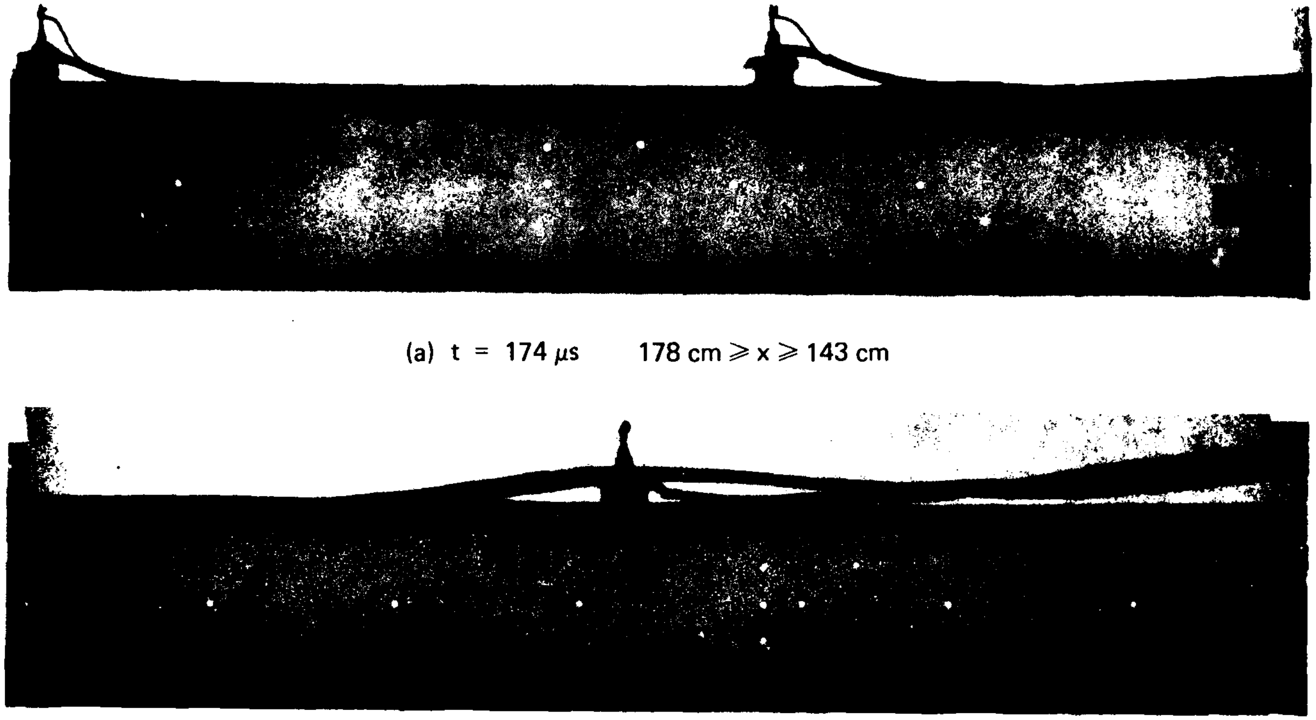

(a) $t = 174\ \mu s \qquad 178\ cm \geq x \geq 143\ cm$

(b) $t = 211\ \mu s \qquad 224\ cm \geq x \geq 187\ cm$

Figure 19 Radiographs of PMMA extension tube downstream from jetting explosive driver in test APC-3.

Figure 20 Aluminum target from test APC-3.

A4107

were a gas. On the other hand, the resolution of the X-ray system would be insufficient to observe individual droplets or particles. For example, the image of a 0.0025 diameter particle moving at a velocity of 1.2 cm/μs would be smeared over 0.048 cm (19.2 diameters) during the 40 ns duration of the X-rays. Therefore it is reasonable to conclude that the jet is a cloud of individual droplets or particles.

Even though a well-defined jet was not visible in the radiographs, the steel step wedges used in this experiment provide a representative value for the average density of the diffuse jet. The very resolvable 0.0025 cm (0.001 inch) step in a steel step wedge with a density of 7.84 gm/cc would be the equivalent to a jet density of 0.0039 gm/cc if the jet mass were uniformly distributed in the 5.08-cm- (2-inch-) i.d. PMMA tube. This value is in reasonable agreement with a density of 0.0065 gm/cc that would be obtained by filling the entire volume inside the PMMA tube with the jet mass as determined from the classical jetting theory described in the previous section. The mass of the driver tube per unit length for this experiment was 8.7 gm/cm. Assuming that the jet is generated by 90 cm of the driver tube (distance from the point where the jet trajectory intercepts the detonation trajectory to the end of the explosive section), the jet mass would be 16.1 grams for a collapse angle of 16.5 degrees. If this mass were distributed uniformly throughout the 122 cm (48 inch) length of 5.08-cm- (2-inch-) i.d. tubing, the jet density would be 0.0065 gm/cc. It is also of interest to note that the kinetic energy of a 16.1 gram jet traveling at 1.21 cm/μs would be 1.22 MJ.

Test APC-4 (Symmetrical Baseline). This test was performed to establish the reproducibility of the results obtained in the previous experiment and, if reproducible, to establish the baseline perfomance characteristics of a symmetrical collapse. The 10.16 cm (4 inch) aluminum target was placed in a thick-walled steel cylinder to prevent fracturing so that estimates of the jet energy could be obtained from the penetration profile in the target. Except for the instrumentation added to investigate the properties of the jet, the remaining configuration and test parameters for this experiment were the same as APC-3. The additional instrumentation included a high-speed framing camera positioned to view the jet in the PMMA tube between the explosive driver and the target. Also five small-diameter enameled copper wires were placed across the inside of the PMMA tube at 5 cm intervals. The objective was to determine the location and geometry of the jet flow by the deformation and ablation of these wires since they were visible in the radiographs.

The results of test APC-4 are presented in Figures 21 to 25. The x-t plot given in Figure 21 shows a detonation velocity of 0.60 cm/μs and an average jet velocity of 1.25 cm/μs. The jet velocity among the six individual ionization pins varied between 1.19 cm/μs and 1.44 cm/μs. Figure 22 is a radiograph of the tube collapse which gave a collapsed angle of 17 degrees. Even though the jet boundaries were still undefined in the radiographs shown in Figure 23, the deformation and ablation of the pins and breakwires indicate the jet flow was not planar. Figure 24 shows the jet completely penetrated the 10.16 cm (4 inch) aluminum

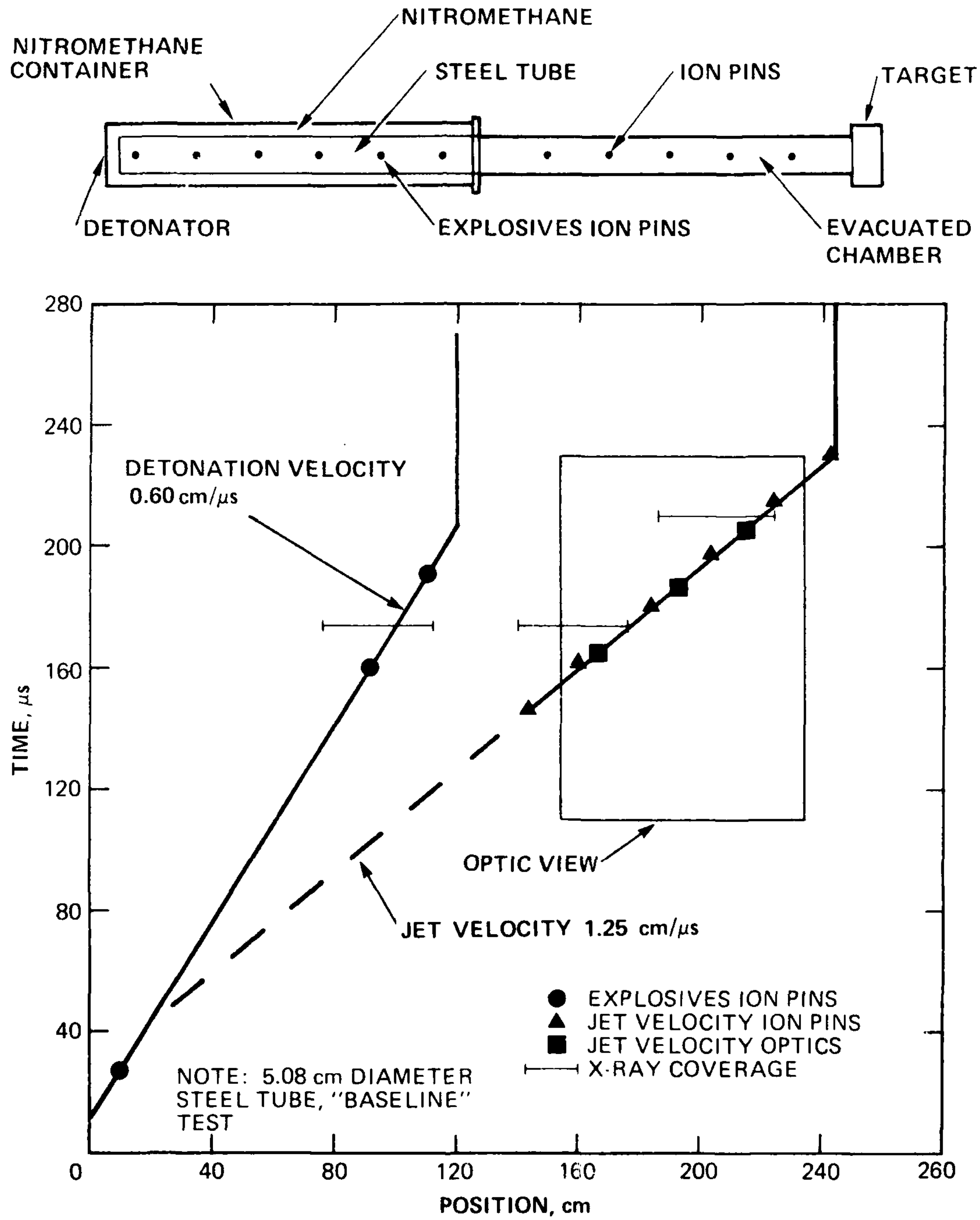

Figure 21 Results from explosive driver test APC-4 (baseline).

A4262

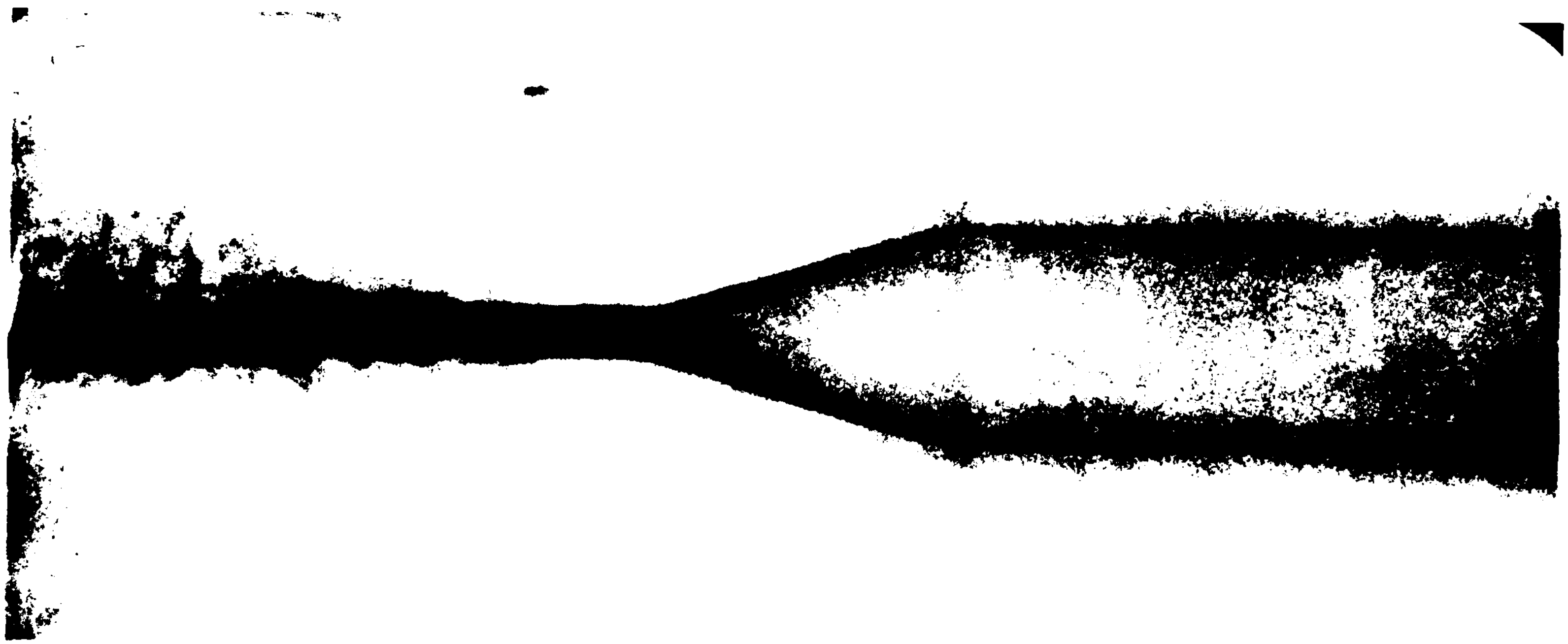

Figure 22 Radiograph of collapsing steel tube in test APC-4 (baseline).

A3709

(a) Position 140 to 178 cm, time - 174 μs

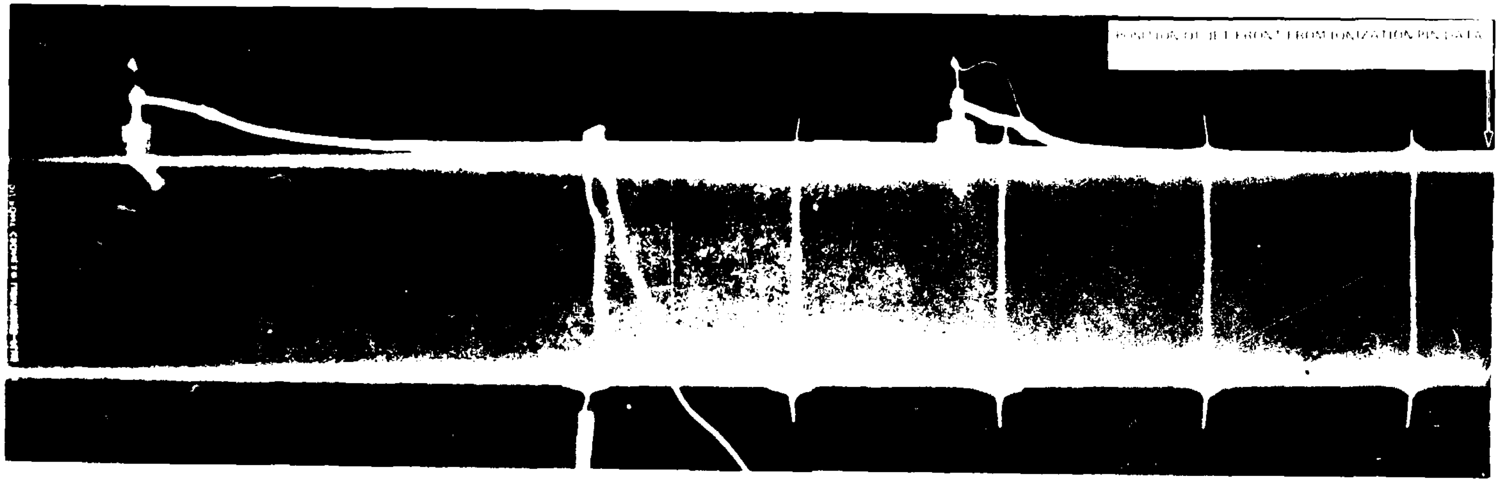

(b) Position 198 to 224 cm, time - 211 μs

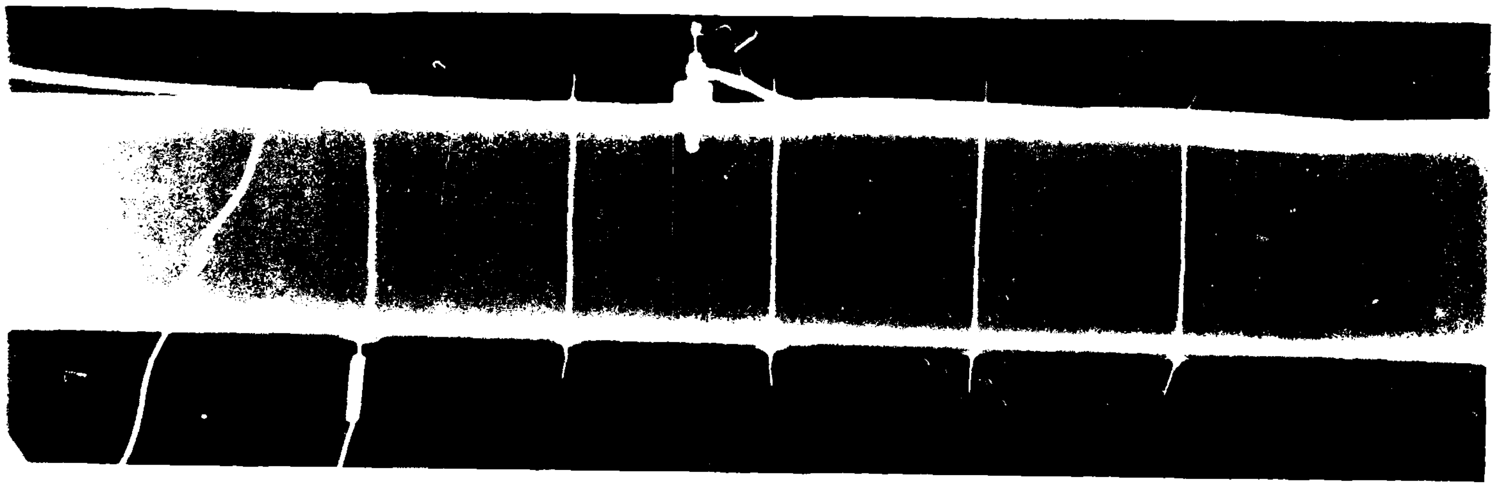

Figure 23 Radiographs of PMMA extension tube downstream of explosive driver in test APC-4 (baseline).

Figure 24 Aluminum target from test APC-4 (baseline).

A3710

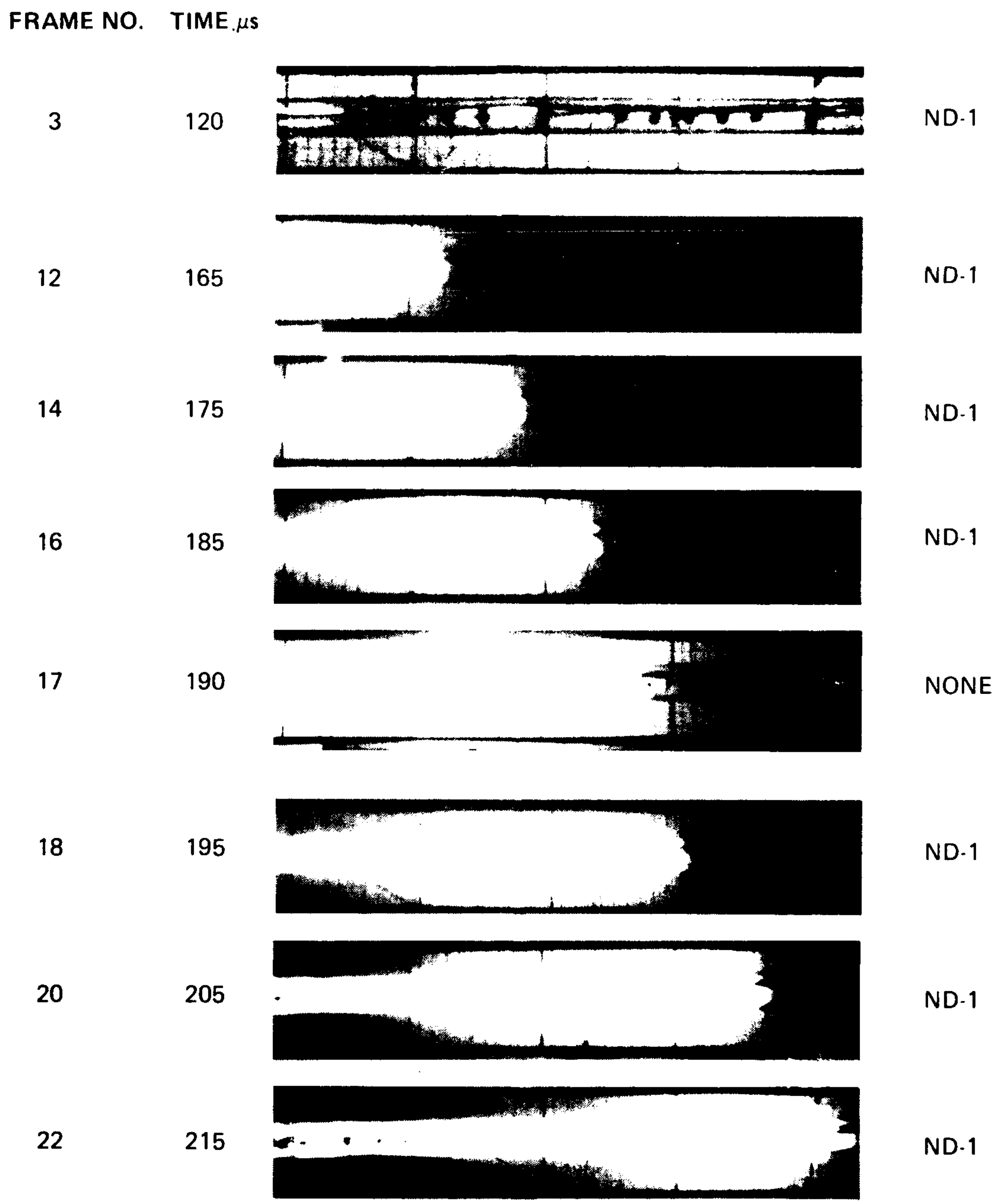

Figure 25 Selected frames from high speed photography of PMMA extension tube downstream of jetting explosive driver in test APC-4 (baseline).

A4106

target and that the steel sleeve indeed prevented residual target fracture. Selected frames from the photographic coverage of the jet are given in Figure 25.

Test APC-5 (Asymmetrical, Lead-Wrapped. This test was the first of the series designed and conducted to investigate the effect of an asymmetrical configuration. A lead ribbon was wrapped in a helical pattern around the outside of the steel driver tube. In principle, the added mass of the lead would cause a reduction in the radial velocity of the tube under the load. Calculations indicated that the addition of 0.081-cm- (0.032-inch-) thick lead would reduce the velocity from 0.18 cm/μs to 0.10 cm/μs. This difference would cause the lead-wrapped side of the tube to encounter the unwrapped opposite side at a position approximately 0.635 cm (1/4 inch) off the centerline of the tube. It was postulated that such an asymmetry would either eliminate any significant jetting or direct the jet to the walls of the tube instead of down the axis of the tube. A 2.54-cm- (1-inch-) wide ribbon was cut from 0.081-cm- (0.032-inch-) thick sheet lead and epoxied to the driver tube in a helical configuration having a 10.16 cm (4 inch) pitch (pitch angle of 32.67 degrees) as shown in Figure 26. This figure also shows the expected collapse conditions. Otherwise, the experiment was designed, fabricated, and instrumented in the same manner as the symmetrical baseline experiment, test APC-4.

The results of test APC-5 are presented in Figures 27 through 31. The trajectories of the plasma jet and detonation wave are shown in the x-t plot of Figure 27. The radiograph in Figure 28 shows the change in collapse conditions resulting from

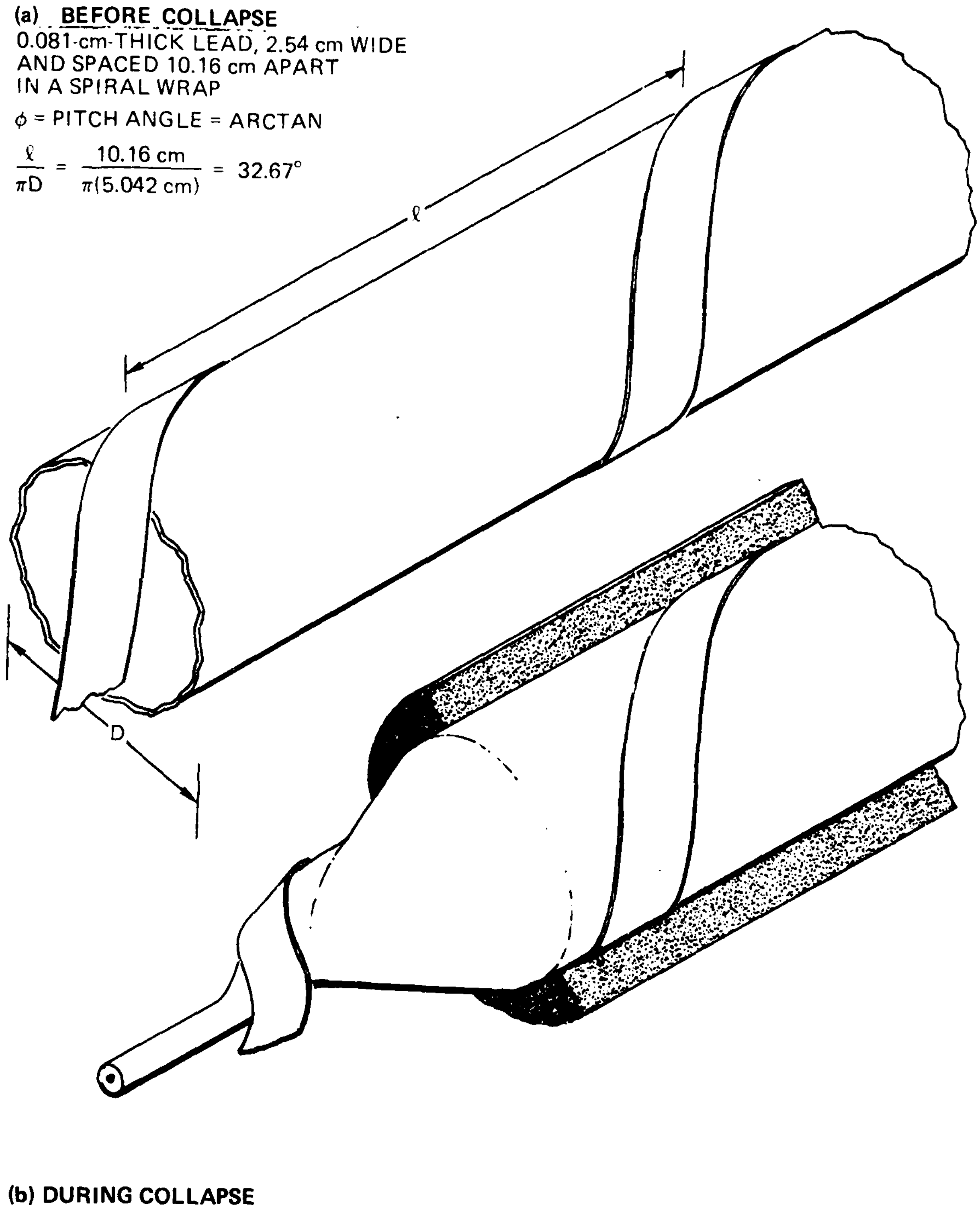

Figure 26 Configuration of explosive driver tube with helical lead ribbon used in test APC-5.

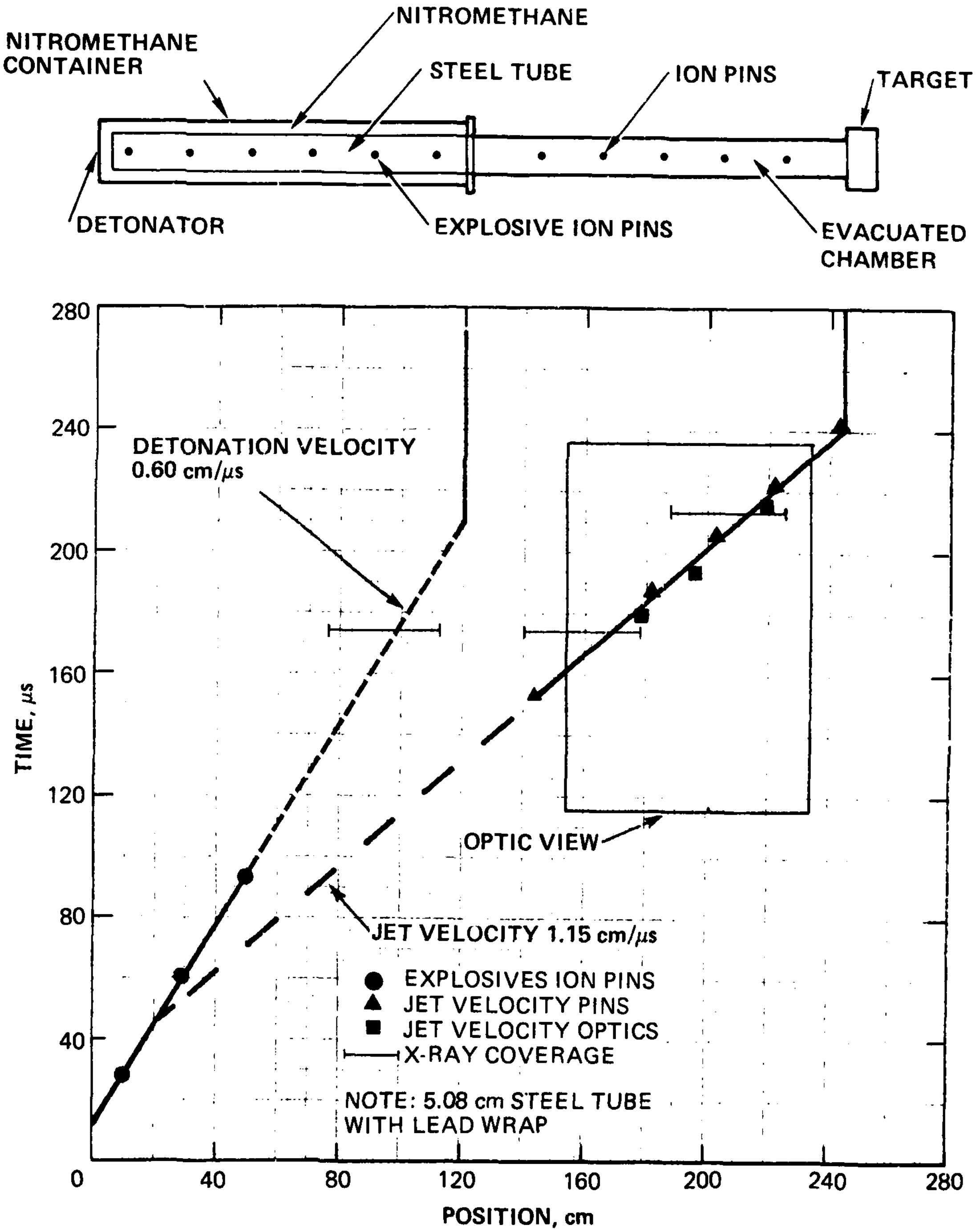

Figure 27 Results from explosive driver test APC-5.

A3765

Figure 28 Radiograph of collapsing steel tube wrapped with helical lead ribbon in test APC-5.

A3737

(a) Position - 140 to 178 cm. time - 174 μs

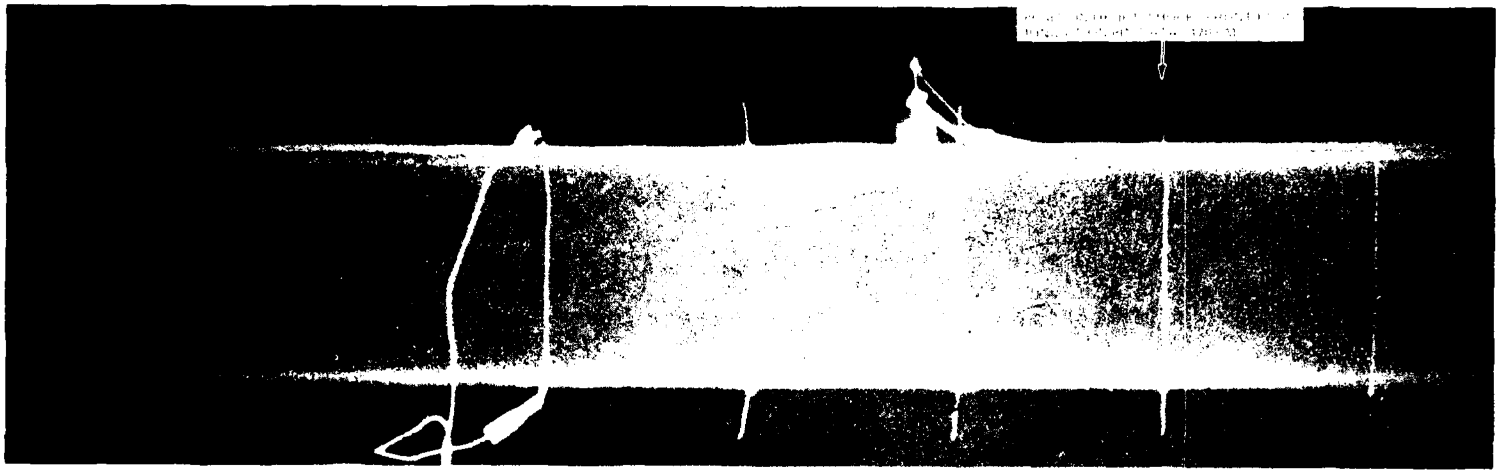

(b) Position - 189 to 225 cm, time - 212 μs

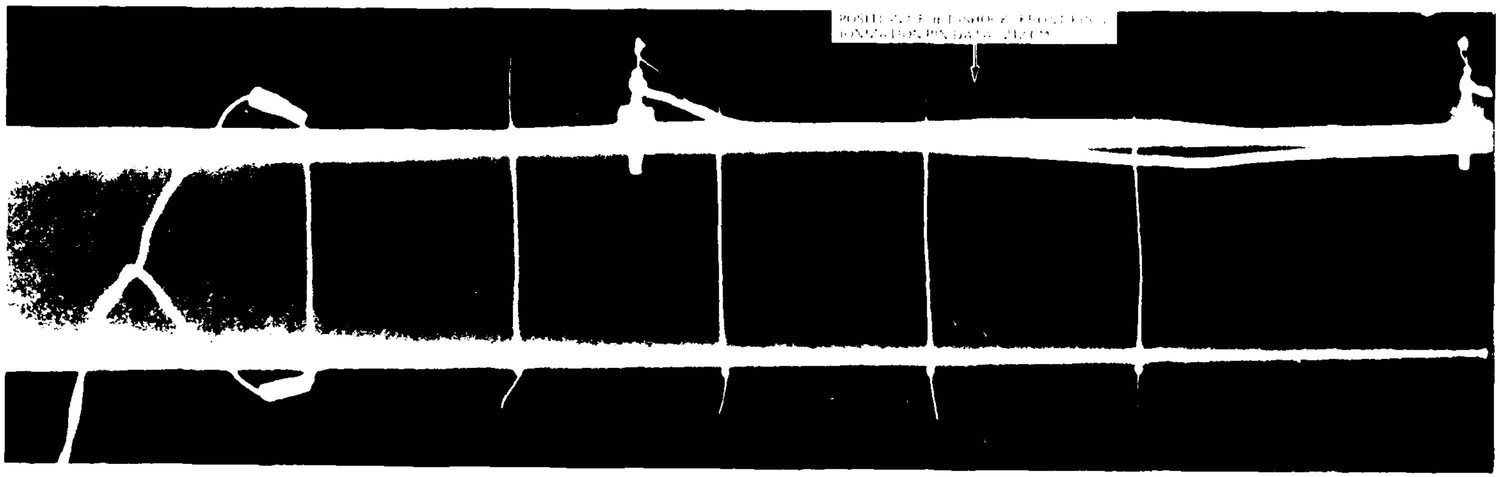

Figure 29 Radiographs of PMMA extension tube downstream of explosive driver with helical lead wrap in test APC-5.

Figure 30 Aluminum target from test APC-5.

A3823

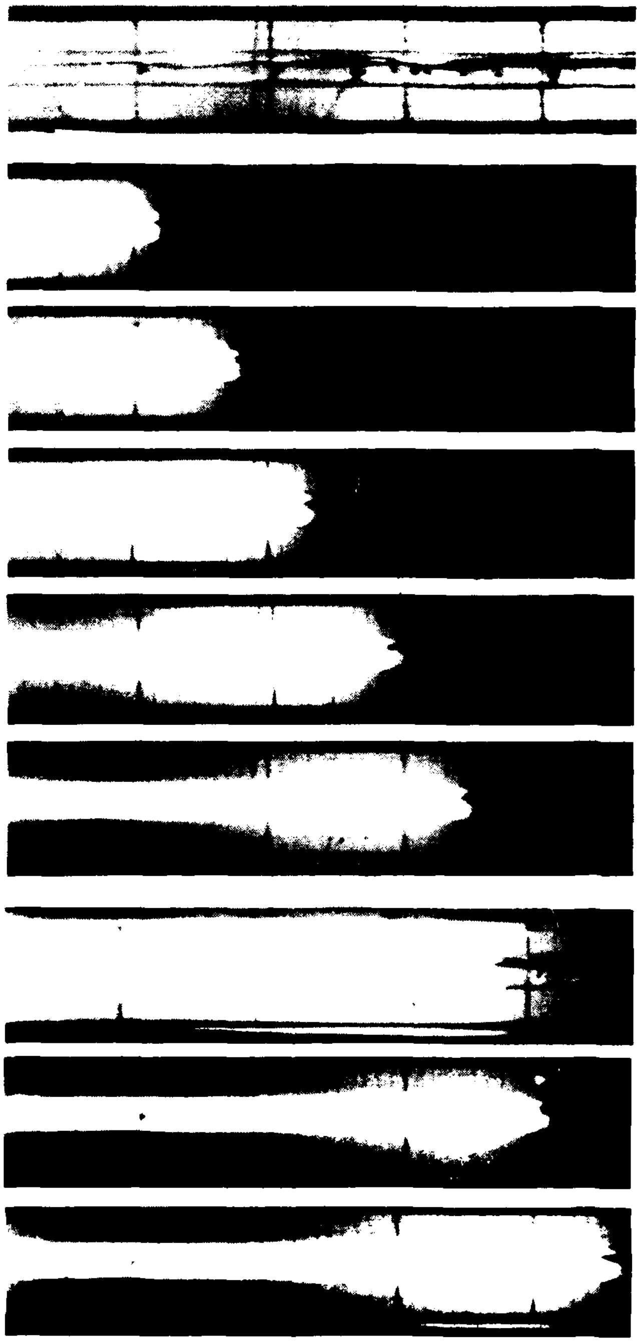

FRAME NO.	TIME, µs	
3	125	ND-1
12	170	ND-1
14	180	ND-1
16	190	ND-1
18	200	ND-1
20	210	ND-1
21	215	NONE
22	220	ND-1
24	230	ND-1

Figure 31 Selected frames from high speed photography of PMMA extension tube downstream of explosive driver in test APC-5 (helical lead ribbon).

A4105

the lead wrap. It also shows that the collapse angle for the unwrapped side of the tube was as expected, approximately 17 degrees. There was very little evidence of jetting in the radiographs in Figure 29, which show no significant deformation or ablation of the breakwires, though the first ionization pin was bent. Figure 30 is a photograph of the target which shows very small surface cratering instead of the full target penetration obtained from the baseline driver. Selected frames from the high-speed photography of the PMMA tube extension are given in Figure 31. This record confirmed that the leading edge of the plasma jet had a velocity of 1.15 cm/μs. Since the target showed considerably less damage than the baseline experiment (indicative of less momentum and energy in the jet), and the jet velocity was not reduced, the mass contained in the flow must have been significantly reduced.

Test APC-6 (Symmetrical--One Atmosphere Air). This experiment was conducted to investigate the effect of having 1 atm. of air in the explosive driver tube instead of the normal 1 mm Hg used in the previous jetting experiments. This parameter change was motivated by the possibility that an air-filled pipe could be used in an add-on experiment on a future underground nuclear test. The results from this experiment are given in Figures 32 through 35. The trajectories of test results in Figure 32 indicate a much lower jet velocity. The observed jet velocity of 0.85 cm/μs is considerably less than the 1.20 cm/μs for the baseline design (APC-4) and higher than would be expected for a nonjetting driver. In the latter case, the progressive collapse of the pipe behaves like a conical shaped piston moving at a constant velocity (detonation velocity) of 0.60 cm/μs into

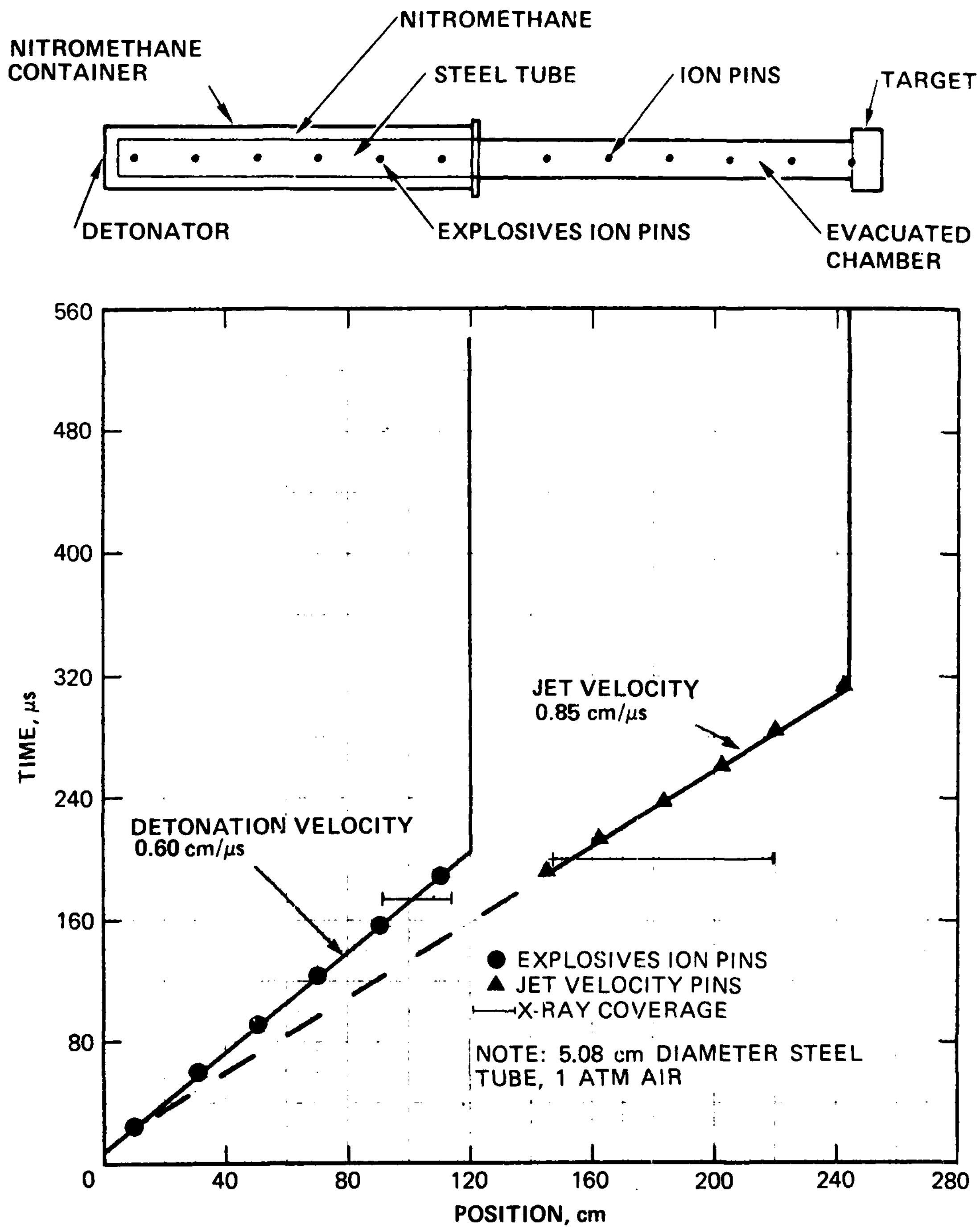

Figure 32 Results of explosive driver test APC-6 (one atmosphere air).

A3794

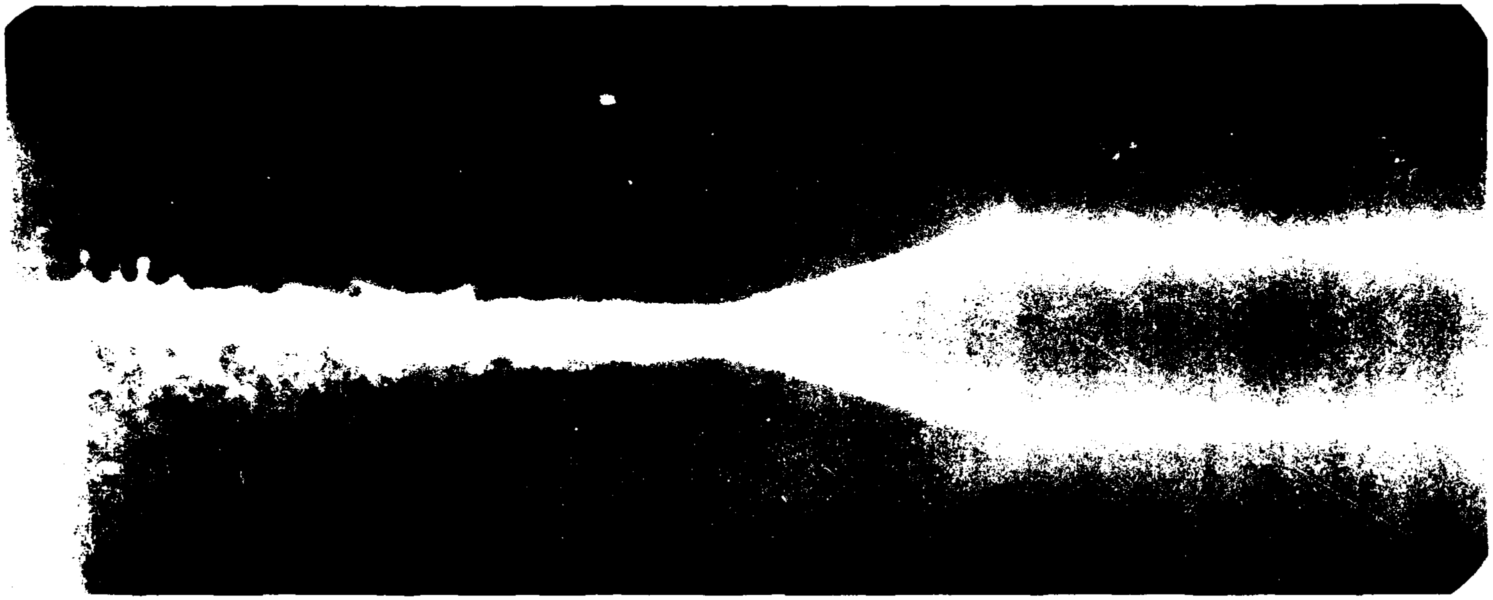

Figure 33 Radiograph of collapsing steel tube in test APC-6 (one atmosphere air).

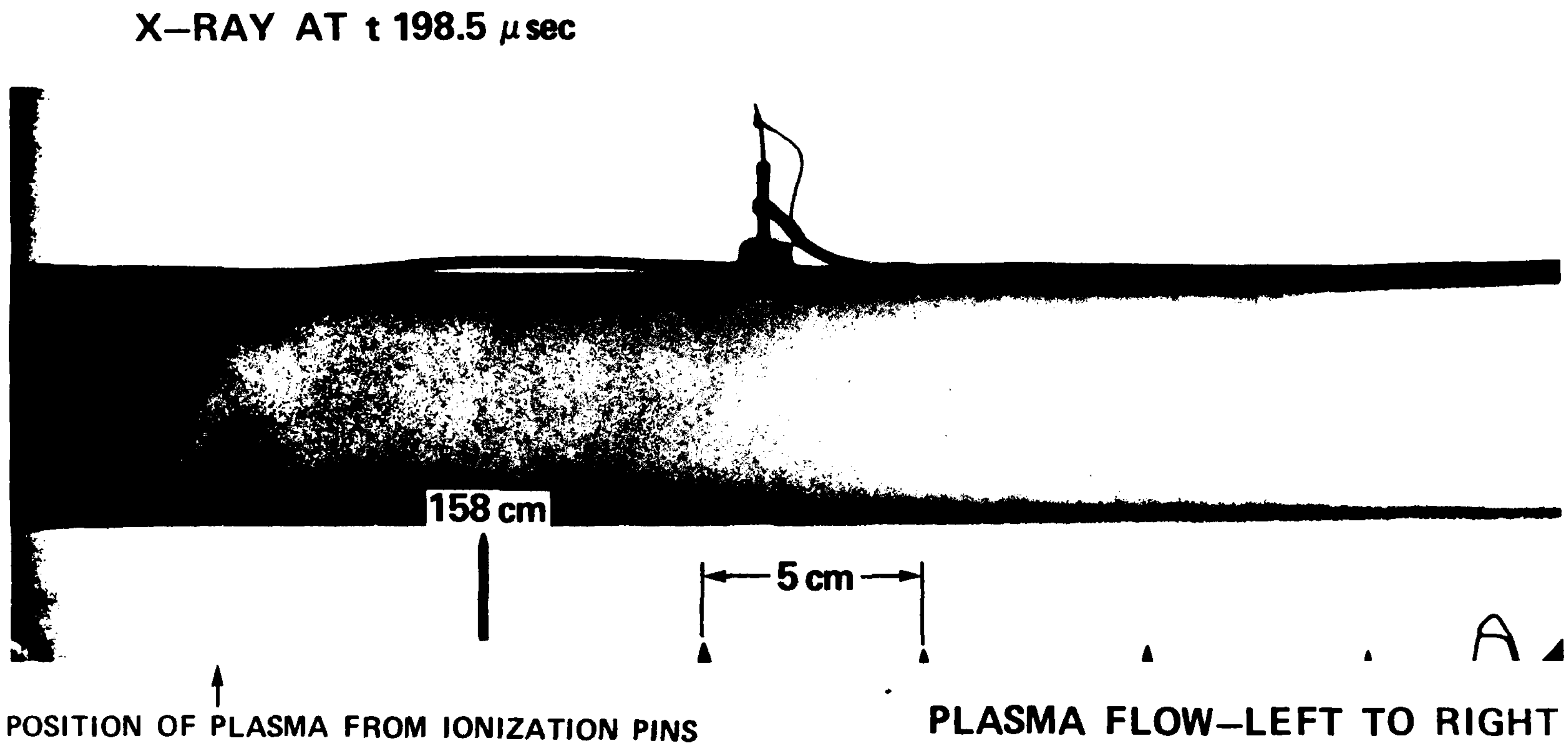

Figure 34 Radiograph of PMMA extension tube downstream of explosive driver in test APC-6 (one atmosphere air).

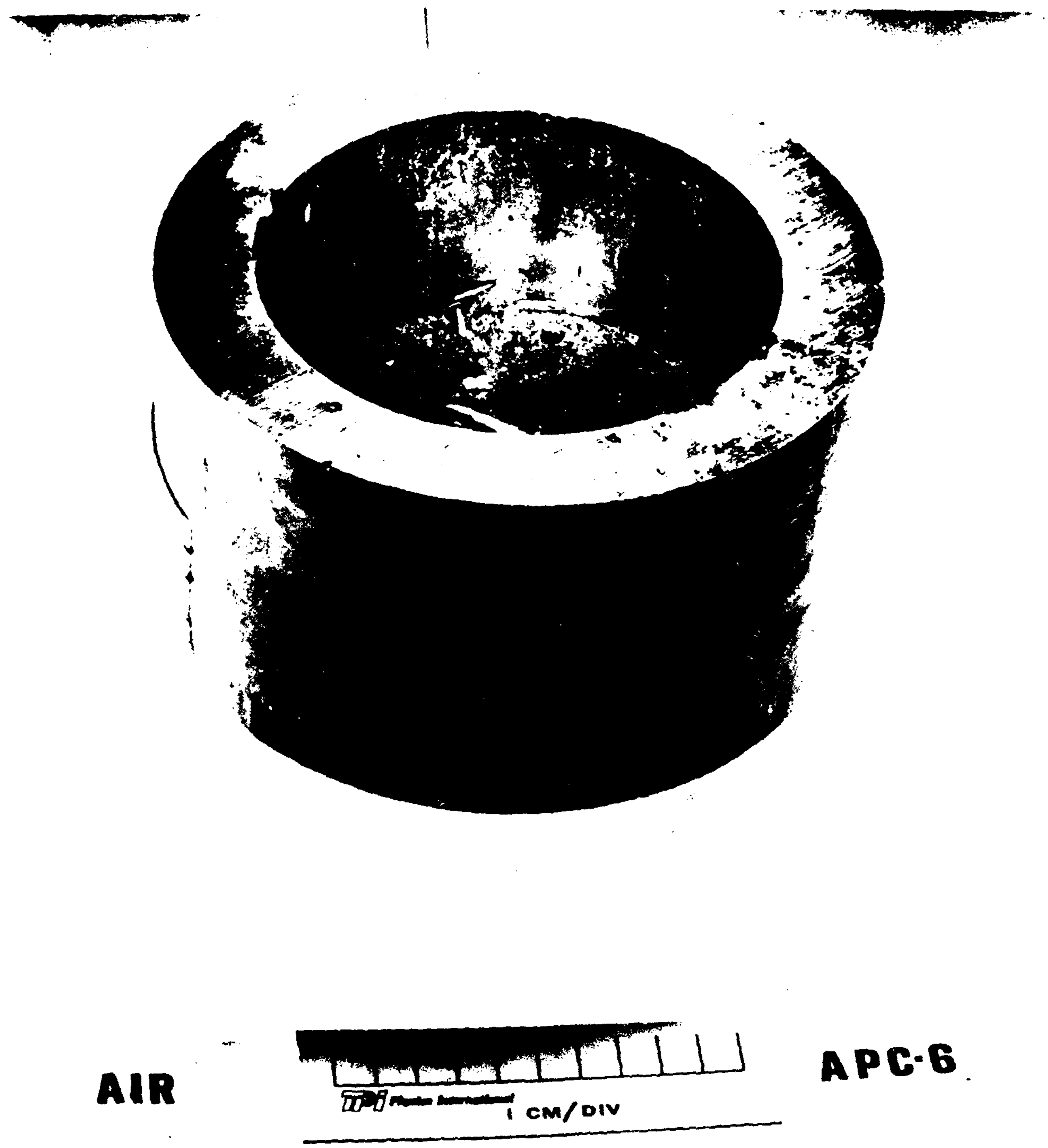

Figure 35 Aluminum target from test APC-6 (one atmosphere air).

A4263

the 1 atm. air environment. This motion generates a shock wave with a shock velocity of $(\gamma+1)/2$ times the detonation velocity, where γ is the ratio of specific heats for the air. Assuming $\gamma = 1.4$ for air (an upper limit), the shock velocity would be 0.72 cm/μs for a piston with a velocity of 0.60 cm/μs. The observed velocity of 0.85 cm/μs indicates some jetting did occur. Figure 33 shows a normal collapse angle (17 degrees), and there is no evidence of jetting indicated in the radiograph in Figure 34. Also, the photograph shown in Figure 35 shows no damage to the target. It was therefore concluded that 1 atm. of air in the driver inhibits the formation of jetting and considerably reduces the energy flow down the axis of an explosively collapsed tube.

<u>Test APC-7 (Asymmetrical--Foam Wrapped)</u>. In this experiment, a ribbon of foam was helically wrapped around the explosive driver tube to cause an asymmetrical collapse. The foam was used to displace some of the nitromethane around the tube and thereby reduce the radial collapse velocity beneath the tube. The reduced velocity would cause an off-axis collapse and eliminate or redirect the jet in the same manner as the experiment using lead wrapping, APC-5. Calculations indicated that a foam with a density of 0.025 gm/cc and a thickness of 0.762 cm (0.3 inch) would give a radial tube collapse velocity of 0.10 cm/μs, the same as calculated for APC-5. The foam ribbon was 2.54 cm (1 inch) wide and epoxied onto the steel driver tube with a 10.16 cm (4 inch) pitch (pitch angle of 32.67 degrees).

Figures 36 through 39 present the results of experiment APC-7. The x-t plot given in Figure 36 indicates a detonation

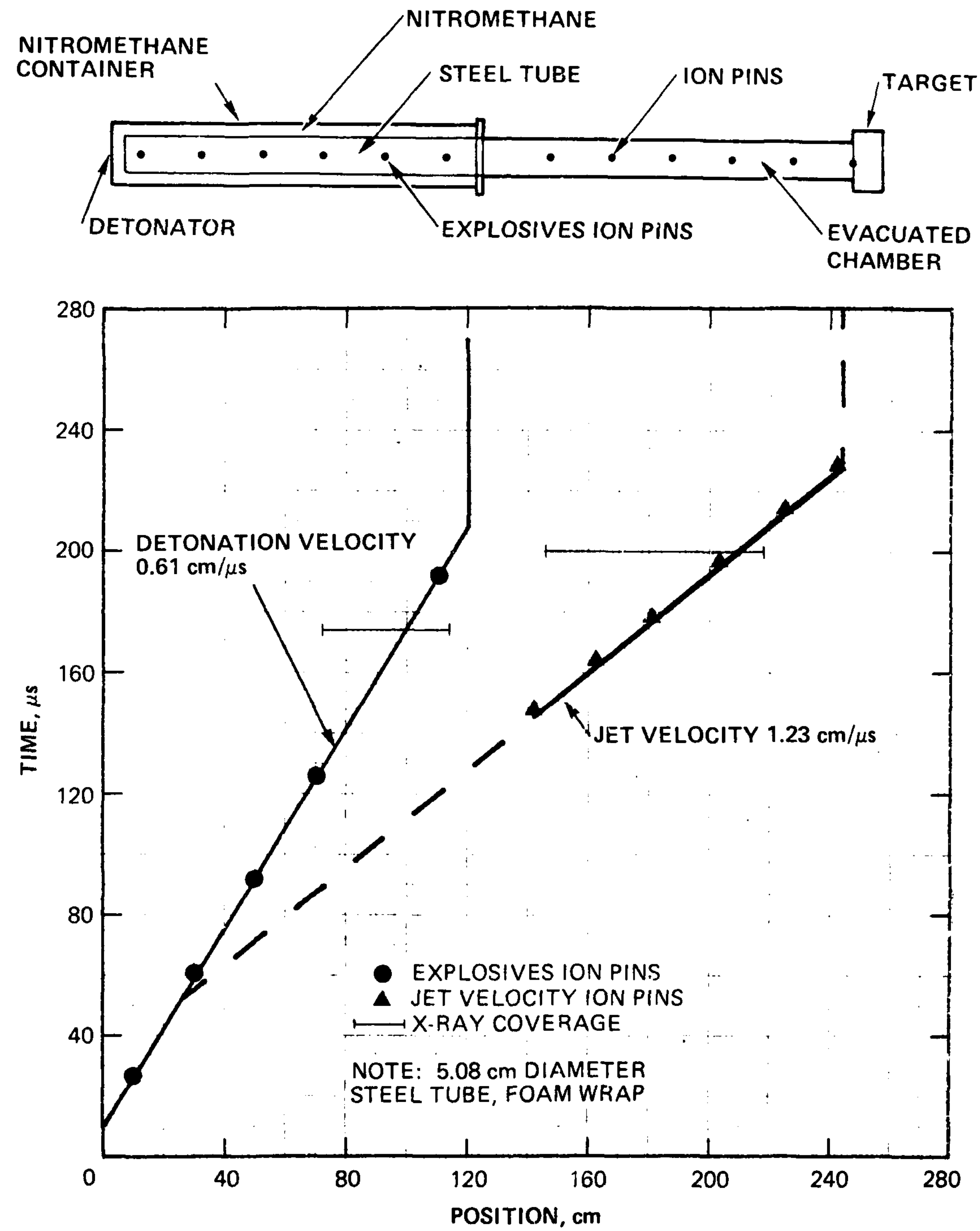

Figure 36 Results from explosive driver test APC-7 (helical foam ribbon).

Figure 37 Radiograph of collapsing steel tube wrapped with helical foam ribbon in test APC-7.

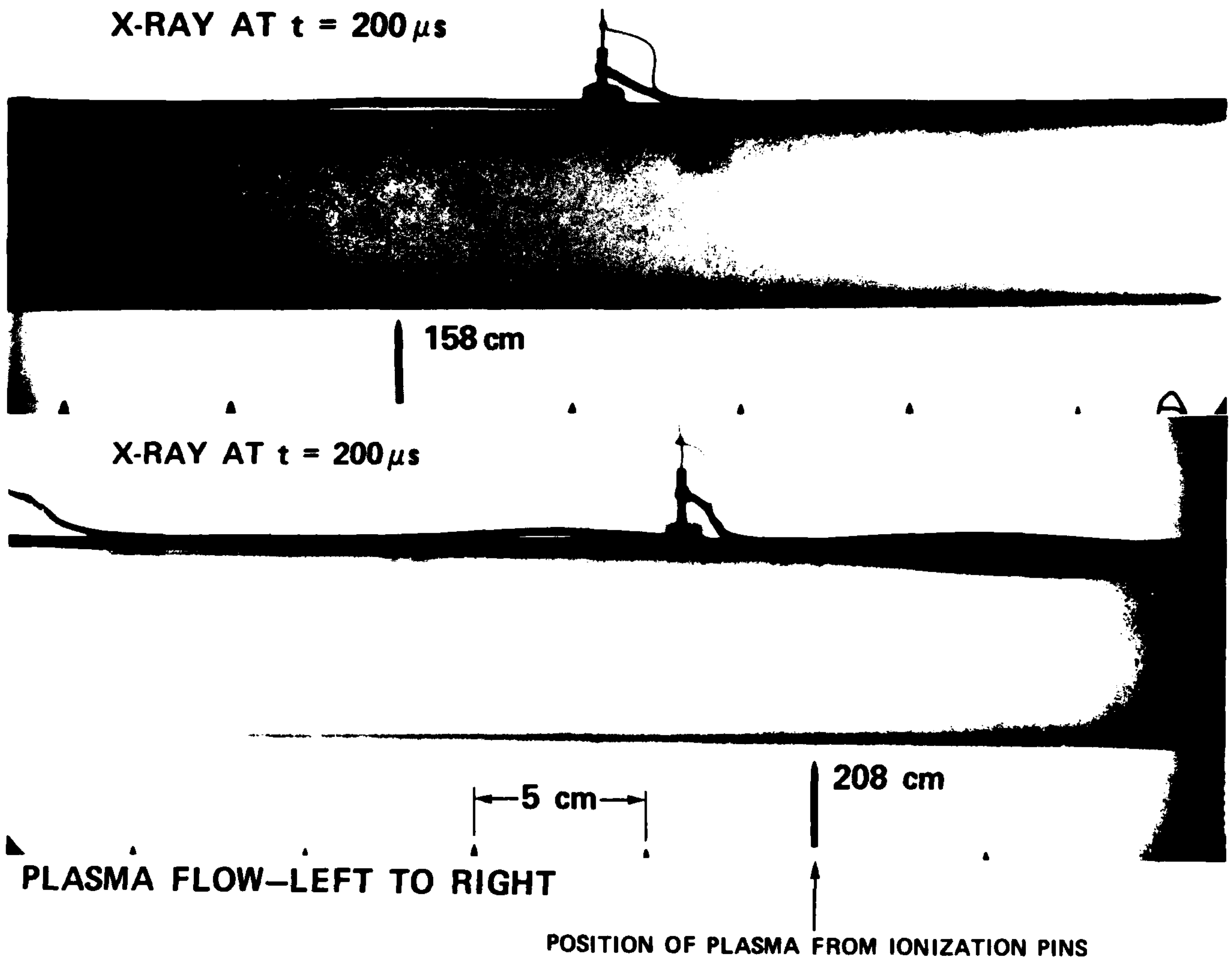

Figure 38 Radiographs in PMMA chamber downstream of explosive driver wrapped with helical foam ribbon in test APC-7.

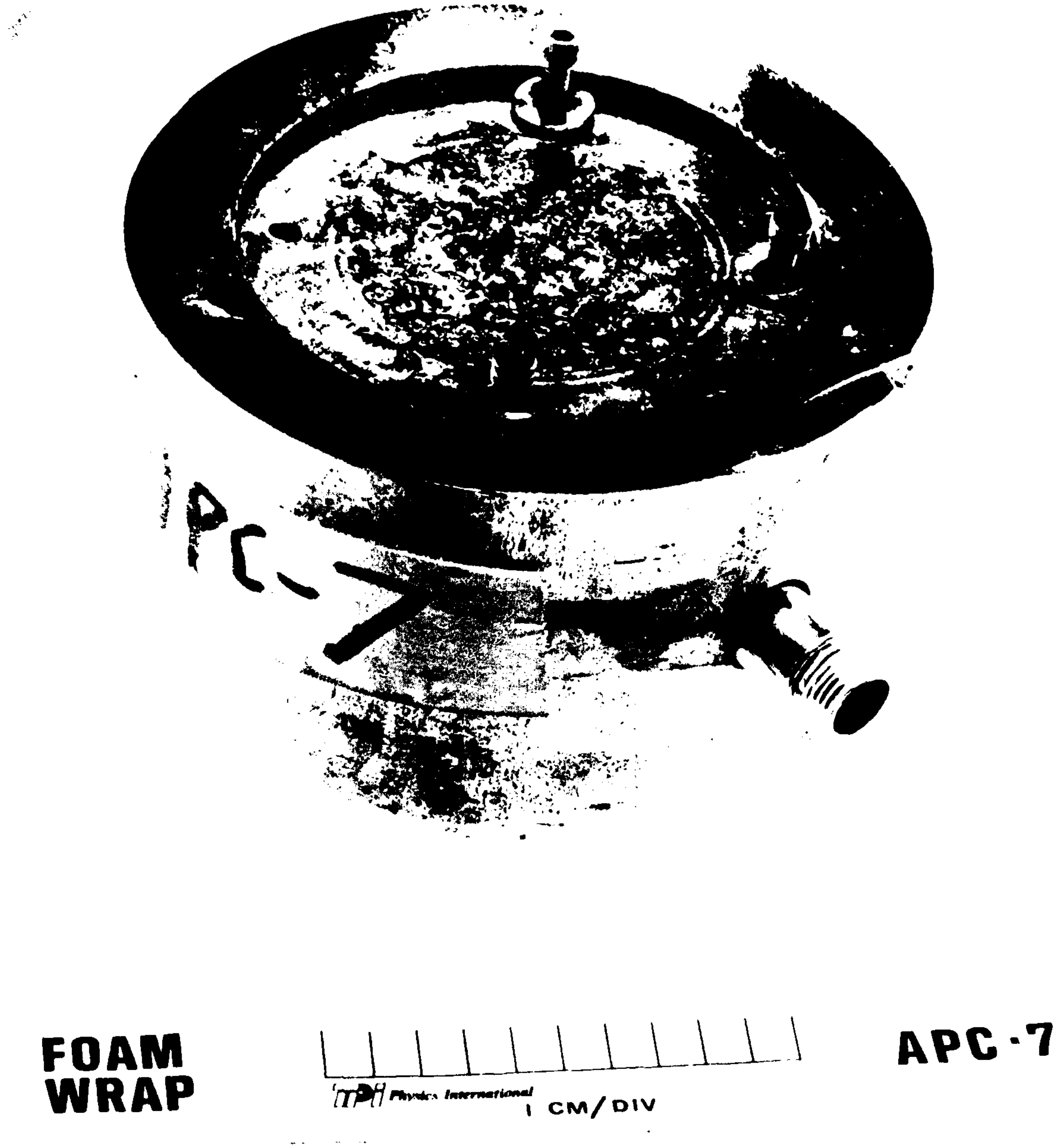

Figure 39 Aluminum target from test APC-7 (helical foam ribbon).

A4264

velocity of 0.61 cm/μs and a jet velocity of 1.23 cm/μs. The effect of the foam ribbon can be seen in the radiograph of Figure 37. The collapse angle on the side without foam appears to be approximately 17 degrees. There was no evidence of jetting in the radiographs of the extension tube given in Figure 38, even though images of the cloth tape used to secure the ionization pin cables were quite visible. The damage to the target was greater than that using lead wrapping but still quite insignificant as can be seen in Figure 39. Once again, asymmetries apparently reduced the mass contained in the jet of an explosively collapsed tube.

Test APC-8 (Asymmetrical--Square Driver). The third method of introducing asymmetries into the collapse of a tube was to change the cross-section of the explosive driver. Square steel tubing, with a cross-section of 5.08 cm (2 inches) by 5.08 cm (2 inches) and a wall thickness of 0.124 cm (0.049 inch) was selected for this experiment. The greater thickness was required to withstand a vacuum with the square cross-section. The nitromethane was contained in a square Lucite box which surrounded the square steel tube. The thickness of the nitromethane was 1.99 cm (0.785 inch), which gave an explosive mass-to-metal mass ratio of 2.3:1. This value was chosen to give the same collapse angle as had been used in the cylindrical drivers. The Lucite extension tube was also square and of the same internal dimensions as the driver.

The results of experiment APC-7 are presented in Figures 40 through 42. The x-t plot given in Figure 40 indicates a detonation velocity of 0.62 cm/μs and a jet velocity of

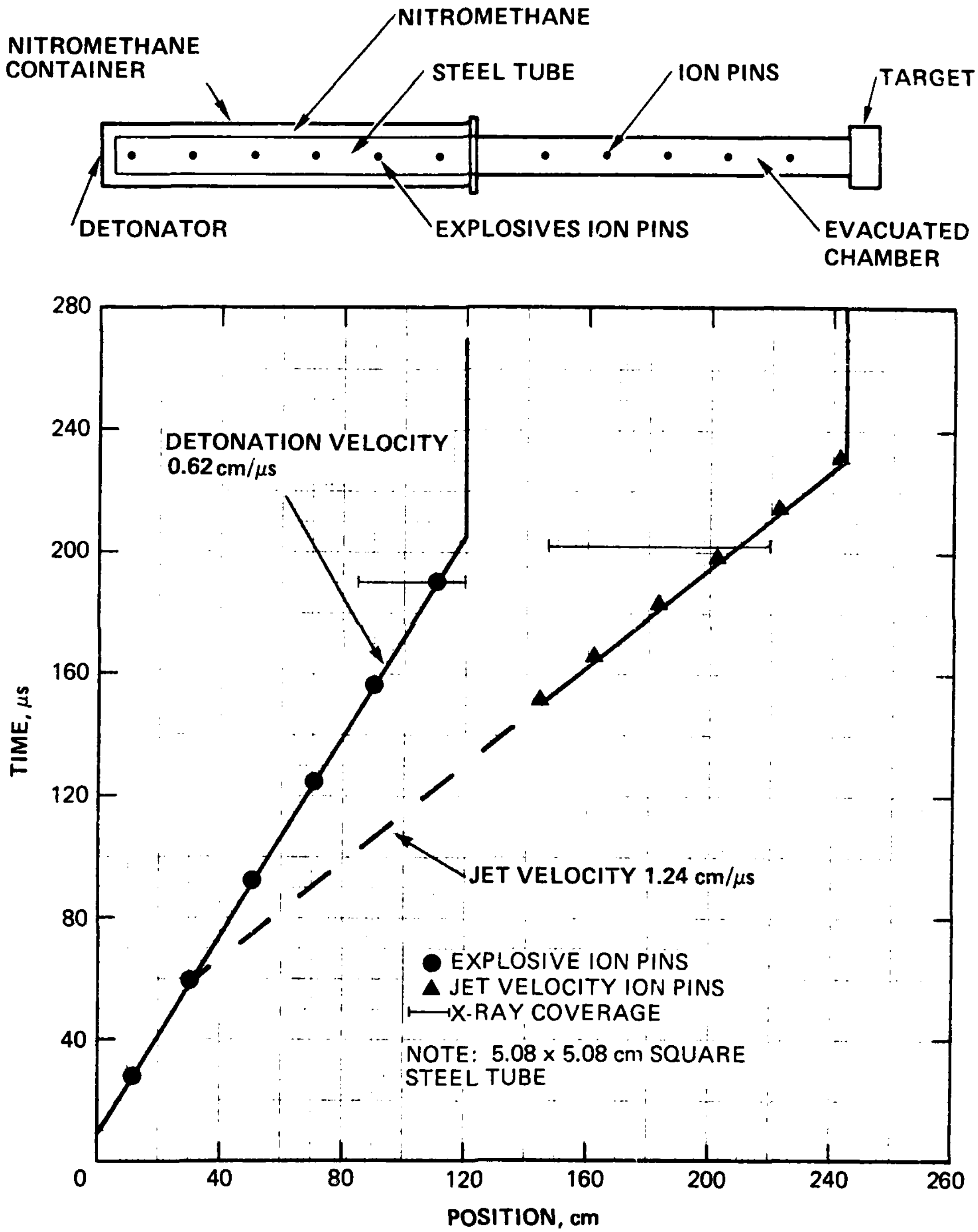

Figure 40 Results from explosive driver test APC-8 (square driver).

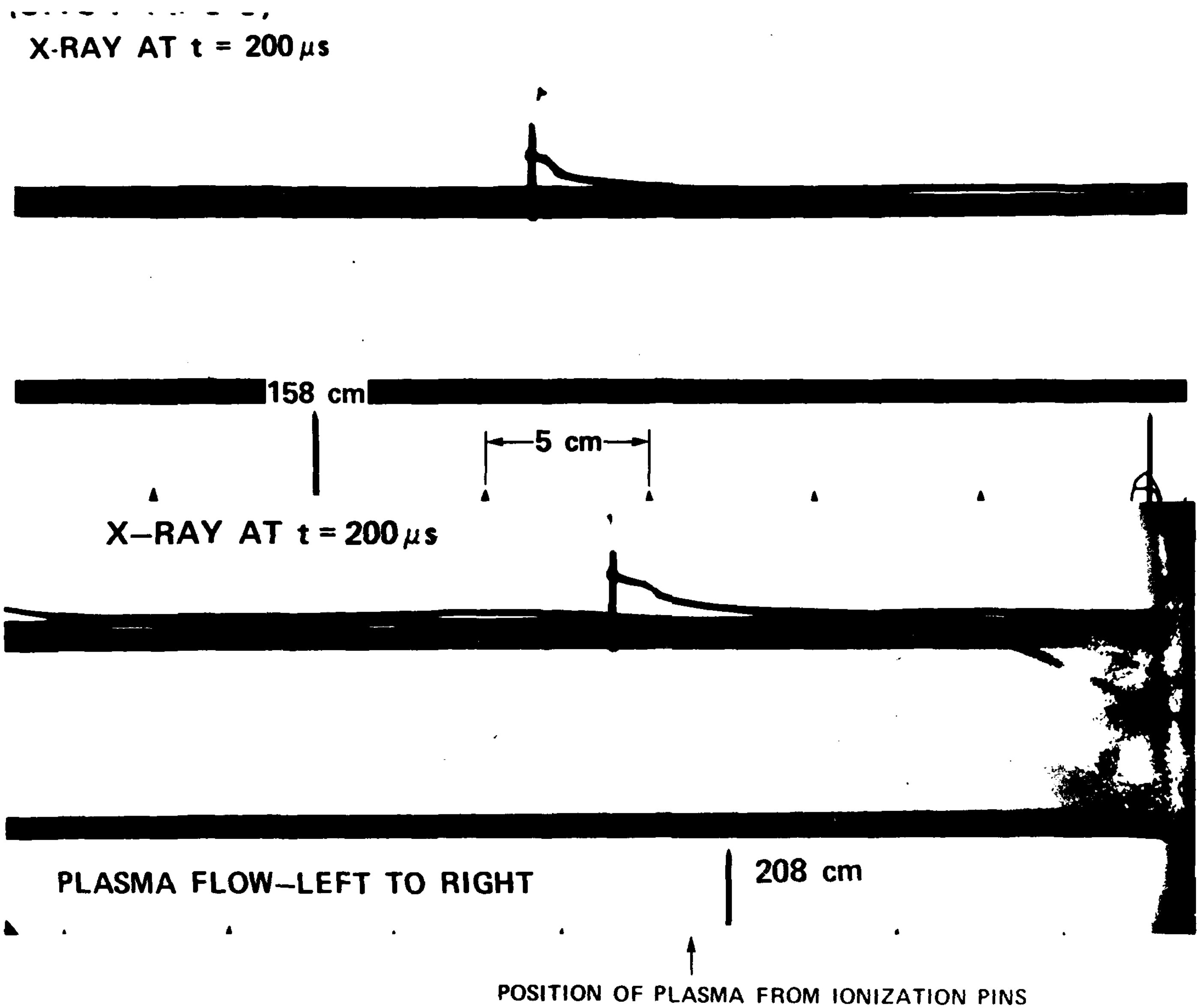

Figure 41 Radiographs of PMMA chamber downstream of explosive driver with square cross section in test APC-8.

Figure 42 Aluminum target from test APC-8 (square driver).

A4265

1.24 cm/μs. Radiographs of the collapse region were not obtained because the X-ray cassette was damaged by the blast and debris from the higher explosive weight required on this experiment. There was no evidence of jetting on the radiographs given in Figure 41. The white pattern on the left of one of the radiographs is pressure printing of the film due to the severe airblast environment. Figure 42 shows that the target damage was definitely less than that produced by the baseline driver, APC-4, but considerably more than that of the lead wrapped driver, APC-5.

Test APC-9. This experiment was conducted to determine if the jetting characteristics generated by the collapse of a stainless steel tube were the same as those generated by the previously used carbon steel tubes. The motive for obtaining results on stainless steel tubes is the requirement to use smaller diameter tubes in the spherical high explosive experiment described in the next section. Attempts to grind the outside surface of smaller diameter (1.27 to 2.54 cm [1/2 to 1 inch]) carbon steel tubing to the desired wall thickness had produced unacceptable variations in dimensions and uniformity. Such pre-existing variations could mask the effects of added asymmetries. Since stainless-steel tubing is commercially available in small diameters with a wider range of wall thicknesses and smaller tolerances, it became the preferable material to use for the drivers. This experiment was used to isolate any effects which might possibly be due to this material change before reducing tube dimensions. Except for the use of stainless steel tube in the explosive driver, there were no changes in the experimental configuration.

Figures 43 through 46 show that the results from this experiment were practically identical to those from the baseline experiment, APC-4. The tajectories of the detonation wave and plasma jet, given in Figure 43, indicate velocities of 0.61 cm μs and 1.22 cm/μs, respectively. Except for problems that arose in film processing, the radiograph showing the collapse (Figure 44) appeared quite normal. The collapse angle is 17 degrees. While clearly defined jets were not present in the radiographs of Figure 45, there were cloud-like images behind the front as measured by the ionization pins. The target damage shown in Figure 46 was quite similar to that produced by the baseline experiment.

Test APC-10 (Stainless Steel--1.905 cm [3/4 inch] Diameter). This experiment was expected to establish the baseline performance data for the tubes to be used in the spherical test described in Section 4. The diameter of the explosive driver tube was scaled down by a factor of approximately 2.65 to obtain a wall thickness of 0.028 cm (0.012 inch) and an outer diameter of 1.905 cm (3/4 inch). The length of the stainless steel tube and the PMMA extension tube were the same as in previous experiments. The PMAA tube used to contain the nitromethane had an outer diameter of 3.81 cm (1-1/2 inches) and a wall thickness of 0.476 cm (3/16 inch). The PMMA extension tube had the same dimensions as the nitromethane container, which created an internal area expansion between the driver and the extension tube of $(1.1225/0.726)^2 = 2.4$. This expansion was included as a possible means of determining whether the plasma jet was a gas or whether it consisted of a liquid droplet

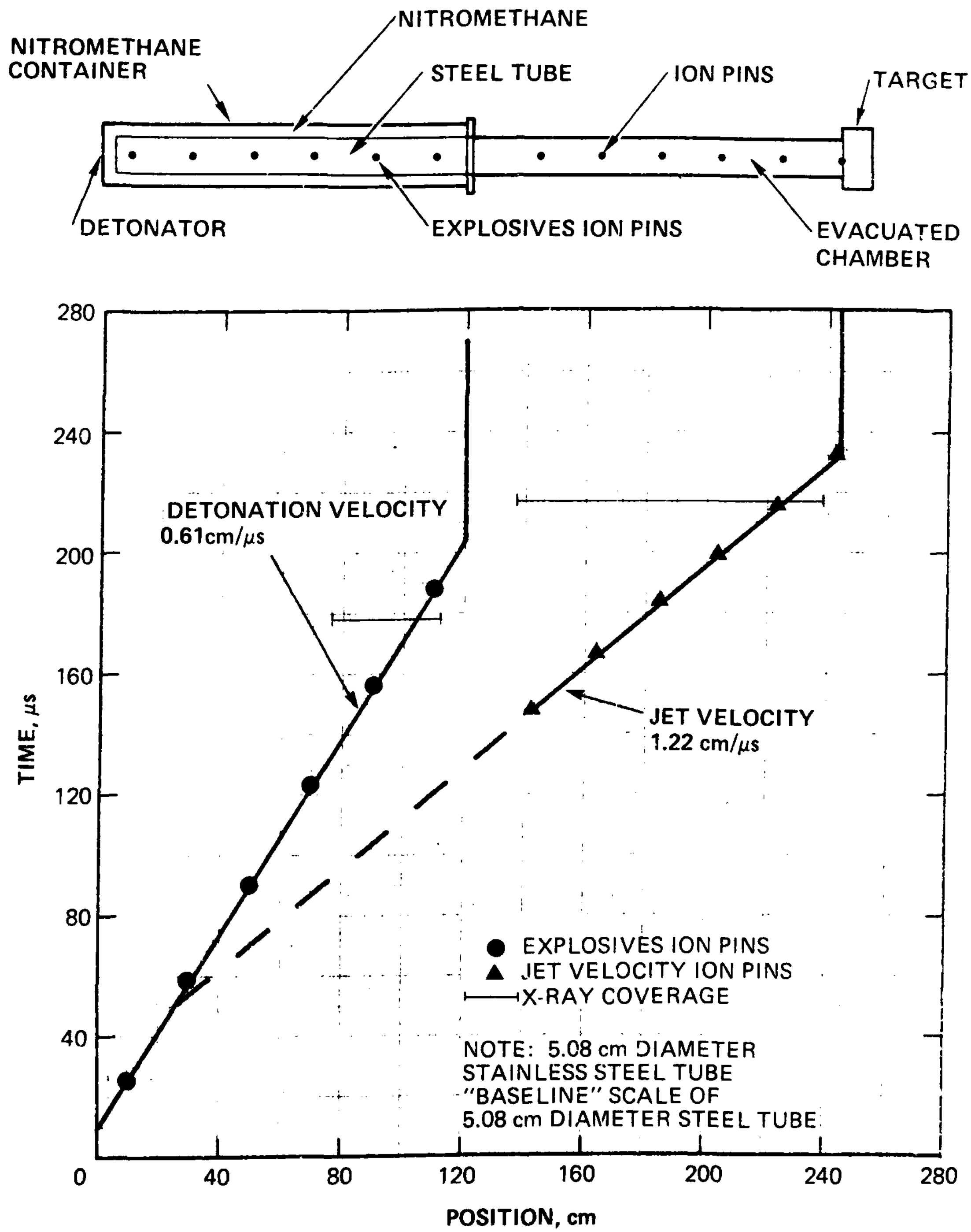

Figure 43 Results from explosive driver test APC-9 (5.08-cm-o.d. stainless steel driver tube).

A4051

Figure 44 Radiograph of collapsing stainless-steel tube in test APC-9 (5.08-cm o.d. tube).

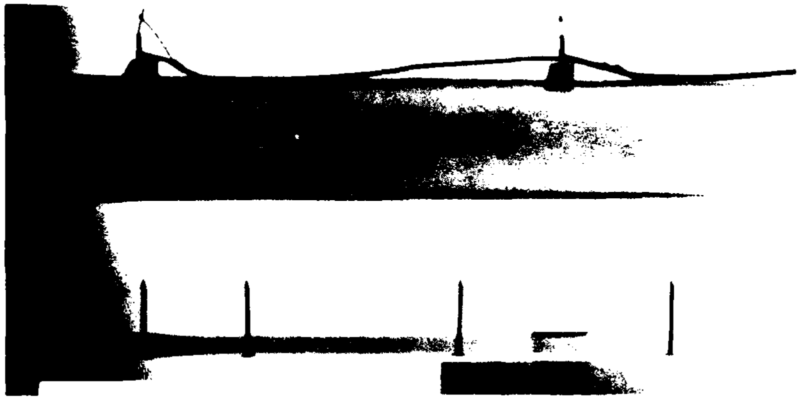

(a) t = 217 μs, x = 135 to 173.5

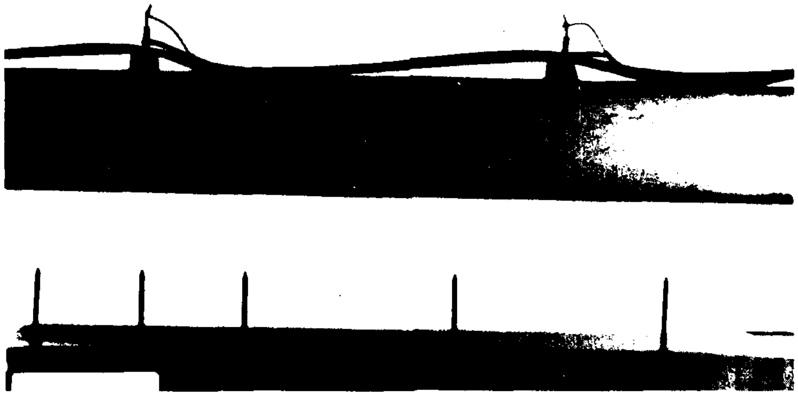

(b) t = 217 μs, x = 175.5 to 214

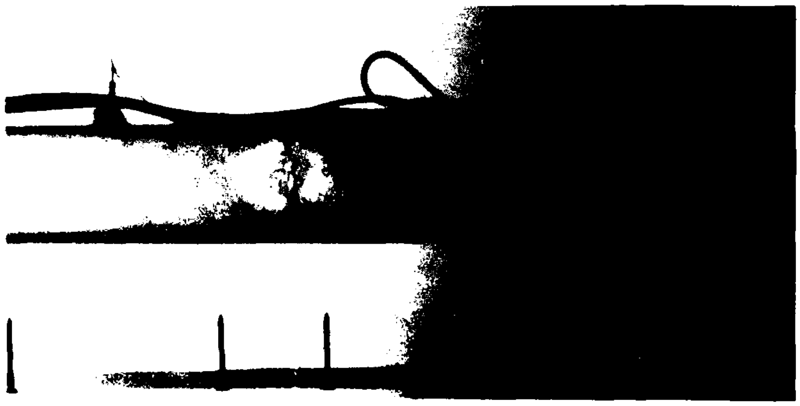

(c) t = 217 μs, x = 216 to 255

Figure 45 Radiographs of PMMA extension tube chamber downstream of jetting driver in test APC-9 (5.08-cm stainless-steel driver tube).

A4053

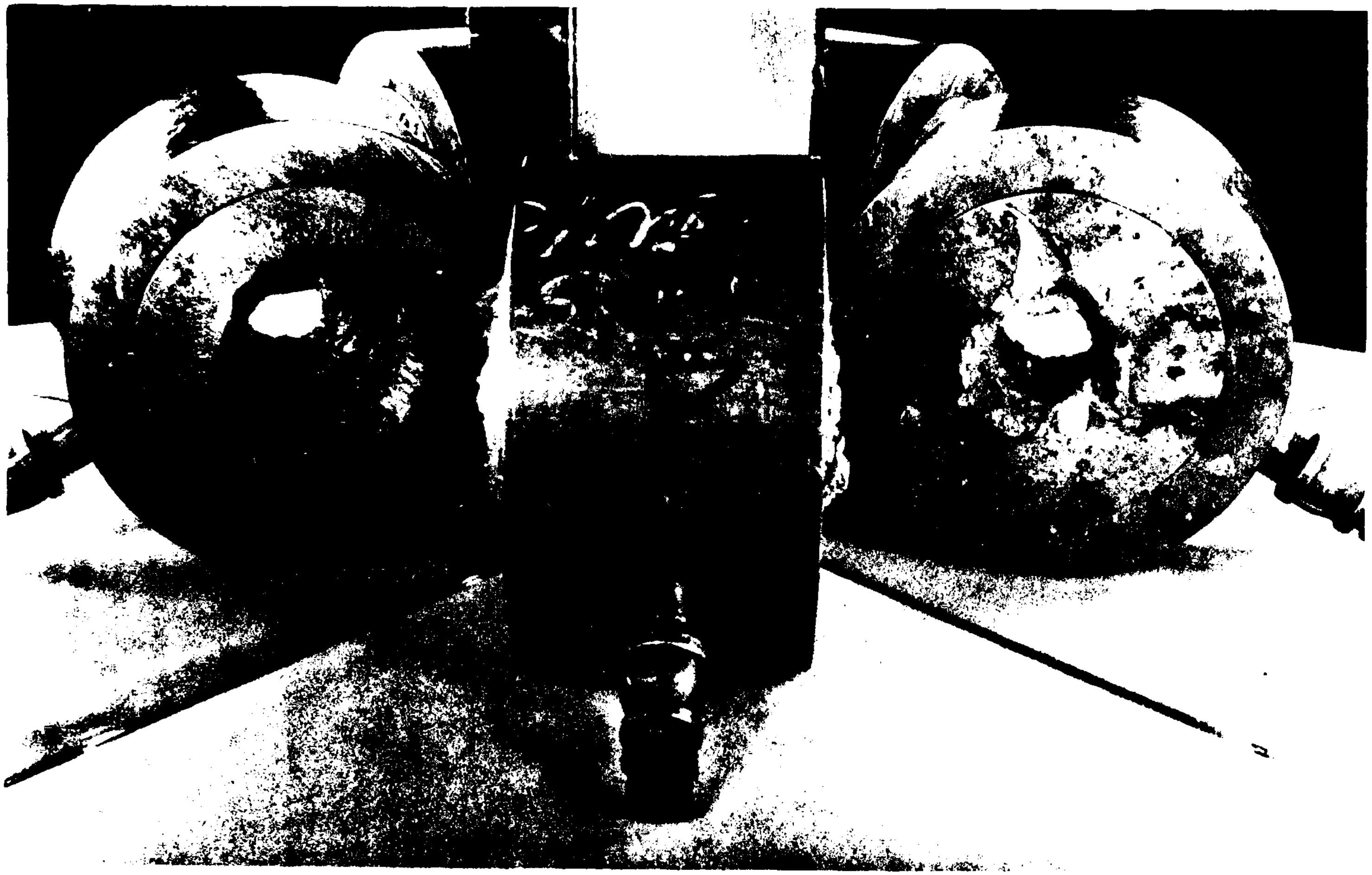

Figure 46 Aluminum target (with mirrors to show end views) from test APC-9 (5.08-cm o.d. stainless-steel driver tube).

spray. As a gas, the expansion would reduce the energy flow along the axis, whereas a droplet jet should be unaffected.

The results of this experiment are presented in Figures 47 through 50. The trajectories of the detonation wave and plasma jet given in Figure 47 yield velocities of 0.61 cm/μs and 1.21 cm/μs, respectively. The radiograph given in Figure 48 shows a normal tube collapse, but a collapse angle of 18.5 degrees. The higher than normal (17 degree) collapse angle was attributed to the greater-than-desired nitromethane thickness resulting from the use of off-the-shelf commercial tubing. Some evidence of jetting is provided in Figure 49 by the deformation and ablation of the ionization pins. In addition, there are small clouds of what appears to be a high density material between the first and second pins. However, there was very little damage to the aluminum target as shown in Figure 50.

Several possibilities emerged as candidates for causing the unplanned reduction of jet energy in this experiment: (1) the collapse process is near a threshold whereby a small increase in the collapse angle changes the material state of the jet, e.g., droplets to a gas; (2) the jet is gaseous and the flow through the area expansion between the driver and extension tube significantly reduced its axial energy; (3) an asymmetric implosion was inadvertently generated because the manufacturing tolerances for the thin-walled stainless steel tubes were considerably greater than the manufacturing specifications, or the tube was not centered in the nitromethane; (4) the lengths of the stainless steel tube and the PMMA extension tube were not reduced in proportion to the reduction in tube diameter, thereby

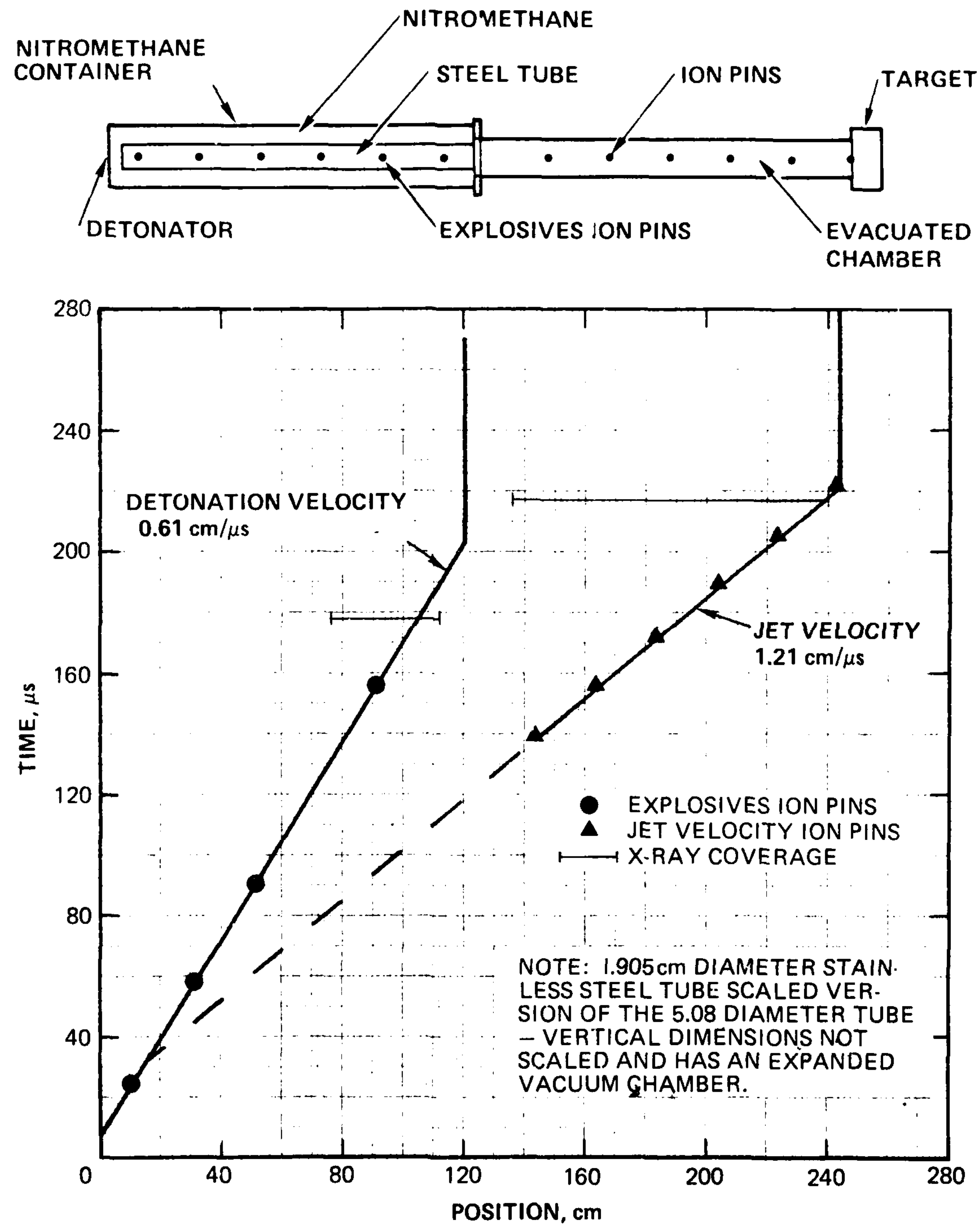

Figure 47 Results from explosive driver test APC-10 (1.905-cm-o.d. stainless-steel driver tube).

Figure 48 Radiograph of collapsing steel tube in test APC-10 (1.905-cm-o.d. stainless steel).

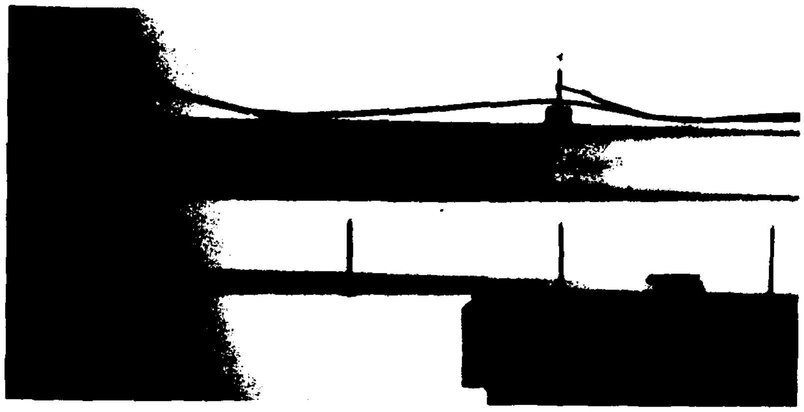

(a) t = 220 μs, x = 136.4 to 175.2 cm

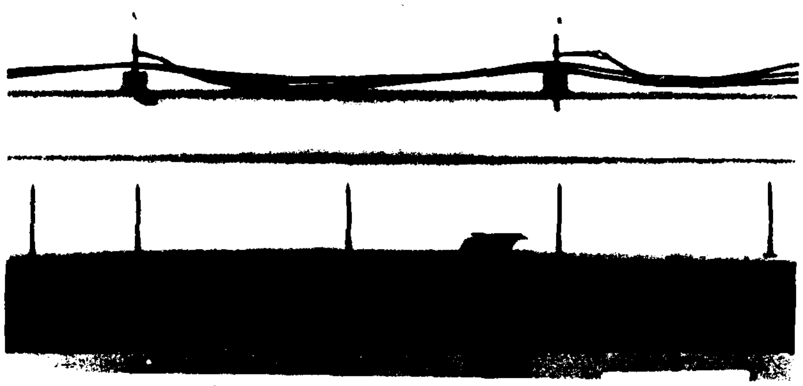

(b) t = 220 μs, x = 176.7 to 215.6 cm

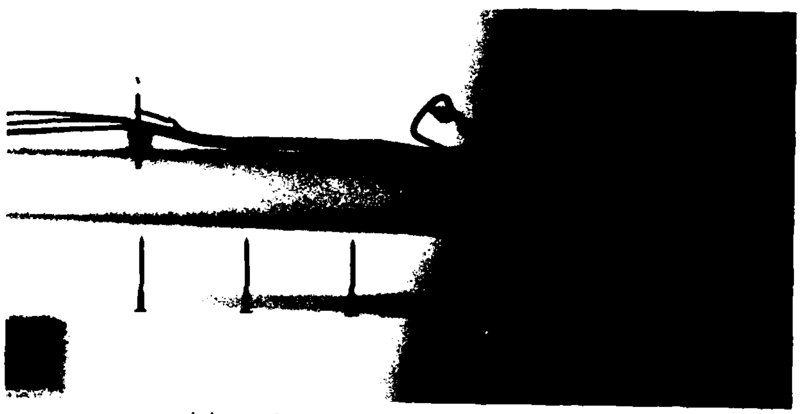

(c) t = 220 μs, x = 217.1 to 256 cm

Figure 49 Radiographs of PMMA chamber downstream of jetting explosive driver in test APC-10 (1.905-cm-o.d. stainless steel driver tube).

A4054

Figure 50 Aluminum target from test APC-10 (1.905-cm-o.d. stainless-steel driver tube).

A4055

causing a length effect such as boundary-layer growth (choking), ablation, and/or condensation on the walls. Since no conclusions could be drawn even after a careful analysis and review of the experimental data, an additional experiment was planned.

APC-11. The unexplained reduction in axial energy flow in the previous experiment led to a design that was more rigorously scaled to the configurations that had produced high energy plasma jets. The lengths of the stainless steel driver tube and the PMMA extension tube were reduced in this experiment by a factor of 0.38, which was the ratio of the outer diameters of the driver tubes (1.905 cm ÷ 5.042 cm). The area expansion used in test APC-10 was eliminated by making the inner diameter of the extension tube approximately equal to that of the driver tube. However, the diameter and wall thickness of the PMMA tube containing the nitromethane was the same as used in Test APC-10. Each component of the experiment was carefully inspected for aherence to tolerances, concentricity, and manufacturing specifications.

Figures 51 through 54 show the results that were obtained for this experiment. The x-t plot given in Figure 51 shows that the detonation velocity was 0.60 cm/μs, and the jet velocity was 1.17 cm/μs. The radiograph of Figure 52 shows the collapse process was normal with a collapse angle of about 18 degrees. The deformation and ablation of the ionization pins and the high density "clouds" present in the radiographs of Figure 53 were quite similar to previous jetting drivers. The conclusive evidence of high energy jet flow was the damage to the 10.16 cm (4 inch) aluminum target shown in Figure 54. The driver had

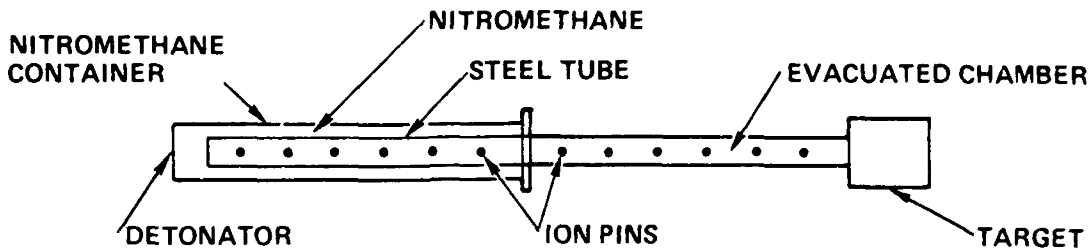

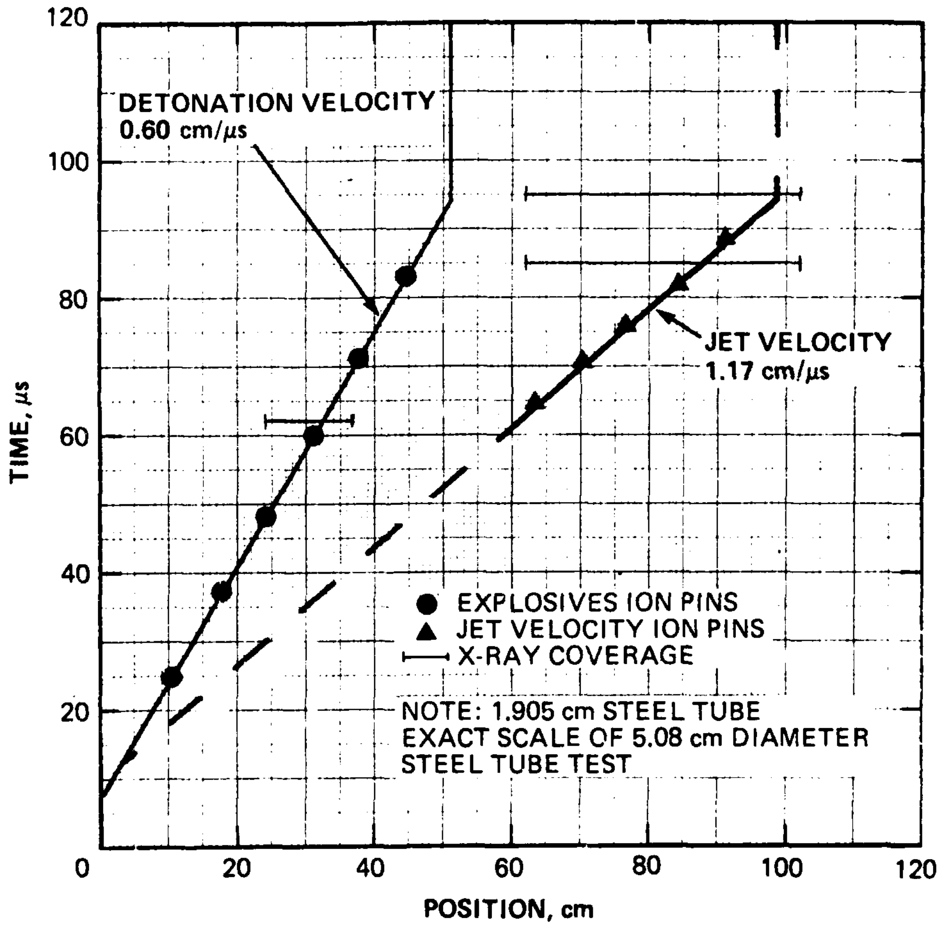

79-3-176

Figure 51 Results from explosive driver test APC-11 (1.905-cm-o.d. stainless-steel driver tube).

A4097

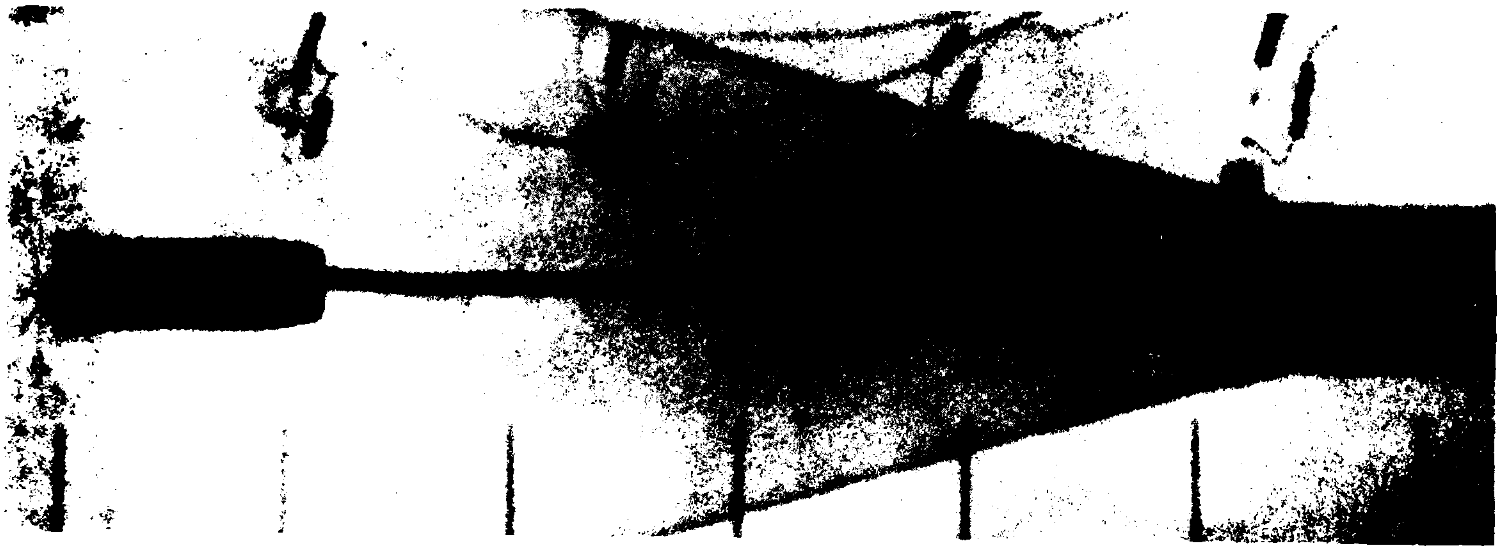

Figure 52 Radiograph of collapsing tube in test APC-11 (1.905-cm-o.d. stainless steel).

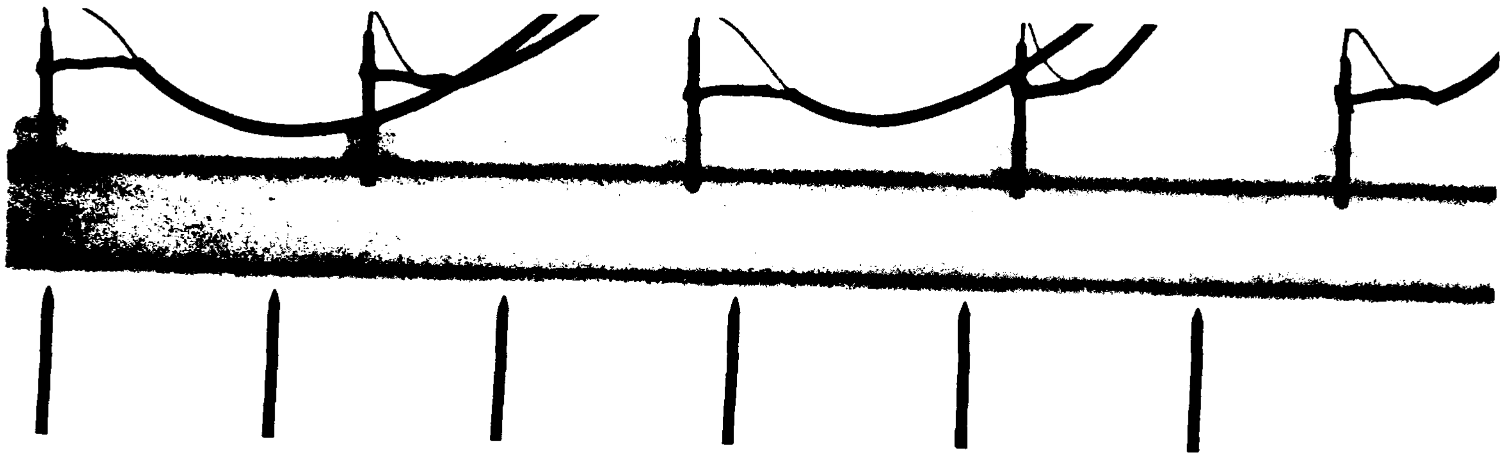

(a) t = 85 μs   X = 62 cm to 102 cm

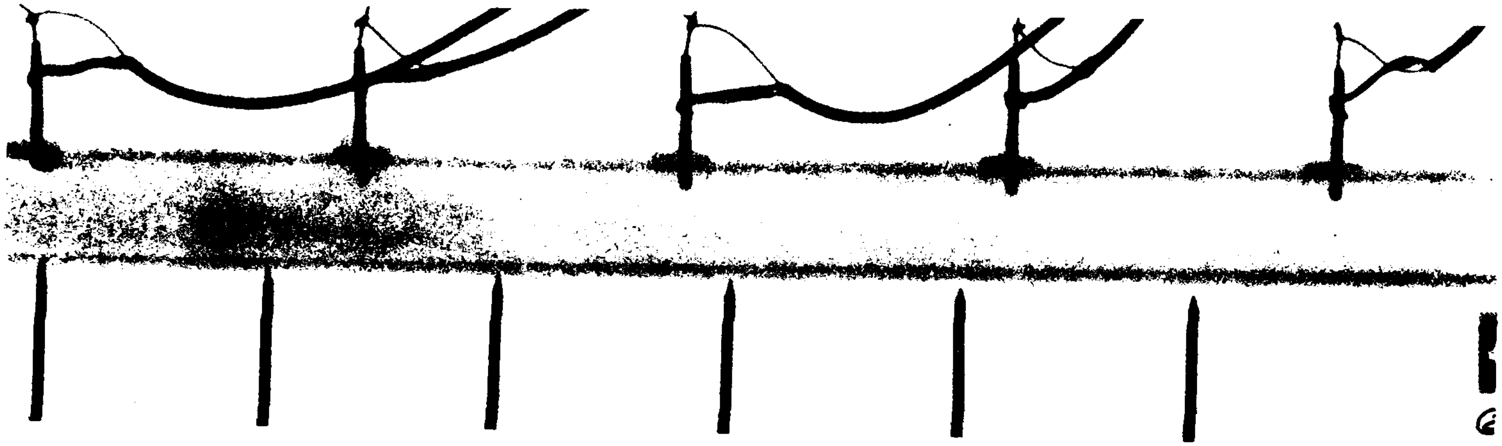

(b) t = 95 = μs   X = 62 cm to 102 cm

Figure 53   Radiographs of PMMA extension tube downstream of jetting explosive driver in test APC-11 (1.905-cm-o.d. stainless-steel driver tube).

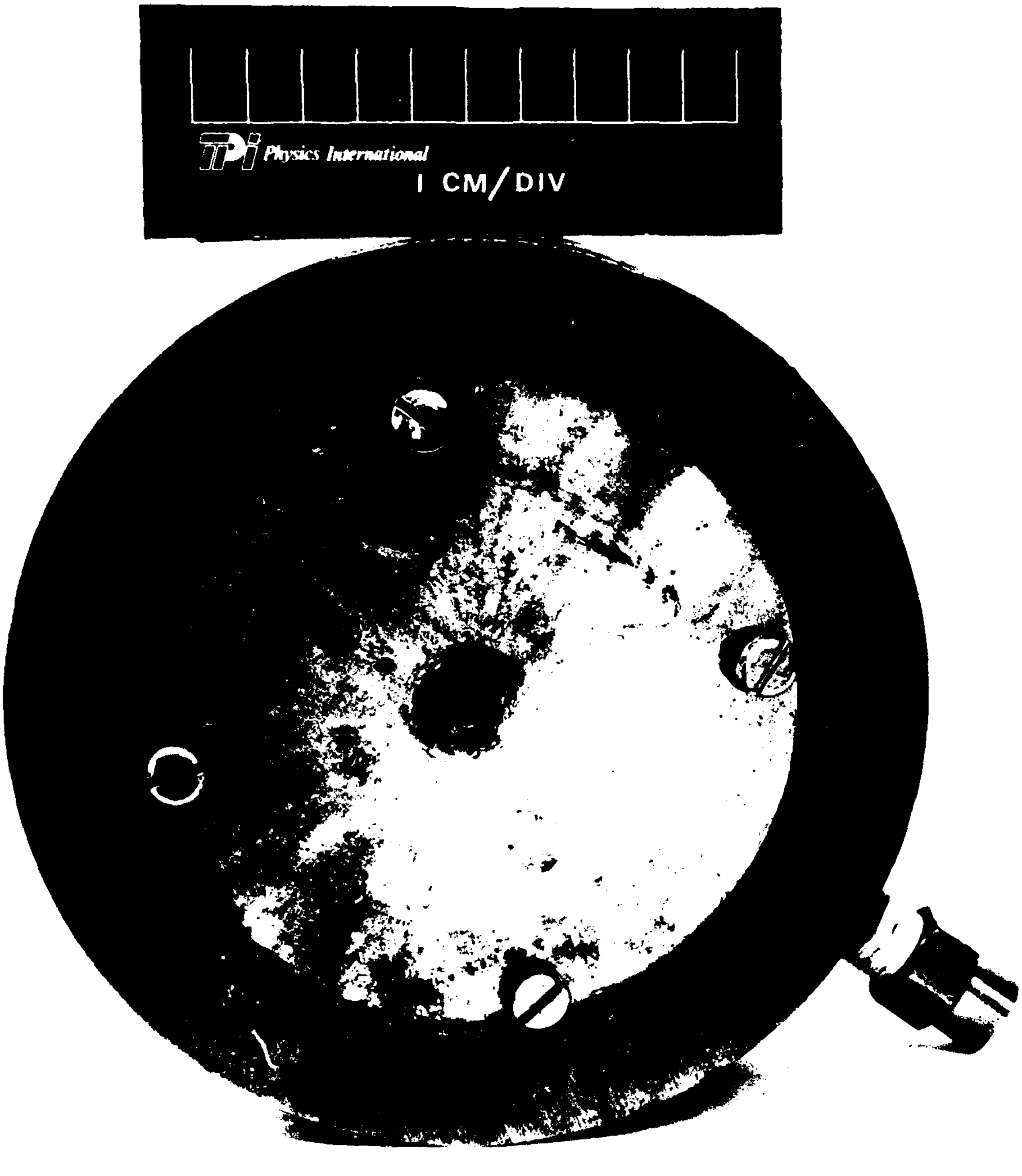

Figure 54 Aluminum target from test APC-11 (1.905-cm-o.d. stainless-steel driver tube).

A4109

produced a 1.905-cm-diameter hole to a depth of 8.4 cm. The crater volume was 29.6 cm^3.

Since several parameters were changed in this experiment, the results could not be used to explain the dramatic loss in axial energy in Test APC-10. However, the high-energy flow that had been achieved with a 1.905-cm-diameter stainless steel tube justified their use in the spherical high explosive experiment described in the next section.

SECTION 3

SPHERICAL HIGH EXPLOSIVE EXPERIMENT (LS-1)

The results of the explosive driver tests described in Section 2 clearly established that asymmetries cause a dramatic reduction of the energy flow in explosively collapsed tubes. However, the collapse conditions for these tests were considerably different from those that would exist for an LOS pipe in an underground nuclear test. In the explosive driver tests, the tube is collapsed by the steady-state, constant detonation pressure of the high explosive which is in direct contact with the tube; whereas, the collapse of an LOS pipe is due to the transient, decaying tangential stress behind a spherically divergent shock wave in the media around the pipe. The spherical high explosive experiment (LS-1) described in this section was designed and conducted to investigate the effects of asymmetries on tubes in a collapse environment that is more representative of the latter case.

3.1 EXPERIMENT DESCRIPTION

Figure 55 shows a cross-section and plan view of the experimental configuration used to provide a small-scale simulation of LOS pipe collapse conditions. This figure will serve as a reference for the orientation and location of all of the apparatus used in this experiment. A fiberglass sphere contained

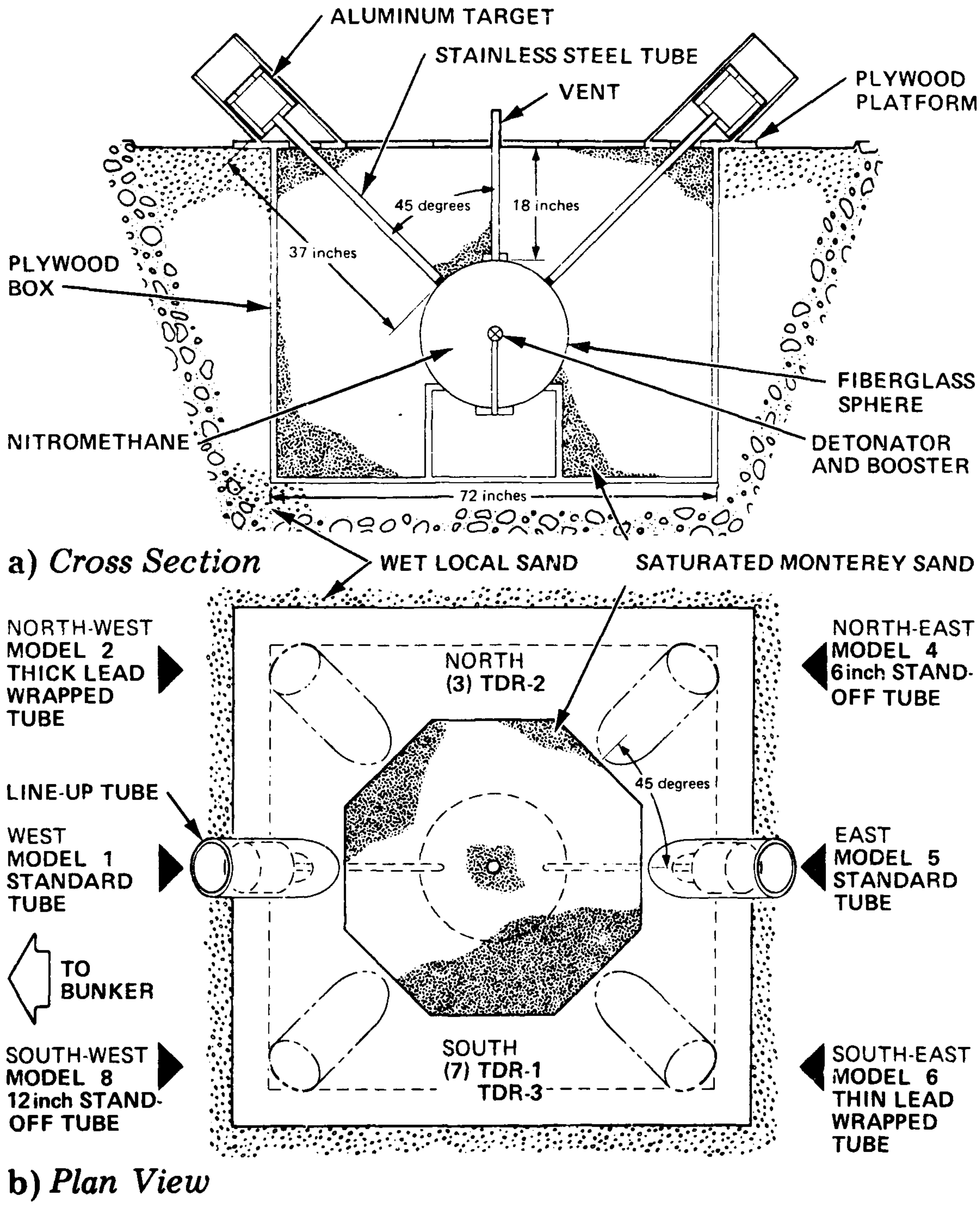

Figure 55 Experimental configuration of spherical high explosive experiment.

AD-A086 217 PHYSICS INTERNATIONAL CO SAN LEANDRO CA F/G 18/3
ASYMMETRIC COLLAPSE OF LOS PIPE.(U)
JUL 79 E T MOORE, R FUNSTON DNA001-77-C-0155
UNCLASSIFIED PIFR-1034 DNA-5023F NL

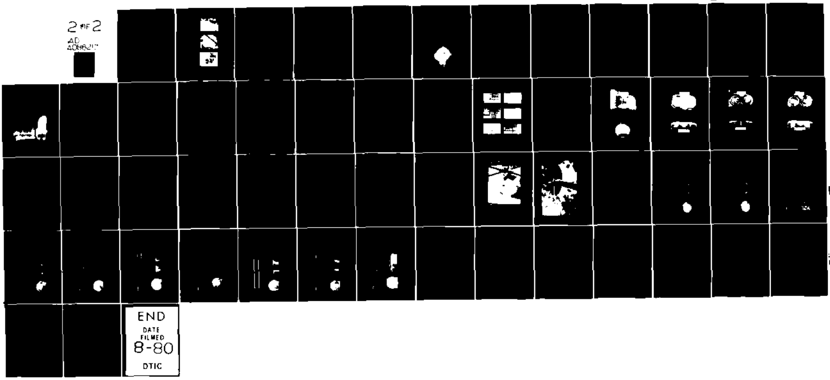

a liquid high explosive, nitromethane. This spherical energy source was placed in a plywood box located below ground level. Six stainless-steel tubes (LOS models) and two instrumentation lines extended radially from the suface of the fiberglass sphere to a plywood platform on the top of the box. The tubes and instrumentation lines were oriented at an angle of 45 degrees with a vertical axis of the sphere and separated by an azimuthal angle of 45 degrees. The box was filled with saturated Monterey sand and surrounded by wet local sand. The photographs in Figure 56 show the experiment during various stages of construction and assembly.

3.1.1 Explosive Sphere. The design approach used for the energy source was to select an explosive sphere size that would generate a spherically divergent shock wave in saturated sand capable of collapsing tubes of the same length and diameter as those used in the explosive driver tests. A preliminary design analysis showed that the sphere size required for the tube dimensions used in these tests would be prohibitively large (and expensive) for a laboratory experiment. Thus, the tube dimensions used in tests APC-10 and ACP-11 were reduced to provide a data base for tubes that could be used in this experiment with a smaller explosive sphere.

Figure 57 shows the peak stress generated in wet sand by the detonation of a 60.96-cm- (24-inch-) diameter sphere of the liquid explosive, nitromethane. The upper curve is the calculated peak radial stress in 100-percent saturated sand as a function of the distance from the center of the sphere (Reference 12). The lower curve is based on free-field stress

(a) **Preparation of test bed.**

(b) **Alignment of LOS Models**

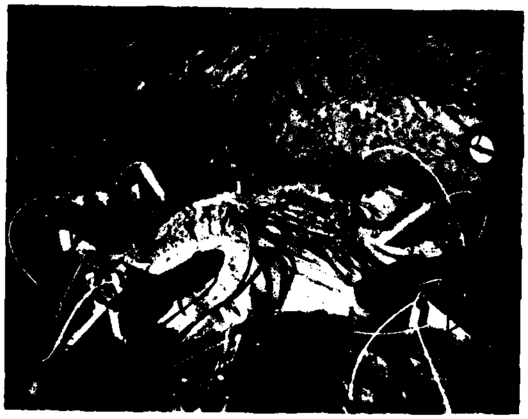

(c) **Configuration prior to firing**

Figure 56 Photographs of spherical high explosive experiment (LS-1).

A4118

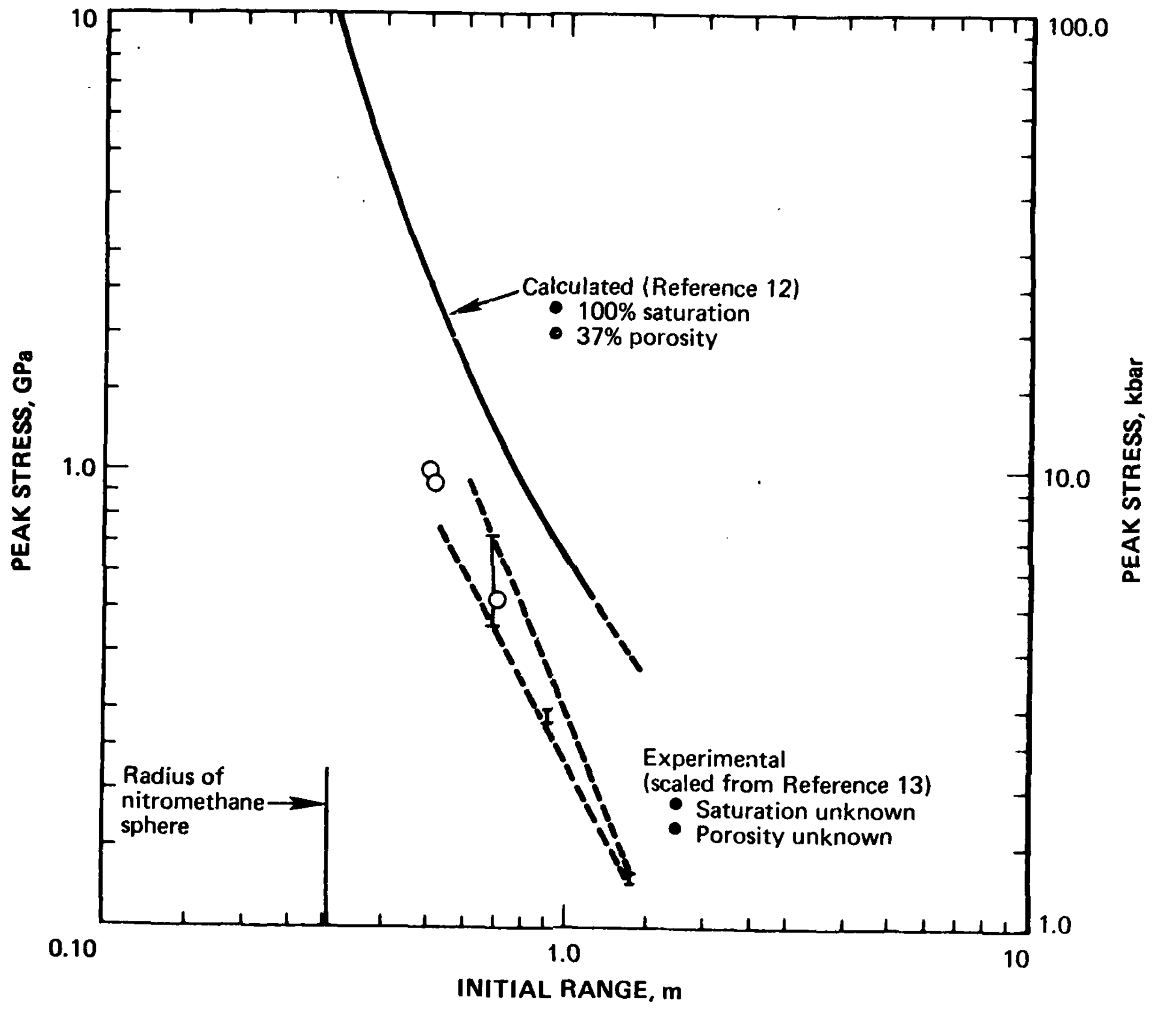

Figure 57 Peak stress in wet sand as a function of distance from 60.96 cm (24 inch) sphere of nitromethane

measurements that were scaled up from experiments using 16-inch-diameter spheres of nitromethane in wet sand of unknown saturation (Reference 13). The scatter in these measurements reflects the variation in water content from experiment to experiment. Collapse is assumed to occur above a stress of 60 kPa (6 kbar). Although collapse may occur below this stress level, the collapse conditions are probably marginal for the formation, progression, and detection of jetting. The configuration and stress-range curves given in Figure 58 indicate the 60 kPa stress is in the range of 11 inches (experimental, wet sand) to 28 inches (calculated, 100 percent saturated sand). This would correspond to a collapse tube length between 15 and 37 diameters of a 1.905-cm- (0.75-inch) diameter tube.

Details of the explosive sphere are given in Figure 59a. Approximately 300 pounds of nitromethane were contained in a 61-cm- (24-inch-) o.d. hollow fiberglass and resin sphere having a wall thickness of 0.102 cm (0.04 inch). The sphere was formed from two hemispherical shells which were joined at the midplane and supported by the use of a plywood flange. Nitromethane was introduced (by gravity) into the sphere through an opening in an aluminum flange located on the bottom of the sphere. This flange also supported an aluminum tube which was used to position a 5.08-cm-diameter C-4 explosive booster containing a RP-3 spherical detonator at the center of the sphere. A similar tube was mounted on a smaller flange at the top center of the sphere to vent the air during the nitromethane filling process. A photograph of the assembled sphere is presented in Figure 59b. This photo also shows the aluminum stand used to support the sphere in the test bed and the small PMMA rings which located the LOS models at the surface of the upper hemisphere.

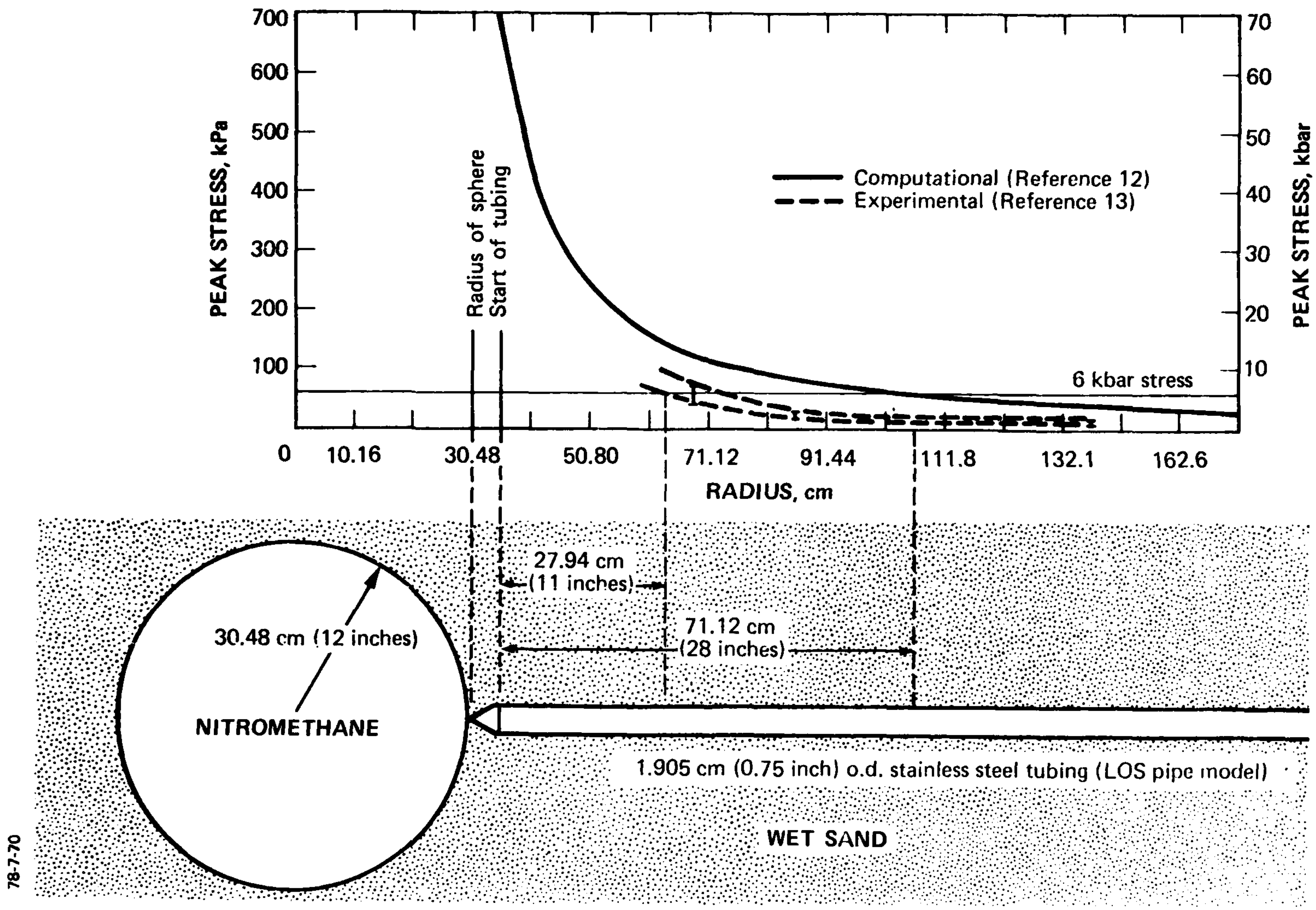

Figure 58 Configuration and stress-range environment for spherical high explosive test (LS-1).

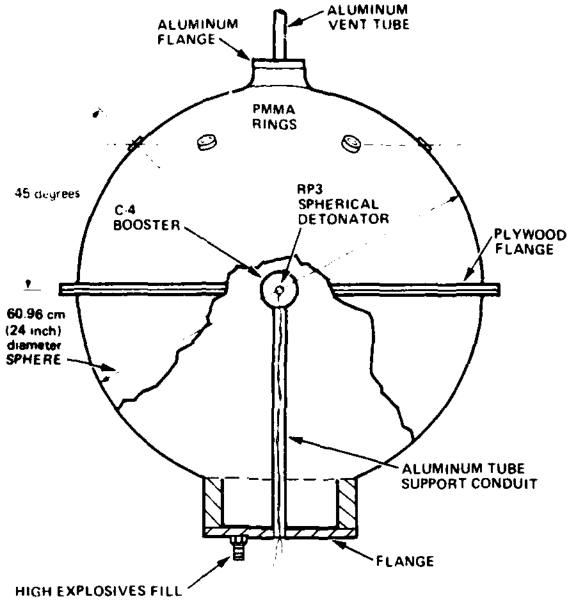

(a) SKETCH OF EXPLOSIVE SPHERE

79-2-77

(b) PHOTOGRAPH OF ASSEMBLED SPHERE

Figure 59 Fiberglass sphere used to contain nitromethane (LS-1).

A4115

3.1.2 <u>Test Bed</u>. A reinforced plywood box was used to contain the saturated Monterey sand. The box had a floor area of 3.34 m^2 (36 ft^2) [1.83 m by 1.83 m (6 ft by 6 ft)] and a height of 1.37 m (4-1/2 ft). Cracks and joints were caulked with a vulcanized rubber sealant to make the box watertight. The box was positioned 1.37 m (4-1/2 ft) below ground level on a compacted sand base. Wet local sand was used to backfill the hole containing the box.

The sand used as the test medium was designated as Lapis Lustre or equivalent from Monterey, California, and met the following specifications:

U. S. Standard Sieve Size	% Passing
#12	100
#16	95-100
#20	40-60
#30	5-15
#50	0-2
#100	0

It should be noted that this is the same sizing of sand that was used in the Boeing Drift Experiment on the DIABLO HAWK event.

The test bed was prepared by slowly pouring individual sacks of sand into a steady stream of water. Care was taken to maintain a thin slurry of sand and water in the box at all times. Hand mixing and pneumatic vibrators were used to maximize the density and saturation. However, no quantitative measurements of porosity or saturation were made.

3.1.3 LOS Models. Six 321 stainless steel tubes (Military specification 8808) were used as LOS models. The outside diameters (0.75 inch) and wall thicknesses (0.010 inch) of the models were the same as the tube used on Test APC-11 described in the previous section. Cross-sections of the planes of the experimental configurations which contain the various models are given in Figures 60 to 62. A small steel plug was welded onto the end of tubes closest to the explosive sphere. The other end of each tube was welded to a steel flange which joined the tube to an aluminum target. The air in the tubes was evaluated through small ports which passed through the 10.16-cm- (4-inch-) thick aluminum targets. The targets were contained in steel line-up tubes located on the plywood platform above the surface of the saturated sand.

The cross-sections of Models 1 and 5 are given in Figure 60. They were considered standard models and expected to provide the baseline performance for symmetrically collapsed tubes. The tubes for these models were 0.94 m (37 inches) long.

The tubes for Models 2 and 6 were also 0.94 m (37 inches) long but were helically wrapped with lead to introduce asymmetries. These models are shown in Figure 61. A 0.89-cm- (0.35-inch-) wide ribbon of 0.025 cm (0.010 inch) sheet lead was epoxied to the outside surface of the steel tube used in Model 6 in a helical pattern having a 3.429 cm (1.35 inch) pitch (pitch angle of 29.8 degrees). The width and pitch of the lead ribbon used in Model 2 was the same as Model 6, but the the thickness was increased to 0.20 cm (0.080 inch).

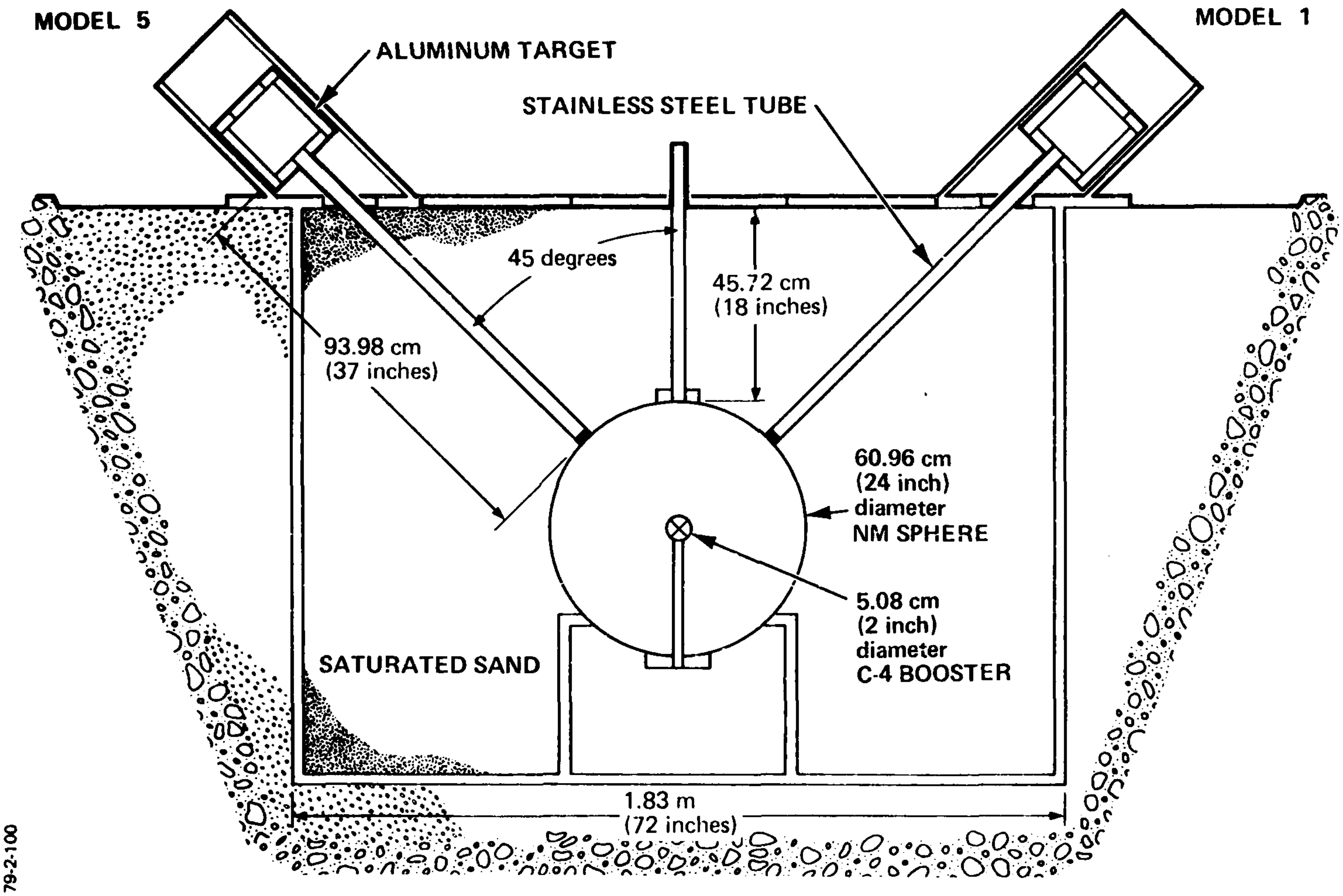

Figure 60 Cross-section of east-west plane containing standard LOS models (LS-1).

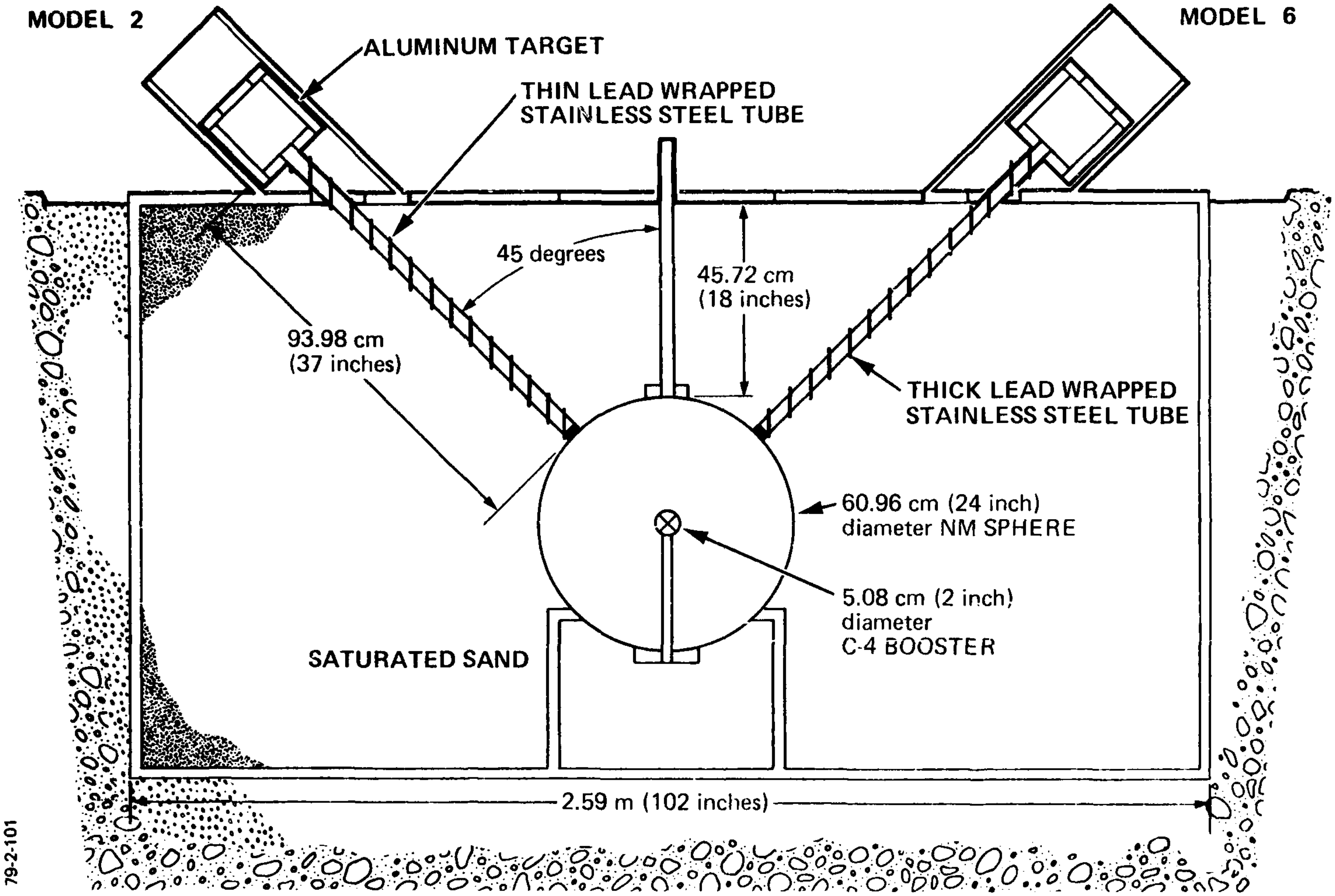

Figure 61 Cross-section of NW-SE plane containing lead-wrapped LOS models (LS-1).

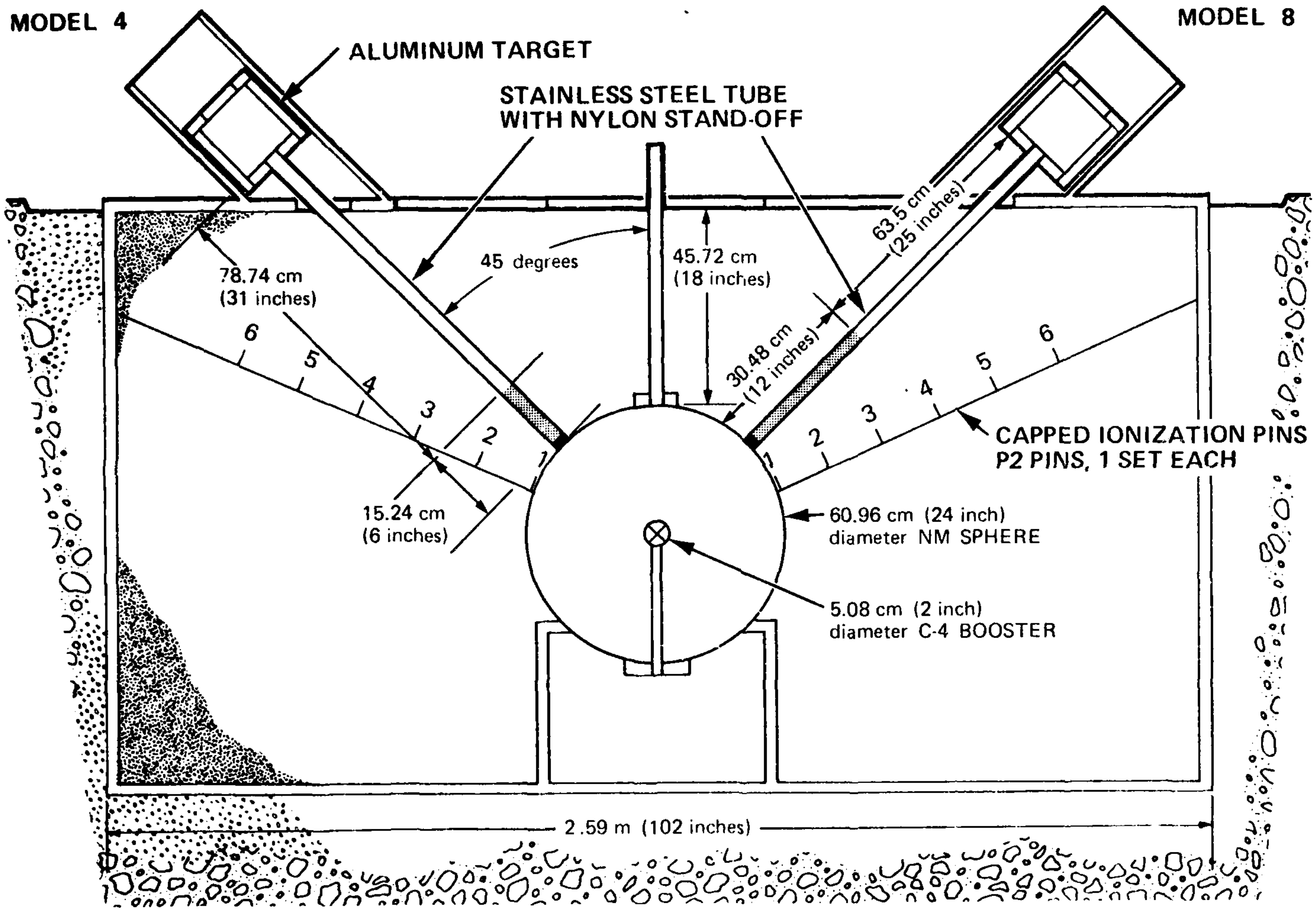

Figure 62 Cross-section of NE-SW plane containing short LOS models (LS-1).

Models 4 and 8 were shorter than the standard models. They were included to investigate the initiation and progression of jetting at two lower stress levels. Cross-sections of these models are given in Figure 62. Model 4 had a tube length of 0.79 m (31 inches). A 15.24-cm- (6-inch-) long nylon rod having the same diameter as the tube was joined to the tube and extended to the surface of the explosive sphere. This rod was used to align the tube radially and to position the tube exactly 15.24 cm (6 inches) from the surface of the sphere. The stress at this distance was expected to be between 150 kPa (1 kbar) and 320 kPa (32 kbar). Model 8 had a tube length of 0.64 m (25 inches) and a nylon rod of 0.30 m (12 inches). The stress at the beginning of the tube (a range of 0.61 m [24 inches]) was expected to be between 60 kPa (6 kbar) and 150 kPa (15 kbar).

A photograph of the LOS models is given in Figure 63. Five of these models were used in the experiment. The model with the 0.61 m (24 inch) nylon rod (extreme right in photograph) was replaced with one having a 15.24 cm (6 inch) rod. Figure 63 also shows an aluminum target, a thick-walled steel cylinder for containing the targets and a steel line-up tube.

3.2 INSTRUMENTATION

The active instrumentation used on this experiment was directed at measuring the time-of-arrival of the shock wave in the saturated sand, the stress behind the shock wave at three different ranges, and the velocity of the jets generated by the collapse of the tubes used in the Models 1 and 5 (standard-symmetrical collapse). The penetration of, and damage to, the

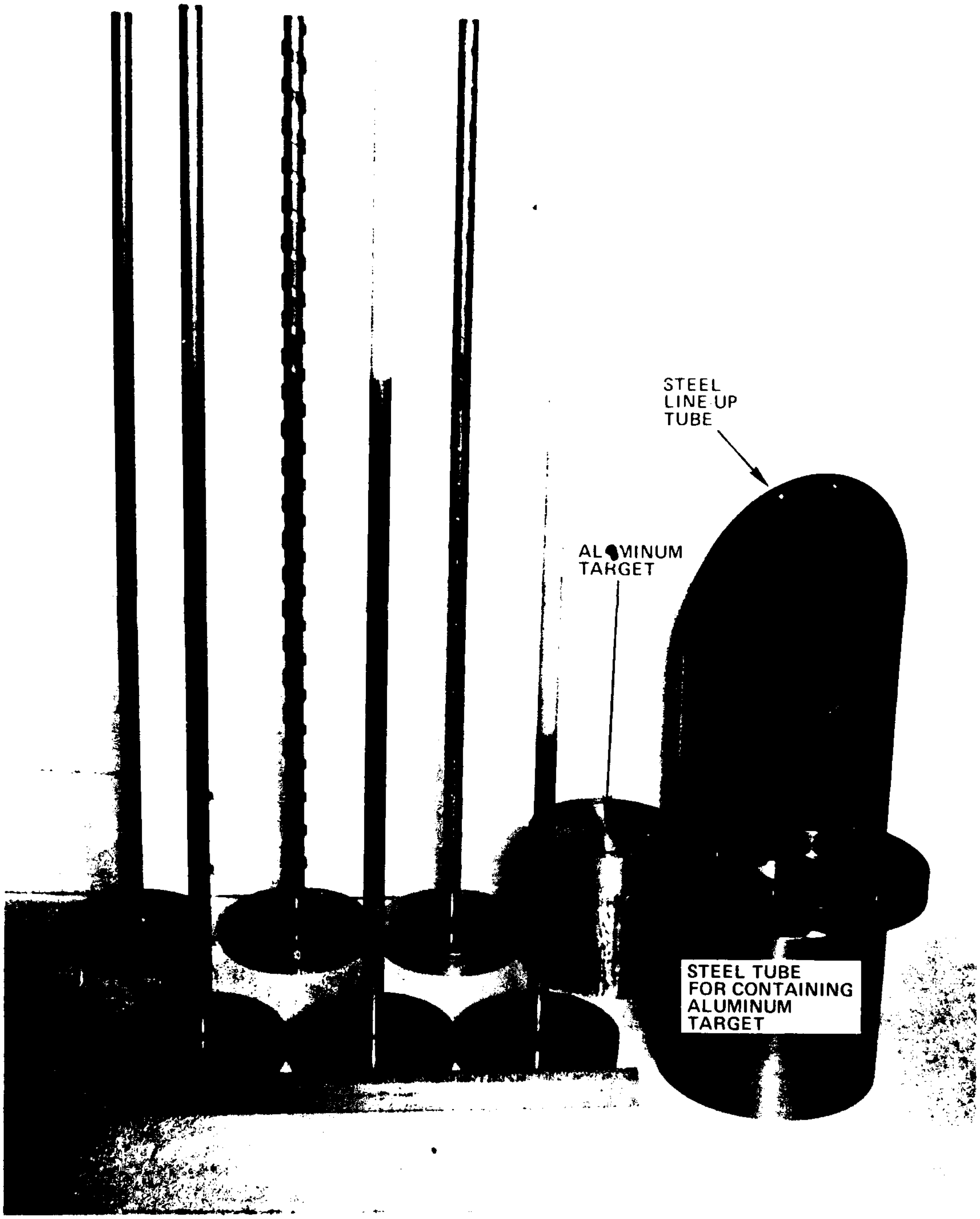

Figure 63 Photograph of LOS Models for spherical high explosive experiment (LS-1).

A4266

10.16-cm- (4-inch-) thick aluminum targets at the end of each tube was used to provide passive, terminal evidence of the jet energy generated by the collapse process.

Three different methods were used to measure the time of arrival of the shock wave in the sand: piezoelectric pins, capped ionization pins, and time domain reflectometry (TDR).* Two radial lines of six PZ pins and six capped pins were placed at 15 cm intervals which extended between 32 cm and 107 cm from the center of the explosive sphere. One line was located in the SE plane (see Figure 55), approximately 68° from a vertical line through the sphere. The other line was in the NW plane and also oriented at a 68° angle from the vertical. The times of shock arrival from these pins were recorded on oscilloscopes and on magnetic tape.

The shock trajectory was also determined by time-domain-reflectometry. The time of arrival was obtained by the reflection of 1000 (20 μs) electrical pulses from the impedance change in coaxial cables as they were being collapsed by the shock wave. Two different types of cable, RG-174 and FSJ1-50 (Super Flex) were used. Two cables, one of each type, were in the S plane (see Figure 55) and extended from the surface of the sphere to the platform at a 45° angle with a vertical line through the center of a sphere. Another FSJ1-50 cable was located in the N plane at the same angle with the vertical. The

*Provided by Tom McKown, Los Alamos Scientific Laboratory, P.O. Box 990, Los Alamos, N. M. 87545, and Dennis Whann of EG&G, 680 East Sunset Road, Las Vegas, Nevada 89112.

trajectory of the shock wave was determined by the round-trip transit time of the electrical pulses which was recorded digitally in a solid state memory and transferred to cassette tapes after the experiment.

Three ytterbium stress gages (flat packs) were used to measure the stress behind the shock wave at three different ranges. Two ytterbium elements in each gage provided dual measurements at each range. Two of the gage were located in the N-S plane (see Figure 55). One gage (B) was in the S plane at a range of 51 cm and 23° from the vertical. The gage (A) in the N plane was at a range of 71 cm and oriented at the same vertical angle. The third gage (C) was at a range of 91 cm and oriented at 45° in the SSW plane. The voltage output from the bridge circuit, where the ytterbium grid forms one leg of the bridge, was recorded on high speed magnetic tape.

Four ionization pins were included on each of Models 1 and 5 to measure the time of arrival of the plasma jet in the symmetrically collapsed tubes. The pins were placed at 7 cm intervals at a range between 98.5 cm and 119.5 cm from the center of the sphere. This range minimized the possibility that the pins and/or their cables would interfere with the collapse process.

3.3 EXPERIMENTAL RESULTS

The time of arrival data for the spherically divergent wave are given in Figure 64. The agreement between the piezoelectric pins, capped pins, and the ytterbium stress gages was quite

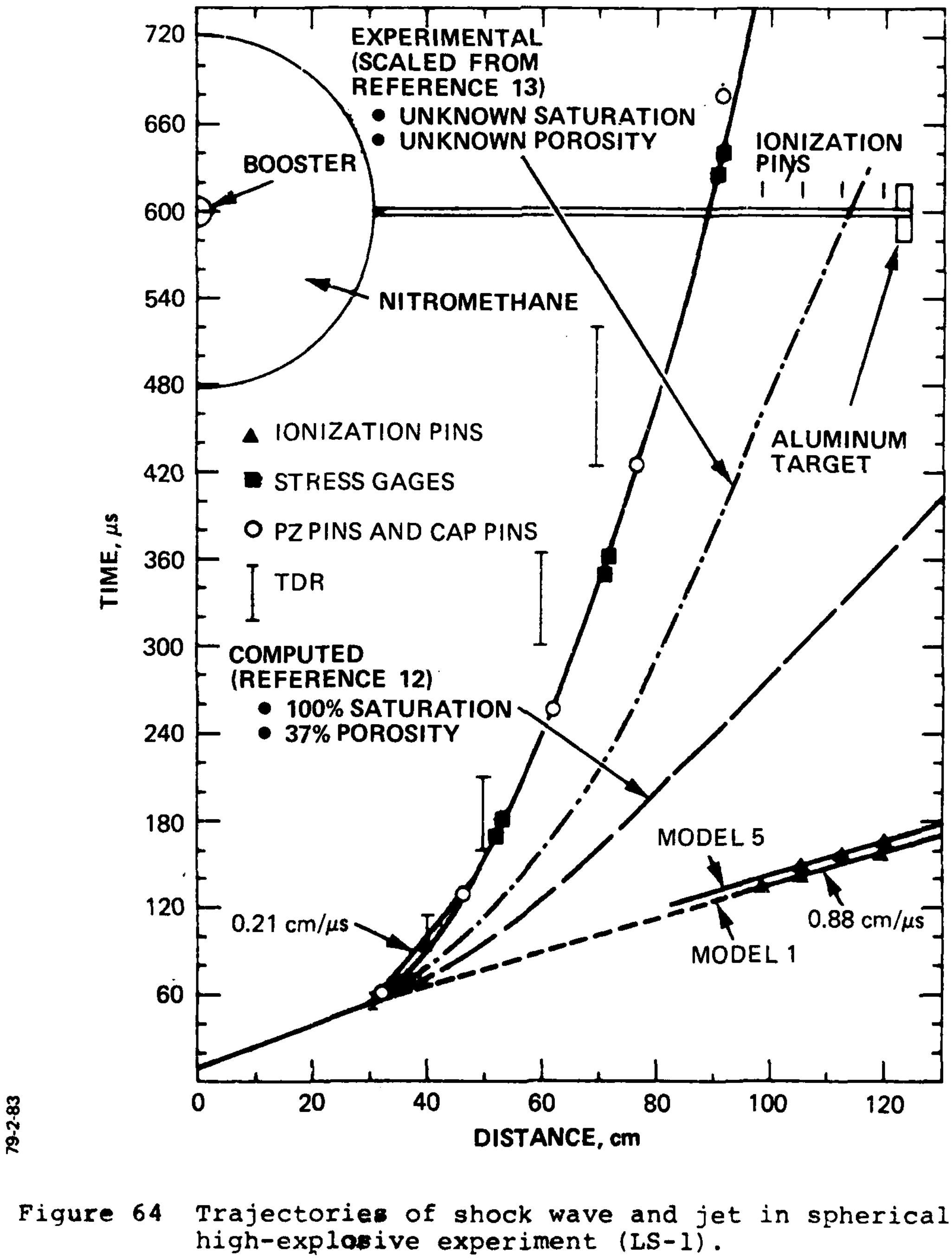

Figure 64 Trajectories of shock wave and jet in spherical high-explosive experiment (LS-1).

good. The TDR data were also in close agreement near the sphere but gave much longer times of arrival at the larger distances (lower stress levels). Representative examples of the TDR data from the RG-174 and FSJ1-50 cables are given in Figures 65 and 66, respectively. The observed trajectory of the wave in Figure 64 (solid curve) shows that the shock velocity was considerably lower than had been expected. The trajectory calculated for the detonation of a 60.96 cm (24 inch) sphere of nitromethane in 100-percent saturated, 37-percent porosity sand given by the dotted curve in this figure) was obtained from Reference 11). The dashed curve was scaled from experimental data for 40.64 cm (16 inch) nitromethane spheres in wet sand of unknown saturation (Reference 12). In this experiment the average shock velocity measured in the first 15 cm of sand was 0.21 cm/μs. This velocity was expected to be between 0.32 cm/μs (experimental-unknown saturation) and 0.43 cm/μs (calculational--100 percent saturated).

A low velocity shock wave was particularly surprising since the stress measurements from this experiment were within the scaled range of stress measurements for the previously mentioned 40.64 cm (16 inch) nitromethane spheres where the water saturation varied from experiment to experiment. This is illustrated in Figure 67. The actual traces for the six stress gages are given in Figure 68. Gages B-1, B-2, and A-1 clearly reached a peak stress before failing. Peaks could not be identified on the other gage records before gage failure.

Figure 64 also shows the times of arrival from the ionization pins in the tubes used for Models 1 and 2. The times

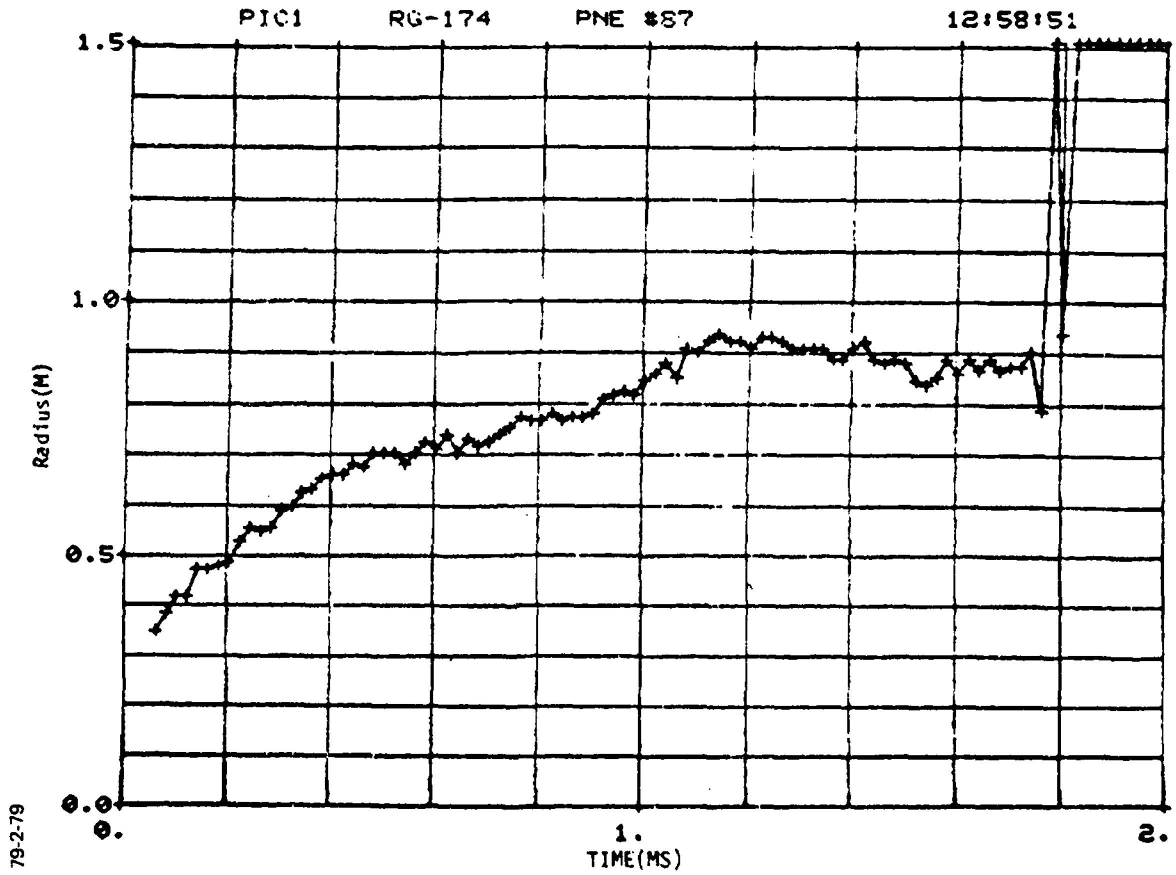

Figure 65 Trajectory of shock wave from TDR using RG-174 cable.

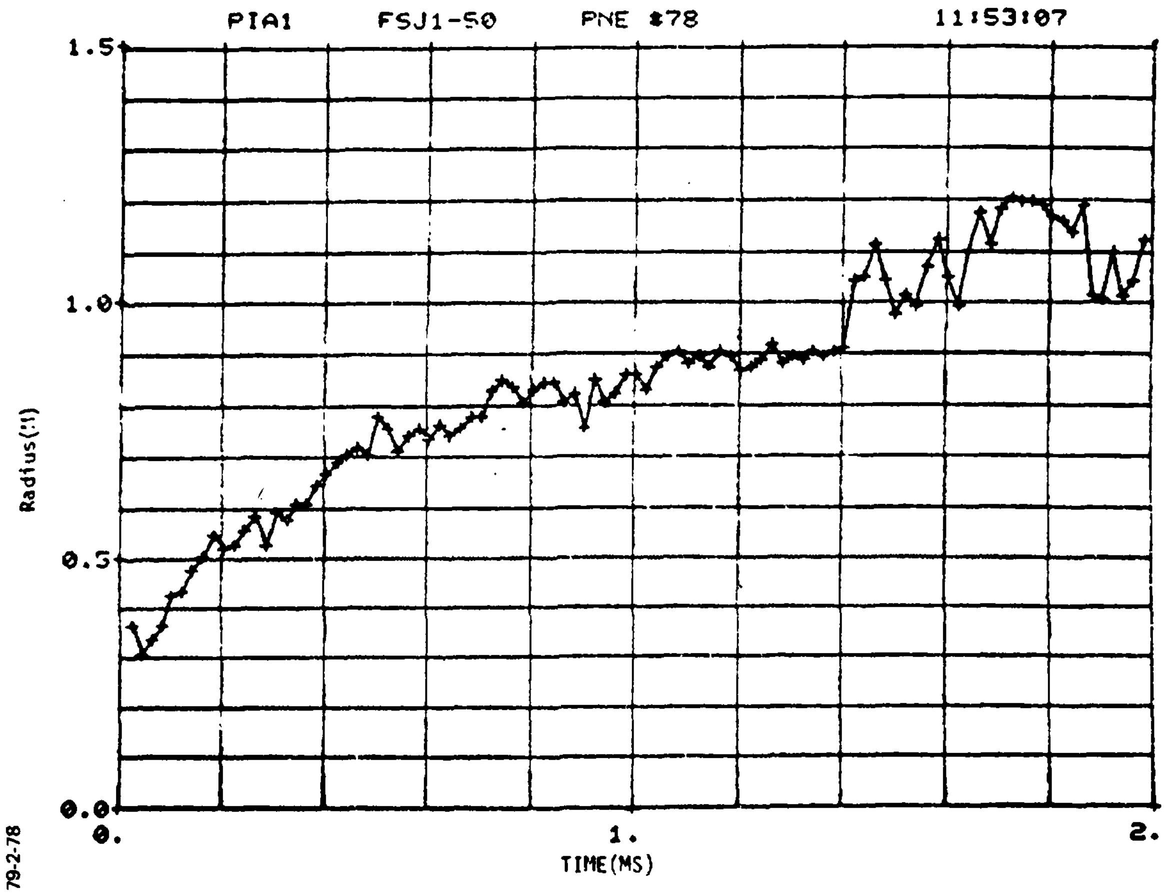

Figure 66 Trajectory of shock wave from TDR using FSJ1-50 cable.

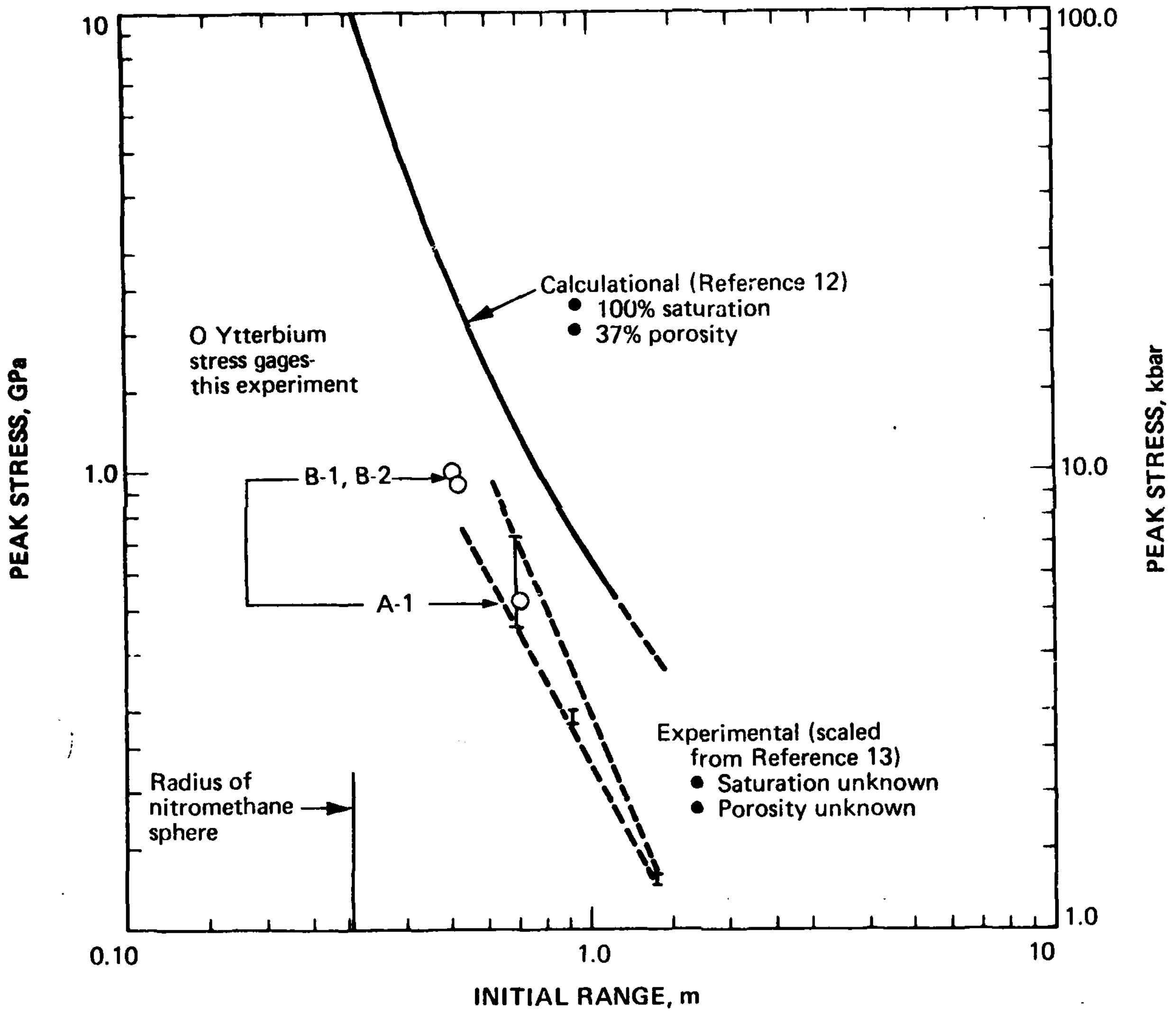

78-7-71

Figure 67 Peak stress in wet sand as a function of distance from nitromethane sphere.

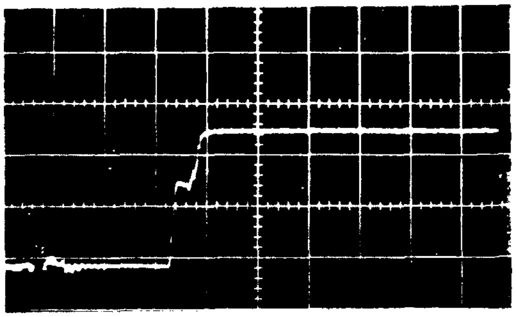

SWEEP 100 μsec/ MAJOR DIV
GAGE B-1 (50-cm)

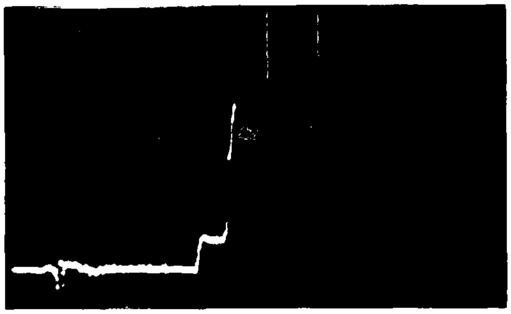

SWEEP 100 μsec/ MAJOR DIV
GAGE B-2 (51.3-cm)

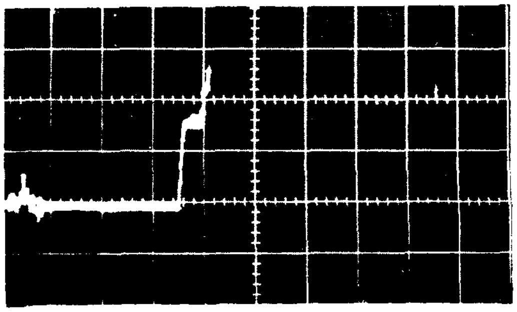

SWEEP 50 μsec/ MAJOR DIV
GAGE A-1 (70-cm)

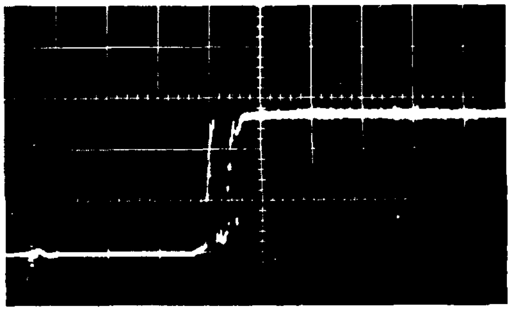

SWEEP 50 μsec/ MAJOR DIV
GAGE A-2 (71.3-cm)

79-2-82

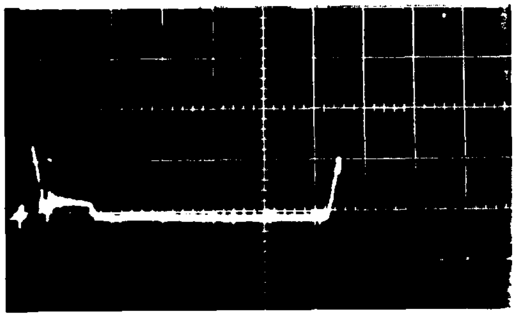

SWEEP 100 μsec/ MAJOR DIV
GAGE C-1 (90-cm)

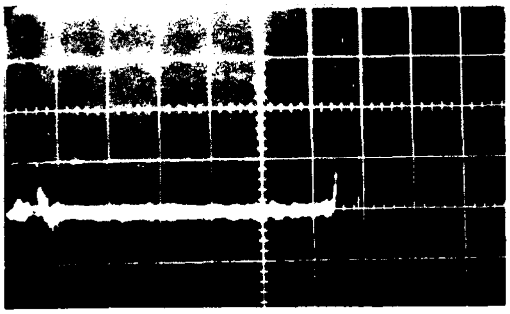

SWEEP 50 μsec/ MAJOR DIV
GAGE C-2 (91.3-cm)

Figure 68 Ytterbium stress gage records for high explosive spherical experiment (LS-1).

A4116

for Model 5 appear to be consistently 7 μs later than those for Model 1. The slope of these data show a velocity of 0.88 cm/μs. This velocity indicates the symmetrically collapsed tubes had indeed produced a jet. Extrapolation of the data indicates the origin of the jet was near the explosive-sand interface as one would expect.

Locating the aluminum targets after the detonation of the explosive proved to be a very difficult and time consuming task. Four of the targets were found between 600 feet and 1500 feet from the explosion. Two targets have not yet been located. Photographs of the recovered targets are given in Figures 69 to 72.

Figure 69 shows the target, flange, and a portion of the tube used in Model 8. The tube showed considerable axial compression, but the target was undamaged. Since the tube began 30.48 cm (12 inches) from the explosive-sand interface, this effect would indicate that the collapse conditions at this distance were insufficient to cause jetting. Figure 67 shows the peak stress was approximately 70 kPa (7 kbar) at this location.

The target from Model 5 is shown in Figure 70. The symmetrical collapse of the standard length tube had produced an irregularly shaped crater. It had a semicircular cross-section with a spiral-like penetration around its periphery. The crater had a diameter of 2 cm, a depth of 2 cm, and a volume of 4.9 cm^3.

Figure 71 shows the target from Model 6. The tube for this model had a thin, helically wound lead ribbon. The crater

(a) ALUMINUM TARGET AND STEEL FLANGE

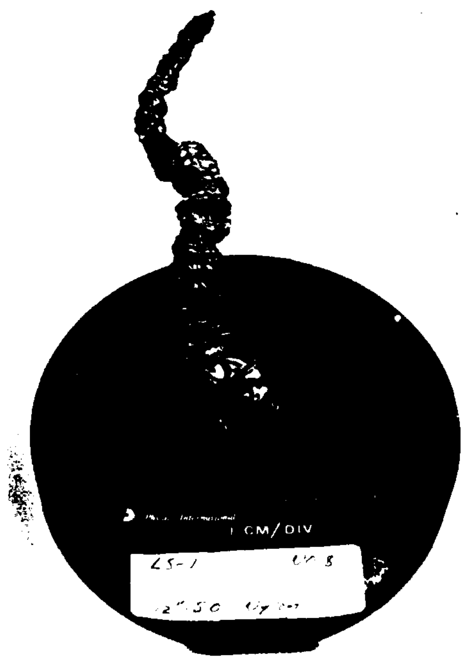

(b) COLLAPSED STAINLESS-STEEL TUBE AND STEEL FLANGE

Figure 69 Target from Model 8 (symmetrical collapse; 30.48 cm standoff; LS-1).

A4114

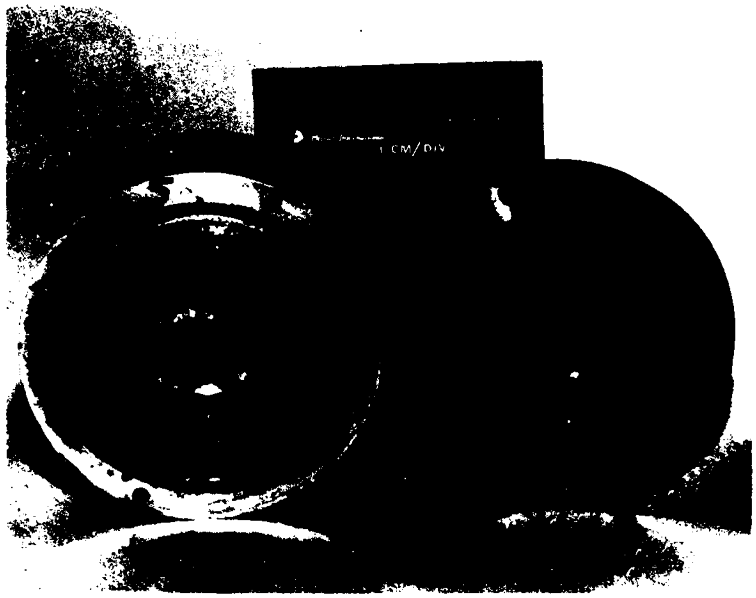

(a) TARGET FLANGE

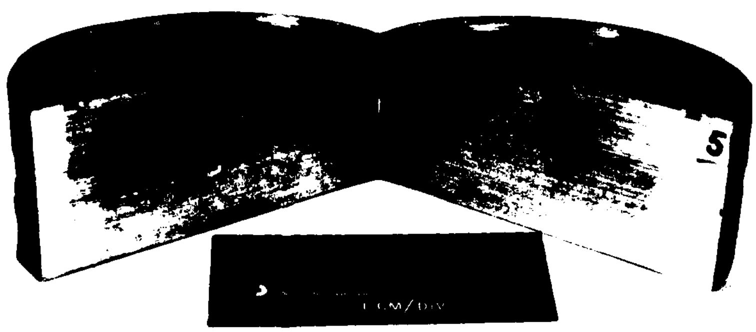

(b) SECTIONED TARGET

Figure 70 Target and flange from Model 5 (symmetrical collapse; standard tube; LS-1).

A4111

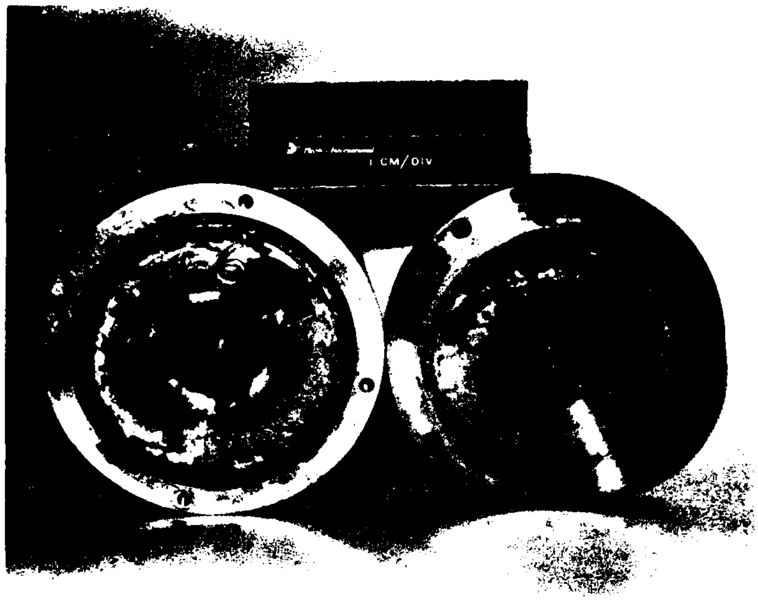

(a) ALUMINUM TARGET STEEL FLANGE

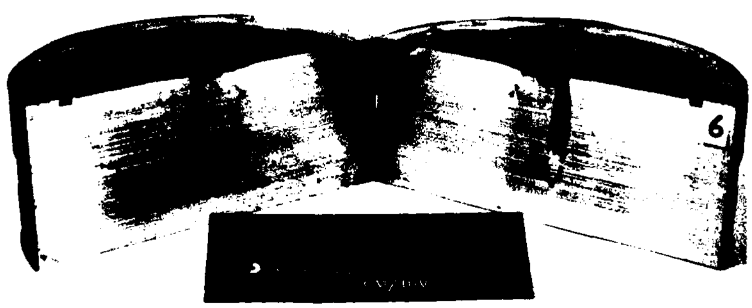

(b) SECTIONED TARGET

Figure 71 Target from Model 6 (asymmetrical collapse; thin lead wrap; LS-1).

A4112

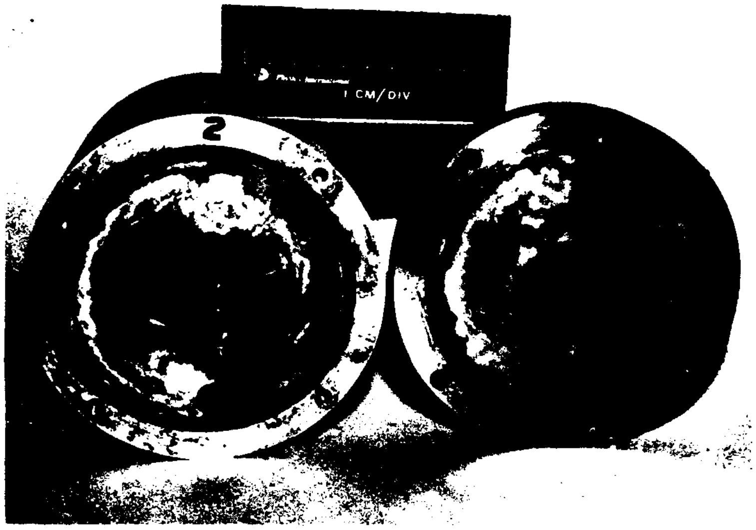

(a) ALUMINUM TARGET STEEL FLANGE

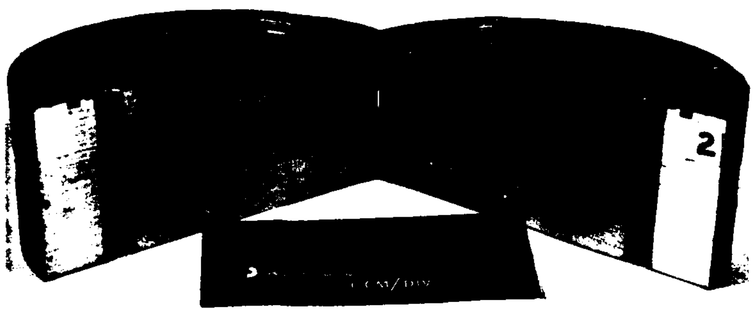

(b) SECTIONED TARGET

Figure 72 Target from Model 2 (asymmetrical collapse; thick lead wrap; LS-1).

A4113

extended into the target like a corkscrew. A final depth of 4.5 cm was achieved in approximately 270 degrees. A dotted line on the sectioned target photograph indicates the maximum penetration. The crater had a diameter of 2 cm and a volume of 4.7 cm^3.

The target from Model 2 was even more unusual. The crater, produced by the tube with a thick lead ribbon, had an annular cross-section with an outer diameter of 2 cm and an inner diameter of 1 cm. It, too, had a corkscrew appearance with a depth ranging from 0.7 cm to a maximum of 2.2 cm. The volume of the crater was 2.9 cm^3. The photograph of the sectioned target shows that the post in the center of the crater (annulus) was undamaged aluminum.

3.3.1 Discussion of Results. The results of the first spherical high explosive experiment were considerably different from the results of the explosive driver tests. The spherically divergent shock wave produced jetting in all of the LOS models that extended to the surface of the explosive sphere, whether or not they included asymmetries. Furthermore, the energy flow in the jets was lower than had been observed in the comparable driver tests. This is illustrated in Table 2. The velocity of the tip of the jet in LOS Model 5 (standard) was 75 percent lower (0.88 cm/μs compared to 1.17 cm/μs) than explosive driver test APC-11. Also, the crater volume and maximum depth of penetration in the aluminum target were respectively 17 percent and 24 percent of those produced by the explosive driver test. These results are reasonably self-consistent. Jet penetration theory shows that the penetration depth, P, is proportional to the jet

TABLE 2

COMPARISON OF JETS FROM THE SYMMETRICAL COLLAPSE OF A 1.9-cm- (0.75-in-) DIAMETER, 0.028-cm (0.011-in-) WALL THICKNESS

Method of Collapse	Test LS-1, Model 5 (spherical shock wave)	APC-11 (explosive)	Ratio: LS-1 to APC-11	Notes/Comments
Jet				
Velocity (V_j), cm/μs	0.88	1.17	0.752	
Length (ℓ_j), cm	~11.4	47.9	~0.238	Assumes ℓ_j for LOS-1 proportional to P_T.
Density (ρ_j), gm/cm^3	$\lesssim$ 0.006	$\lesssim$ 0.006	1.000 (?)	Assumes same ρ_j; ρ_j based on X-ray resolution in APC series.
Area (A_j), cm^3	~ 2.68	2.68	1.000 (?)	Jet assumed to fill tube.
Energy (E_j), e.u.	~ 0.071	0.527	0.135	$E_j = \frac{1}{2} \rho_j A_j \ell_j V_j^2$.
Target Penetration				
Crater volume (V_T), cm^3	4.9	29.6	0.165	
Maximum depth (P_T), cm	2.0	8.4	0.238	
Entrance diameter (d_T), cm	2.0	2.0	1.0	

length, ℓ_j; or $P = \ell_j\ (\lambda\rho_j/\rho_t)^{1/2}$, where ρ_j is the density of the jet, ρ_t is the density of the target, and λ is a constant that equals 1 for continuous jets and 2 for dispersed particle jets. While this description is normally used only for constant velocity jets, it should provide limiting values for the length of jet. If we assume, as a first approximation, that the jets in both experiments were equal in density, the length of the jet for this experiment would be

$$\ell_j\ (\text{LS-1}) = \ell_j\ (\text{APC-11})\ \frac{P\ (\text{LS-1})}{P(\text{APC-11})} \quad \text{or} \quad 11.4\ \text{cm.}$$

This would imply that the jet was formed by the collapse of the tube near the nitromethane-sand interface (30.5 cm + 1.6 cm for the steel plug), which extended for a distance of 11.4 cm to a range of 43.5 cm. The stress at this range was ~ 125 kPa (~ 12.5 kbar) according to the stress measurements (Figure 67). This appears to be a reasonable cut-off range, since steel has a dynamic yield strength of approximately 120 kPa (12 kbar).

The theory of jet penetration (constant velocity jets) shows that the volume of material removed from a semi-infinite target is proportional to the total energy contained in the jet. The ratio of the crater volumes would therefore indicate that the jet from the spherically collapsed tube (LS-1) had 16.5 percent of the energy produced in the drive test (APC-1). A separate estimate can be obtained by comparing the kinetic energy of the jets:

$$\frac{\text{KE (LS-1)}}{\text{KE (APC-11)}} = \left[\frac{V_j\ (\text{LS-1})}{V_j\ (\text{APC-11})}\right]^2 \times \frac{\ell_j\ (\text{LS-1})}{\ell_j\ (\text{APC-11})} \times \frac{\rho_j\ (\text{LS-1})}{\rho_j\ (\text{APC-11})} \times \frac{A_j\ (\text{LS-1})}{A_j\ (\text{APC-11})}$$

$$= \left(\frac{0.88}{1.17}\right)^2 \times \left(\frac{11.4}{47.9}\right) \times 1 \times 1$$

$$= 0.135\ (= 13.5\%)$$

Of course this estimate assumes: (1) the velocity of the jet is constant and equal to the value determined by the ionization pins in both cases; (2) the cross-sectional area and densities of the two jets are comparable; and (3) the lengths of the jets are directly proportional to their penetration depths as discussed above.

It should be noted that three pre-test events may have introduced certain asymmeties and thereby adversely affected the results of the spherical explosive test. The first event occurred while filling the plywood box with saturated sand. When the sand level reached approximately 0.81 m (32 inches), there was a small but perceptible shift in the explosive sphere, and the water level began to recede. It was estimated that the sphere had dropped as much as 9.5 mm (3/8 inch). From all indications, the sand underneath the box had settled, and a watertight seal in the box had been ruptured by the process. The models were then realigned, and the explosive sphere was carefully referenced to an external benchmark so that any further shifts in position would be observed. Up to the time of firing, the sphere had dropped less than 3 mm (1/8 inch). The water flow was also adjusted to compensate for the leak.

The second event was a misfire, which occurred when the RP-3 detonator failed to initiate. The continuity of the exploding bridgewire detonator circuit was found to be open after the firing attempt. Since the circuit had been checked immediately before firing, it was postulated that the settling process (first event) had broken a watertight seal between the detonator and firing cable and had shunted the firing current. As a result, the bridgewire burned out instead of exploding and detonating the 50.8-mm- (2-inch-) diameter C-4 explosive booster. A separate RP-1 detonator was then lowered through the aluminum vent tube (see Figure 59) and positioned on top of the C-4 booster. This caused initiation to occur 25.4 mm (1 inch) above the center of the sphere. When combined with the settling of the sand, the total unplanned asymmetries could have caused the detonation wave to be tilted by approximately 6.4 degrees with respect to the longitudinal axes of the models.

The third event was a loss of saturation in the sand. The compensating water flow was turned off after the misfire and remained off for a period of two hours while the misfire was diagnosed and corrected. Since water was not reapplied, the saturation conditions were unknown at the actual time of firing.

SECTION 4

SPHERICAL HIGH EXPLOSIVE EXPERIMENT LS-2

The results from the first spherical experiment (LS-1) indicated that there was very little correlation between the effects of asymmetries on the jetting produced by the steady-state explosive drivers and those produced by a transient, spherically-divergent, shock wave. Therefore, the primary objective of the experiment described in this section was to evaluate alternative methods of inhibiting or eliminating the jetting phenomena resulting from the collapse of LOS models by spherically divergent shock waves. A secondary objective was to confirm the results of the first spherical test, which had been clouded by a loss of saturation and the introduction of unplanned asymmetries.

4.1 EXPERIMENT DESCRIPTION

The experimental configuration used for LS-2 is given in Figure 73. The saturated sand test bed was contained in a 2.44-m- (8-ft-) diameter, 6.35-mm- (1/4-inch-) wall, steel cylinder. The cylinder was mounted on a 101.6 mm (4 inch) concrete pad. The interface between the cylinder and pad was joined with a cement grout and a water-based epoxy sealant. The concrete pad was constructed on compacted sand in the bottom of the crater resulting from the previous spherical test, LS-1. The explosive sphere was mounted on a 304.8-mm- (12-inch-) diameter

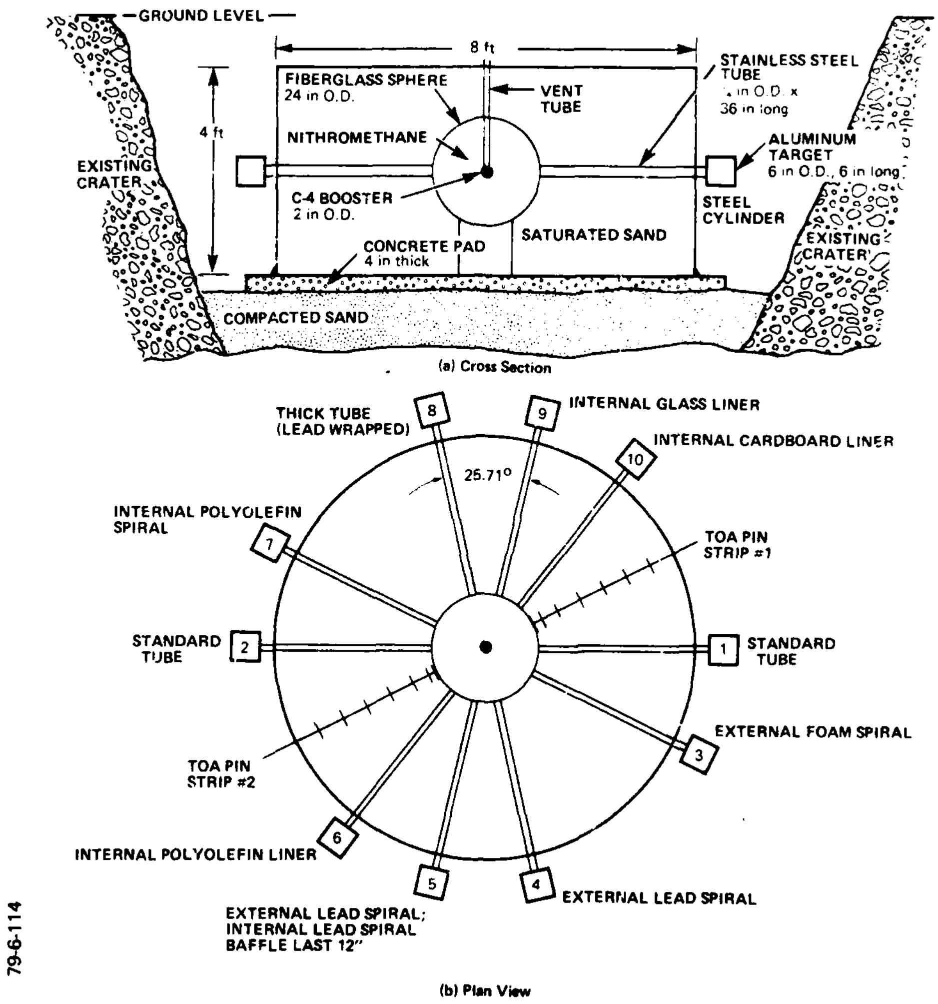

Figure 73 Experimental configuration of experiment LS-2.

vertical steel cylinder embedded in the concrete pad. Except for the initiation system, the explosive source was similar to that used in LS-1 (Section 4.1.1). The initiation system consisting of an RP-2 detonator, 1.22 m (48 inches) of mild detonating fuse (MDF), a spherical tetryl pellet and a 50.8 mm (2 inch) sphere of C-4 explosive, was inserted into the nitromethane sphere through the vertical vent tube. The water used to saturate the Monterey sand was injected into the test bed through a perforated PVC pipe located around the inside bottom perimeter of the sand containment cylinder.

As shown in Figure 73b, the horizontal midplane of the explosive sphere was divided into fourteen equal segments of 25.71° each. Two of these segments contained time-of-arrival instrumentation lines, ten contained LOS models, and two were left vacant since they contained the flange which coupled the two hemispherical shells of the explosive container. The LOS models extended from the surface of the explosive sphere to the outside surface of the sand confinement cylinder. An aluminum flange was fastened to the end of each model to accommodate a vacuum port, and a 0.25 mm (0.010 inch) Mylar diaphragm which separated the models from their aluminum targets. Each target had a diameter of 15.24 cm (6 inches) and a length of 15.24 cm (6 inches). The targets were contained in thick-walled steel cylinders and supported on steel cradles which were welded onto the side of the sand confinement cylinder. The photographs given in Figure 74 show the experiment before and after sand emplacement.

Stainless steel tubing (321 welded and drawn, Military Specification 8808) was used for the LOS models. Each model had

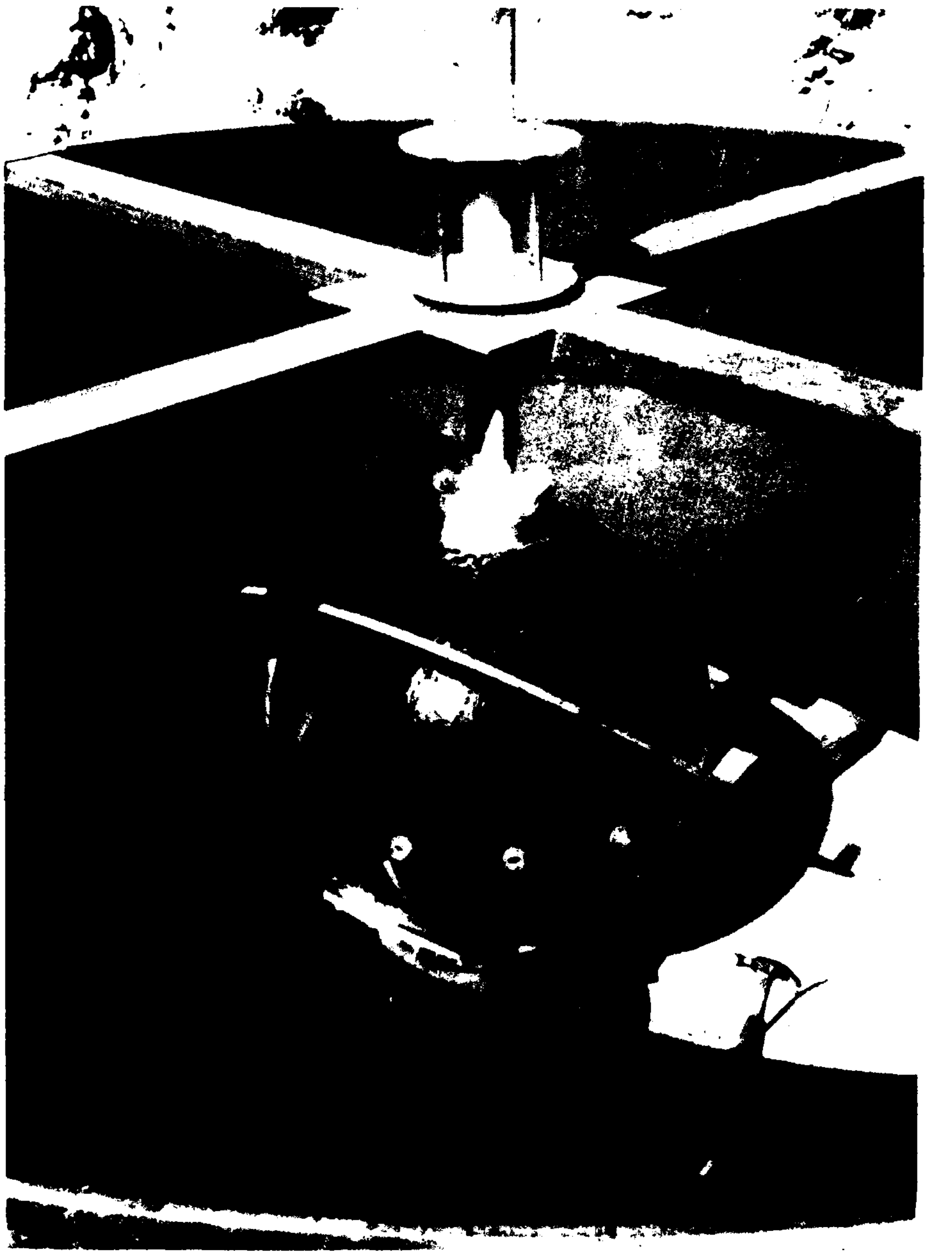

79-6-100

(a) Explosive sphere prior to model installation and sand emplacement

Figure 74a   Photograph of experiment LS-2.

79-6-97

(b) Experiment just prior to firing

Figure 74b   Photograph of experiment LS-2.

an outer diameter of 1.905 cm (3/4 inch) and a wall thickness of 0.028 cm (0.012 inch). A description of the individual models is given in Figures 75 to 84 of Section 4.3. Models 1 and 2 were standard models with no asymmetries. Model 3 had a foam ribbon helically wound around the external surface of the stainless steel tubing. A lead ribbon helix was used on Model 4. Model 5 was similar to Model 4 except for a lead helix on the inside surface of the tube for the last 30.48 cm (12 inches). Model 7 had a polyolefin ribbon on the inside surface of the tube. The wall thickness of Model 8 was increased from 0.3 mm (0.012 inch) to 2.34 mm (0.092 inch) by wrapping sheet lead around the tube. Models 6, 9, and 10 had polyolefin, glass, and cardboard liners respectively.

4.2 INSTRUMENTATION

The penetration of, and damage to, the aluminum targets was used as the principal evidence of the jet energy generated by the collapse process. The only active instrumentation used on this experiment was directed at measuring the time-of-arrival (TOA) of the free-field shock wave in the saturated sand. Two radial TOA pin lines were used. The pin lines were positioned on opposite sides of the explosive sphere. Each line contained seven capped ionization pins and seven piezoelectric pins. A pin of each type was located at distances of 32 cm, 37 cm, 47 cm, 62 cm, 77 cm, 92 cm, 107 cm, and 122 cm from the center of the sphere.

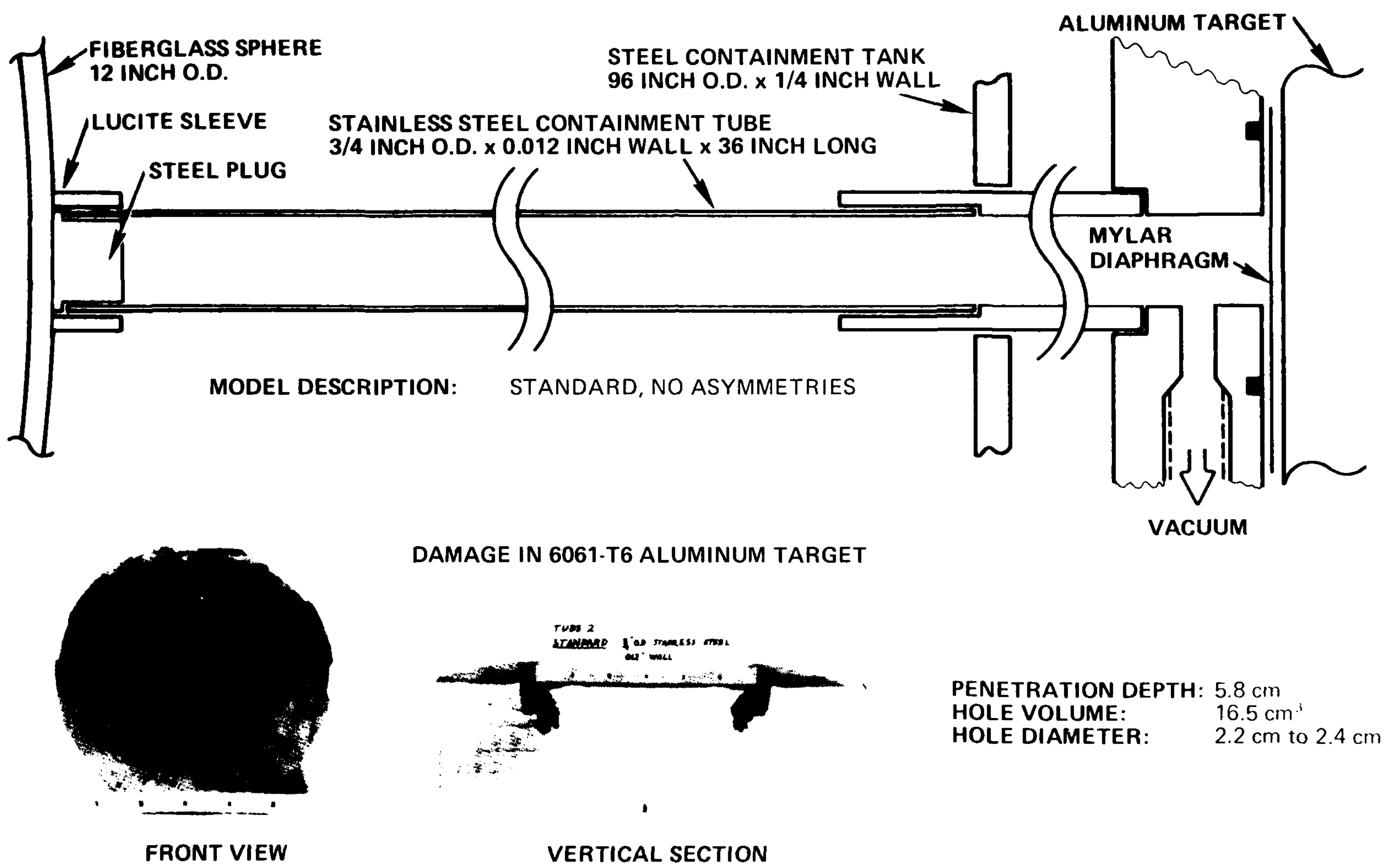

Figure 75 Configuration and target damage for LOS Model 1 (Experiment LS-2).

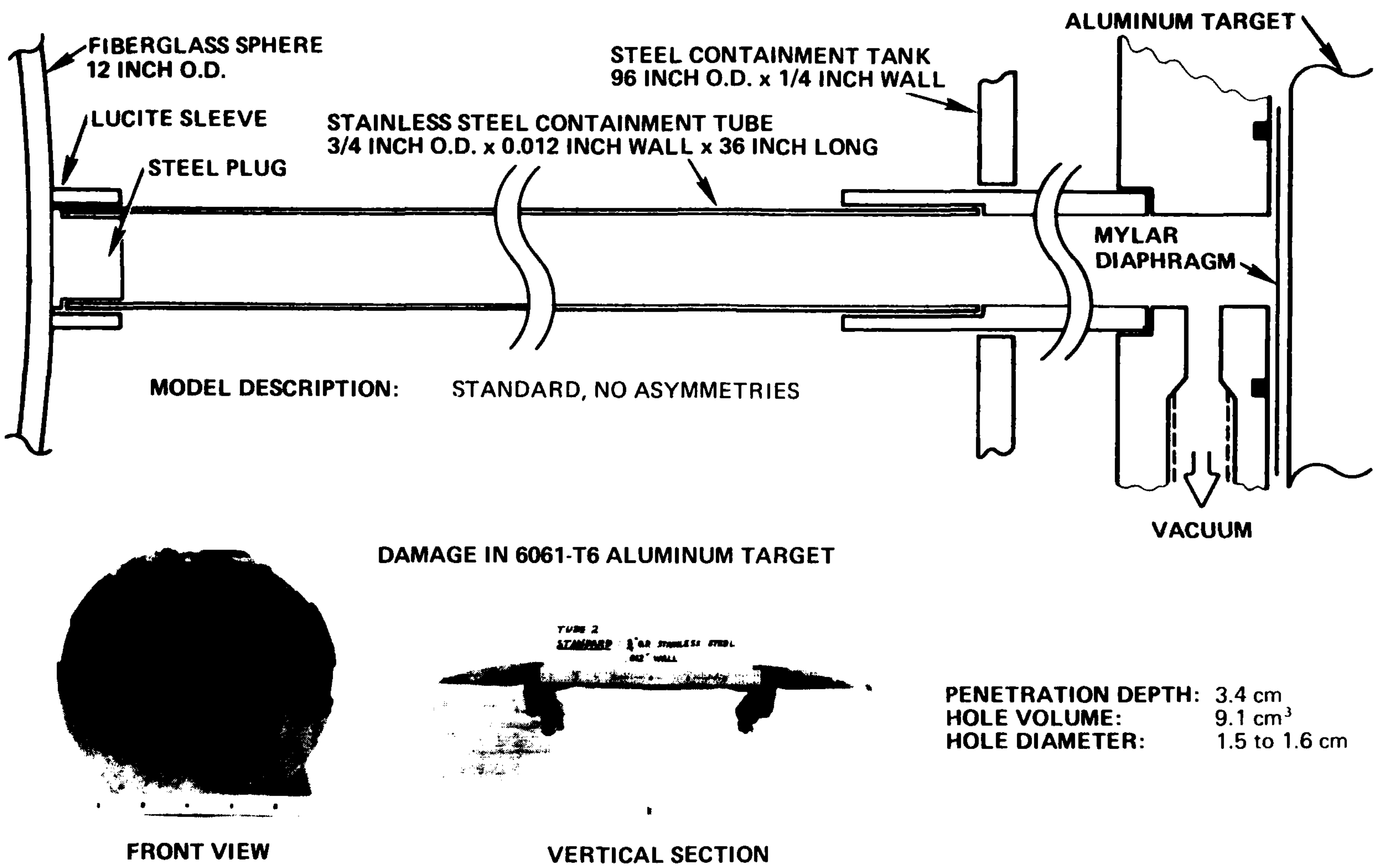

Figure 76 Configuration and target damage for LOS Model 2 (Experiment LS-2).

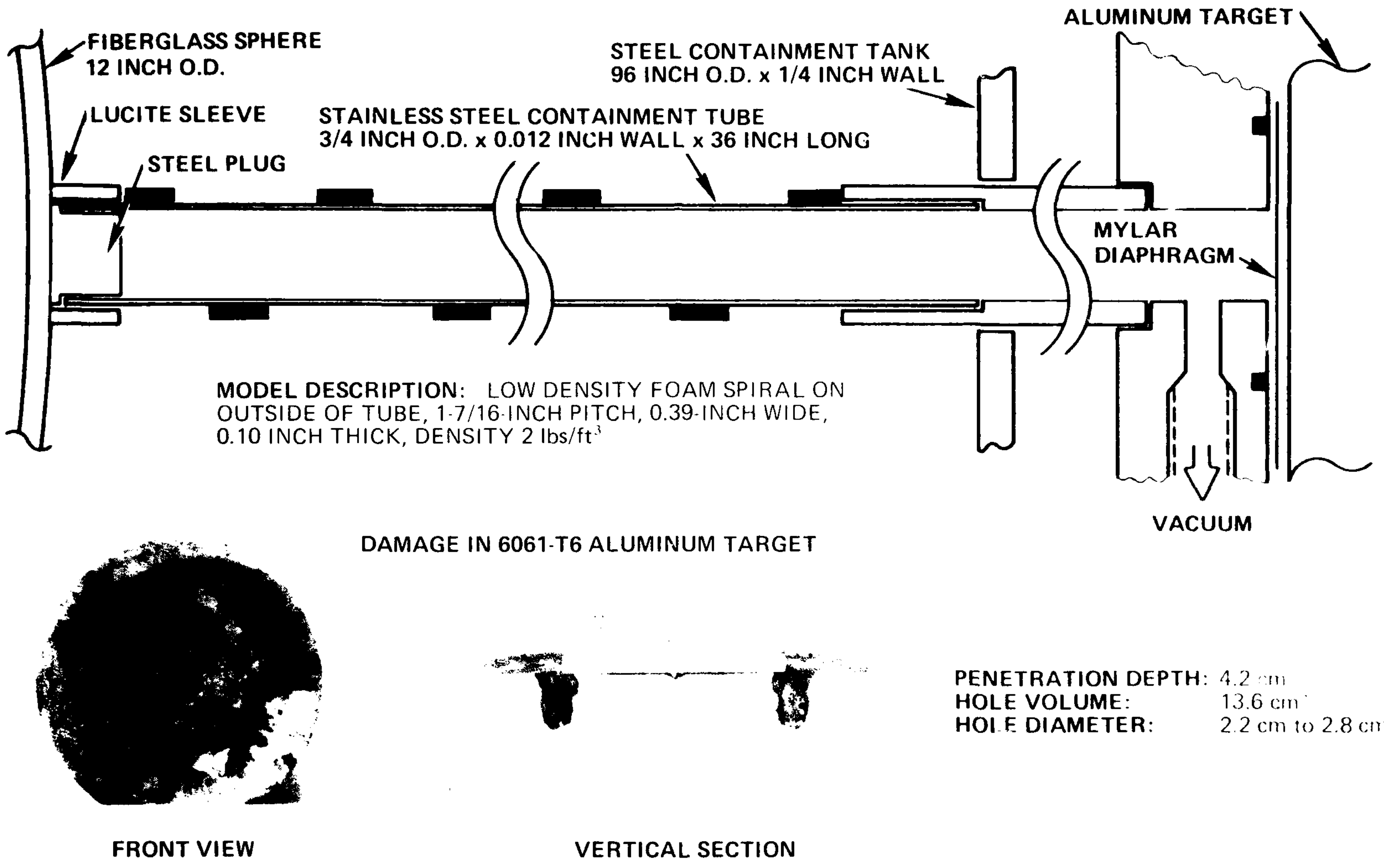

Figure 77 Configuration and target damage for LOS Model 3 (Experiment LS-2).

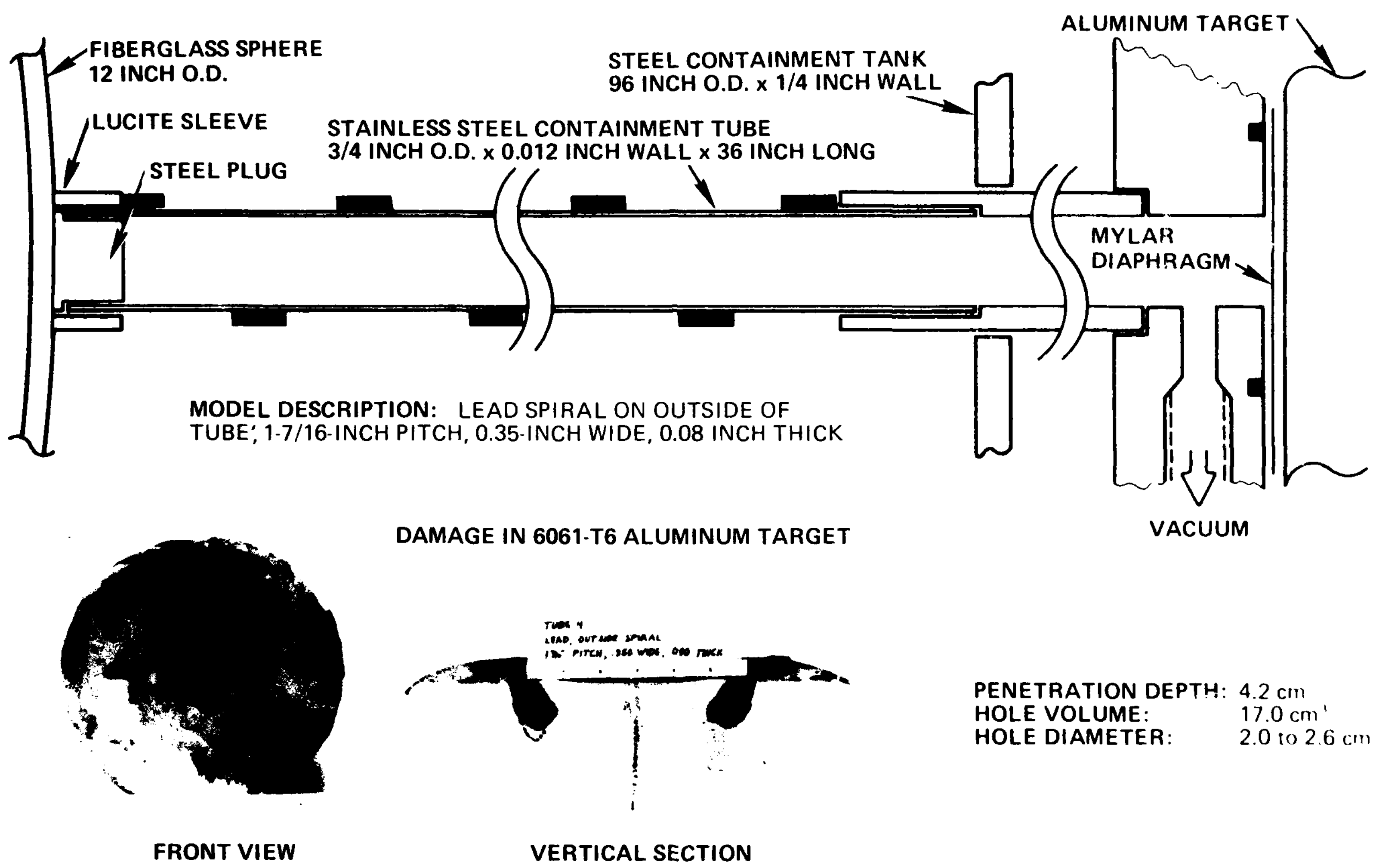

Figure 78 Configuration and target damage for LOS Model 4 (Experiment LS-2).

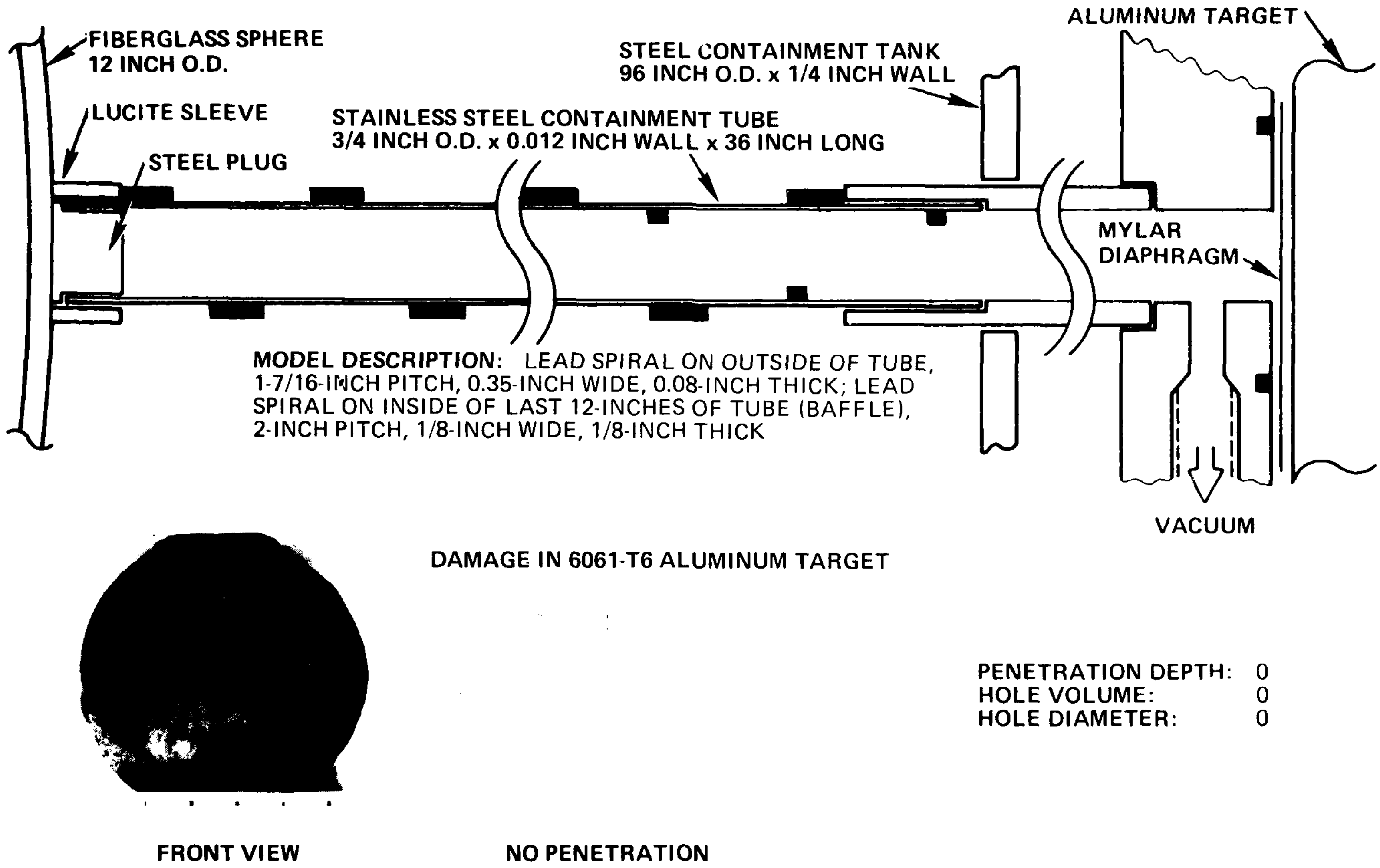

Figure 79 Configuration and target damage for LOS Model 5 (Experiment LS-2).

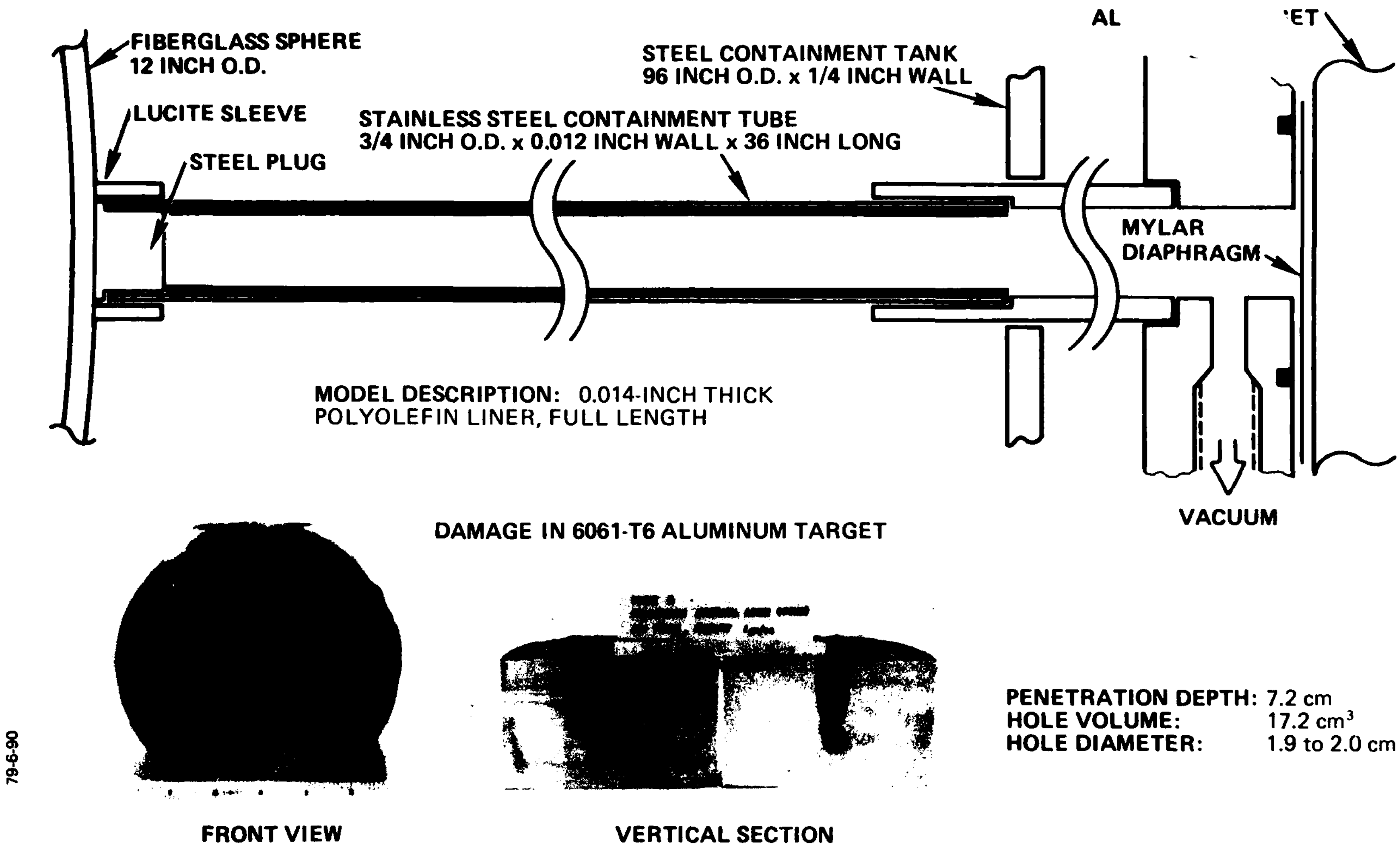

Figure 80 Configuration and target damage for LOS Model 6 (Experiment LS-2).

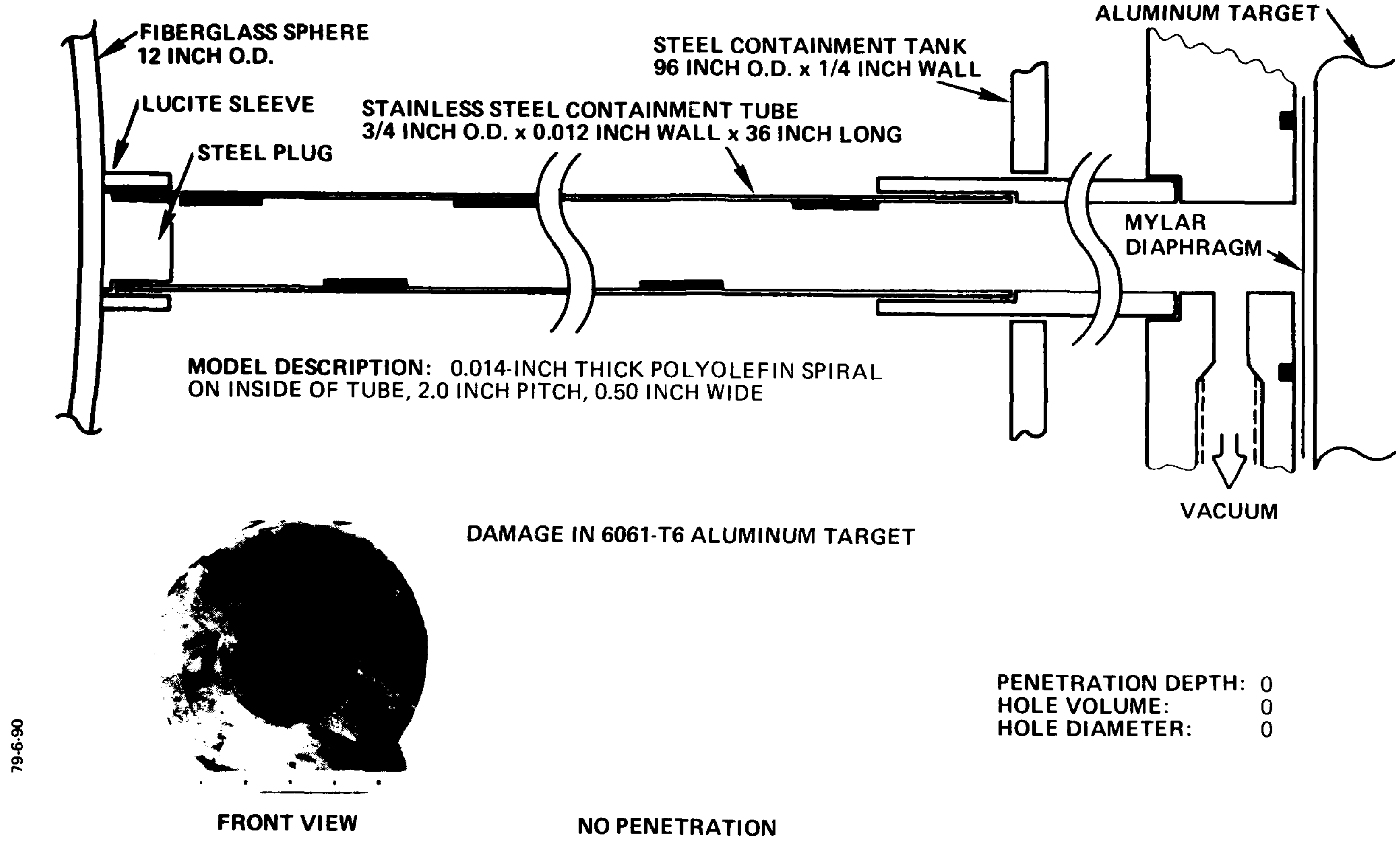

Figure 81 Configuration and target damage for LOS Model 7 (Experiment LS-2).

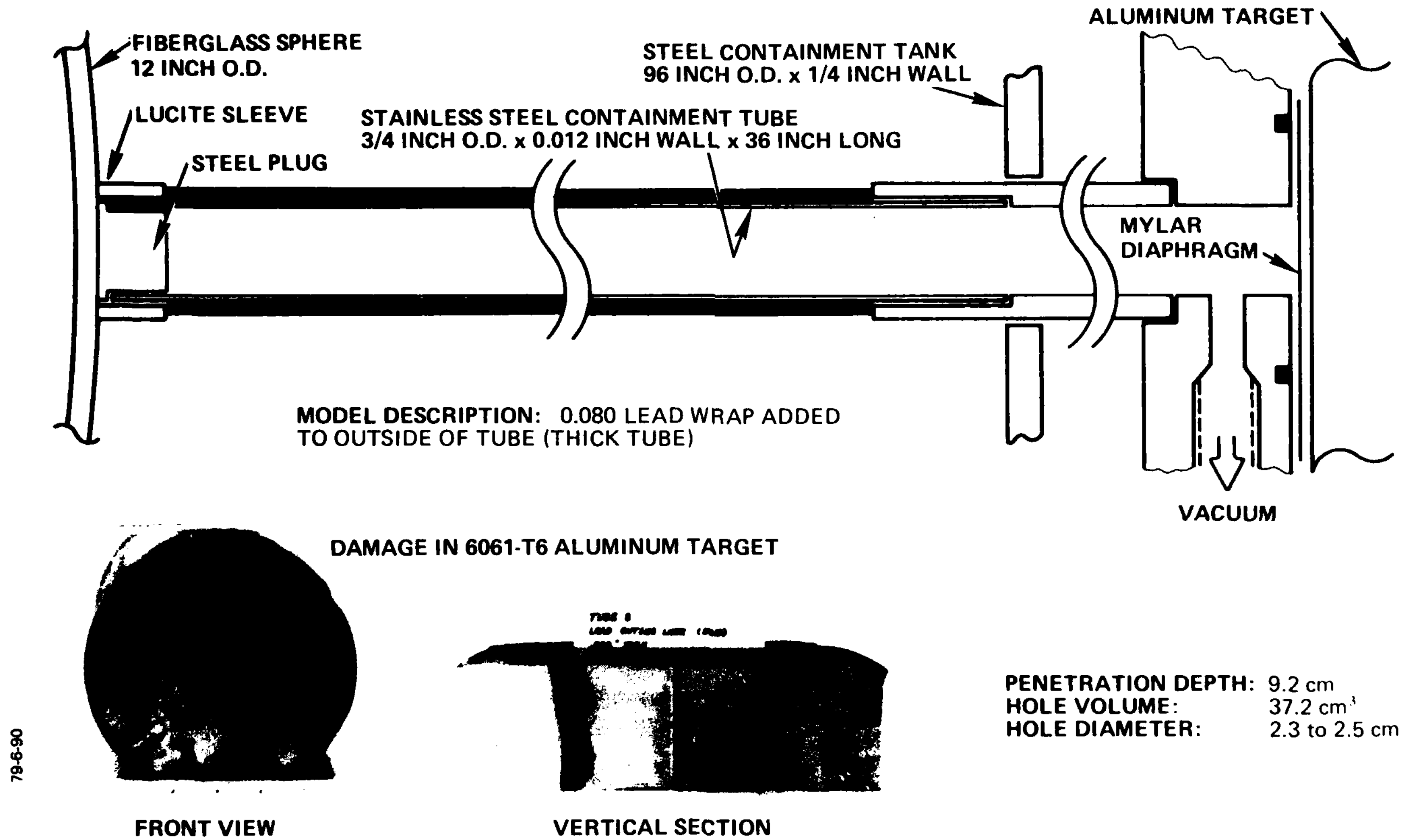

Figure 82 Configuration and target damage for LOS Model 8 (Experiment LS-2).

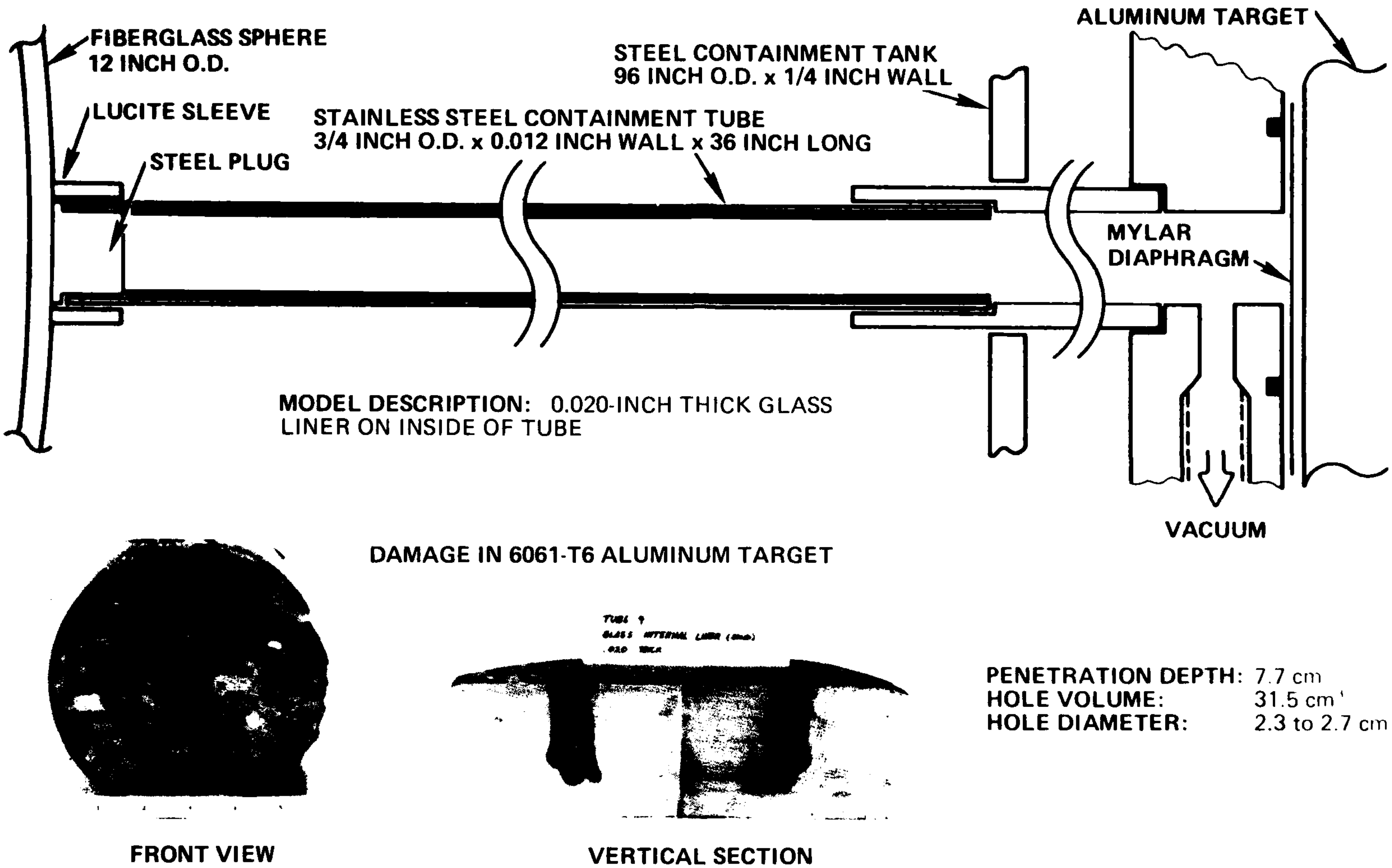

79-6-90

Figure 83 Configuration and target damage for LOS Model 9 (Experiment LS-2).

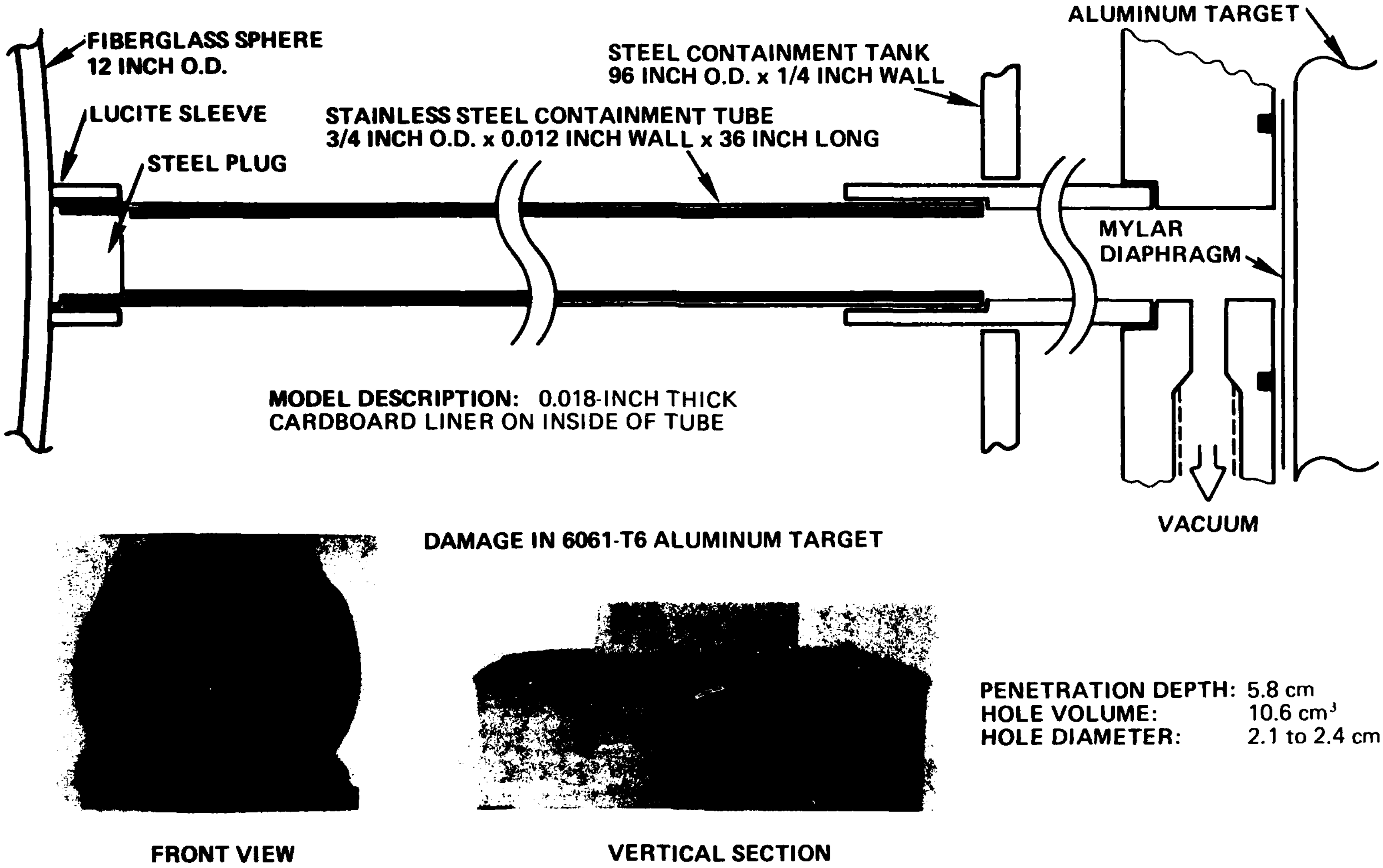

Figure 84 Configuration and target damage for LOS Model 10 (Experiment LS-2)

4.3 EXPERIMENTAL RESULTS

The most salient results of Experiment LS-1 are given in Figures 75 to 84. These figures show the initial configuration and the target damage for each of the ten LOS models. The penetration depth, crater diameter, and crater volume produced in the aluminum target by the jet from each LOS model are summarized in Table 3. The models are also ranked according to target damage (crater volume and penetration depth) in this table. These data show that jetting was essentially eliminated in the two LOS models with internal spirals, Model 5 and Model 7, and that the most severe target damage was produced by the collapse of the thick lead wrapped tube (Model 8) and the glass-lined tube (Model 9).

The trajectory of the spherically divergent shock wave in the saturated Monterey sand is shown in Figure 85. The trajectory is based on the time-of-arrival measurements on opposite sides of the explosive spheres. Only one set of data is shown since the times-of-arrival for the two locations were identical within the resolutions of the measurement. It should be noted that the time coordinate of Figure 85 is depressed by 172 microseconds. This is the time required to initiate the C-4 explosive booster using the mild detonating fuse and the exploding bridgewire detonator, which was outside the explosive sphere.

The velocity and trajectory of the free-field shock wave for LS-2 was quite close to the trajectory calculated for a 37 percent porous, 100 percent saturated sand (Reference 12). In

TABLE 3

SUMMARY OF RESULTS (EXPERIMENT LS-1)

Model Number	Model Description	Target Damage: Penetration Depth (cm)	Crater Diameter (cm)	Crater Volume (cm^3)
1	Standard (baseline)	5.75	2.2 - 2.4	16.5
2	Standard (baseline)	3.40	1.5 - 1.6	9.1
3	Foam spiral - External	4.15	2.2 - 2.8	13.6
4	Lead spiral - External	4.20	2.0 - 2.6	17.0
5	Lead spiral - External, Lead spiral - Internal	Nil	Nil	Nil
6	Polyolefin liner - Internal	7.20	1.9 - 2.0	17.2
7	Polyolefin spiral - Internal	Nil	Nil	Nil
8	Lead wrap - External	9.2	2.3 - 2.5	37.2
9	Glass liner - Internal	7.7	2.3 - 2.7	31.5
10	Cardboard liner - Internal	5.8	2.1 - 2.4	10.6

	Model Number	Crater Volume (cm^3)	Model Number	Penetration Depth (cm)
Least Target Damage	7	Nil	7	Nil
↓	5	Nil	5	Nil
	2	9.1	2	3.40
	10	10.6	3	4.15
	3	13.6	4	4.20
	1	16.5	1	5.75
	4	17.0	10	5.80
	6	17.2	6	7.20
	9	31.5	9	7.70
Most Target Damage	8	37.2	8	9.20

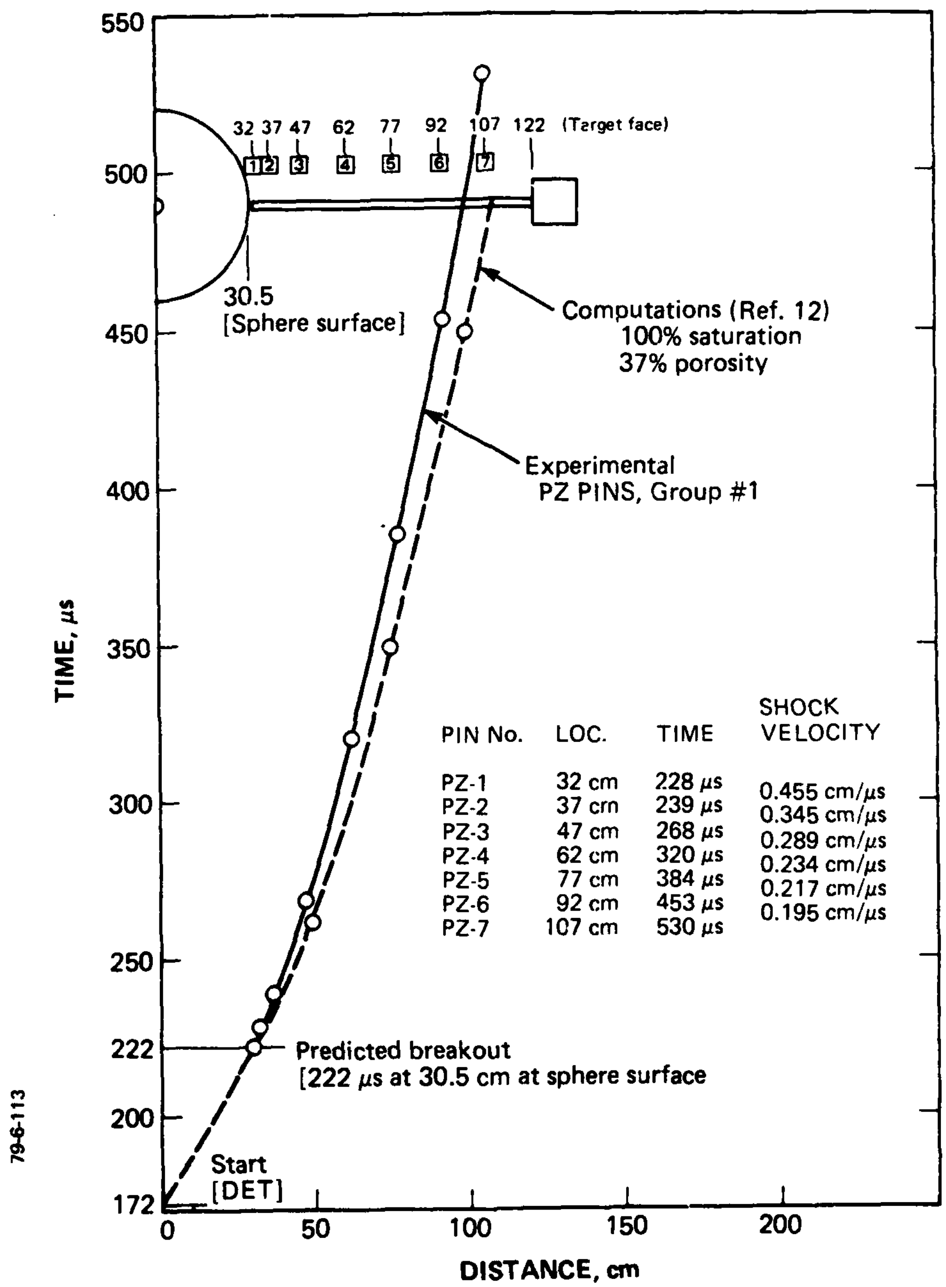

Figure 85 Free-field shock trajectory in saturated Monterey Sand for LS-2.

fact, the agreement supports the postulate that a considerable amount of water was lost in the first experiment (LS-1).

4.4 DISCUSSION OF RESULTS

Based on the observed target damage, jetting did not occur in Models 5 and 7. Both of these models had asymmetries on the inside surface of the stainless steel tube. However, they were designed to evaluate two entirely different phenomena. The lead helix used in Model 5 was placed in the last 0.305 m (12 inches) of the tube as a means of suppressing an already formed jet. This model also had an external lead helix along its entire length. Conceptually, the internal lead helix would serve as a baffle and interrupt the annular-like jet flow which was inferred from the target damage observed in LS-1 (Figures 70-72 and Section 4.3). Model 7, on the other hand, had a polyolefin helix inside the entire tube. This helix was directed at reducing or eliminating the jet at its source by: (1) placing an asymmetry precisely where the jet is formed; and (2) using a material with low melting and vaporization points. Conceptually, the jet would either be disrupted by the presence of the asymmetry, or the plastic would be converted to a gas by the collapse process. In the latter case, it was postulated that the energy and momentum in a gas jet could be reduced more easily than a liquid and/or a solid jet.

The most disquieting results of LS-1 were the rather wide variations in target damage which were produced by the two "standard" LOS designs, Models 1 and 2. Even though both of these models were designed, fabricated, assembled, installed and tested in the same manner, Model 1 produced 81 percent more crater volume and 69 percent greater penetration depth than Model 2. The data base is insufficient to assess whether this result was an anomaly or within the normal reproducibility spread of jetting phenomena.

The target damage resulting from Models 3 and 4 provides convincing evidence that asymmetries on the external surface of a tube do not inhibit the formation of a jet when the tube is collapsed by a spherically divergent shock wave. In fact, the foam and lead helixes used in these models produced target damage within the range of that produced by Models 1 and 2, which had no asymmetries.

The target damage produced by Models 6, 9, and 10 indicates that internal liners are also not an effective way of eliminating the jet from a collapsing tube. However, it does appear that the liner material replaces the tube material in the jet. This observation is based on the recognition that the target damage from a glass liner (Model 9) was greater than that for a polyolefin liner (Model 6) which was, in turn, greater than that for a cardboard liner (Model 10). Since the target damage resulting from the glass liner was so much greater than the other materials, these results may also indicate the importance of the melting and vaporization properties of the tube and liners.

The final observation is that the lead wrapped tube used in Model 8 produced the greatest target damage. This is not unexpected since, according to classical jetting theory, the mass of the jet is directly related to the mass of the tube and the collapse angle (Section 2.2). Not only was the tube mass per unit length of Model 8 over 11 times greater than the "standard" tube, but the thicker tube undoubtedly resulted in larger collapse velocities and thus larger collapse angles as it converged on axis.

REFERENCES

1. E.T. Moore, Jr., "Explosive Hypervelocity Launchers," NASA CR-982, National Aeronautics and Space Administration, Washington, D.C., February 1968.

2. H.F. Waldron, E.T. Moore, Jr., G.B. Steel, and C.S. Godfrey, "A Mechanism for the Conversion of the Chemical Energy of Explosives to the Kinetic and Internal Energy of a Gas," Paper No. 67-178, presented at the AIAA 5th Aerospace Sciences Meeting, New York, New York, January 23-26, 1967.

3. J.K. Crosby and S.P. Gill, "Feasibility Study of an Explosive Gun," NASA CR-709, National Aeronautics and Space Administration, Washington, D.C., April 1967.

4. S.P. Gill and R.C. Goettelmann, "Implosively Accelerated Shock Tube Driver," NASA CR-950, National Aeronautics and Space Administration, Washington, D.C., November 1967.

5. E.T. Moore, Jr., "Explosively Driven Shock Tubes," AEDC-TR-66-238, Arnold Engineering Development Center, Arnold Air Force Station, Tennessee, November 1966.

6. H.F. Waldron, W. Wolny, and G.B. Steel, "Explosive Drivers for Shock Tunnels," AEDC-TR-68-115, Arnold Engineering Development Center, Arnold Air Force Station, Tennessee, June 1968.

7. G.B. Steel, E.T. Moore, Jr., and C.S. Godfrey, "Simulation of Nuclear Surface Bursts Using an Explosive Driver Technique," DASA-2102, Part I, Defense Atomic Support Agency, Washington, D.C., August 1968.

8. D.W. Baum, E.T. Moore, Jr., and D.M. Mumma, "FLARE, Fast Launch and Recovery Experiments," PIFR-103, Physics International Company, San Leandro, California, May 1969. Prepared for University of California Los Alamos Scientific Laboratory, Los Alamos, New Mexico.

9. J.R. Barthel private communication.

10. G. Birkhoff, D.P. MacDougall, E.M. Pugh, and G. Taylor, "Explosives with Lined Cavities," J. Appl. Phys., 19, 563 (1948).

11. J.L. Ploss, private communication.

12. D. Patch, private communication.

13. D.E. Grady, C.W. Smith, and L. Seaman, "In Situ Constitutive Relations of Rocks," Stanford Research Institute, Menlo Park, California, January 1973. Prepared for Defense Nuclear Agency, Washington, D.C., DNA-3172 Z.

DISTRIBUTION LIST

DEPARTMENT OF DEFENSE

Assistant to the Secretary of Defense
Atomic Energy
ATTN: Executive Assistant

Defense Nuclear Agency
ATTN: DDST
ATTN: SPTD, T. Kennedy
4 cy ATTN: TITL

Defense Technical Information Center
12 cy ATTN: DD

Field Command
Defense Nuclear Agency
ATTN: FCPR
ATTN: FCTK, C. Keller
ATTN: FCTMD, W. Summa

Field Command
Defense Nuclear Agency
Livermore Division
ATTN: FCPRL

Field Command Test Directorate
Test Construction Division
Defense Nuclear Agency
ATTN: FCTC, J. LaComb

Undersecretary of Def. for Rsch. & Engrg.
ATTN: Strategic & Space Systems (OS)

DEPARTMENT OF THE ARMY

Harry Diamond Laboratories
Department of the Army
ATTN: DELHD-N-P

DEPARTMENT OF THE NAVY

Naval Surface Weapons Center
ATTN: Code F-31

DEPARTMENT OF THE AIR FORCE

Air Force Weapons Laboratory
ATTN: SUL

OTHER GOVERNMENT AGENCY

Department of Interior
U.S. Geological Survey
Special Project Center
ATTN: R. Carroll

DEPARTMENT OF ENERGY

Department of Energy
Nevada Operations Office
ATTN: R. Newman

DEPARTMENT OF ENERGY CONTRACTORS

Lawrence Livermore Laboratory
ATTN: Document Control for D. Oakley
ATTN: Document Control for B. Hudson
ATTN: Document Control for B. Terhune
ATTN: Document Control for J. Shearer

Los Alamos Scientific Laboratory
ATTN: Document Control for R. Brownlee
ATTN: Document Control for E. Jones
ATTN: Document Control for F. App
ATTN: Document Control for A. Davis

Sandia Laboratories
ATTN: C. Mehl
ATTN: C. Smith

DEPARTMENT OF DEFENSE CONTRACTORS

General Electric Company-TEMPO
ATTN: DASIAC

Pacifica Technology
ATTN: G. Kent

Physics International
ATTN: E. Moore

R & D Associates
ATTN: C. MacDonald

SRI International
ATTN: A. Florence

Systems, Science & Software, Inc.
ATTN: R. Duff

Terra Tek, Inc.
ATTN: S. Green

END

DATE

FILMED

8-80

DTIC